A Novel Capacitively Coupled Contactless Conductivity Detection System for Microfluidic Devices: Design, Optimisation and Application

A thesis submitted for fulfilment of the degree of
Doctor of Philosophy

Leigh D. Thredgold

BTech (Forens&AnalytChem), BSc (Hons)

Faculty of Science & Engineering
School of Chemical and Physical Sciences

February 2015

Declaration

'I certify that this thesis does not incorporate without acknowledgement any material previously submitted for a degree or diploma in any university; and that to the best of my knowledge and belief it does not contain any material previously published or written by another person except where due reference is made in the text.'

Leigh D Thredgold.

.... on ....

Acknowledgements

The successful completion of a PhD cannot be achieved without surrounding yourself with an incredible network of support. Consequently, the contents of this thesis are not the result of an individual effort alone; rather they are the culmination of the support and encouragement from everyone involved in the journey of the last four years. Therefore, there are many people to thank.

First and foremost my supervisory team of Assoc. Professor Claire Lenehan and Professor Amanda Ellis. Claire, thank you for taking me on as your Honours student in 2010 and for showing unwavering belief in my capabilities as a research scientist since that time. Your incredible knowledge has been an amazing resource to draw on and your ability to somehow turn what seemed like unassailable negatives into achievable positives never ceases to amaze me. Amanda your support of this project, particularly in the early days, has been invaluable. Your feedback has always been honest, to the point and provided great food for thought but all the way it resulted in better outcomes.

To think I started this PhD with almost no knowledge of microfluidics is extraordinary. For teaching me the fundamentals of microfluidics and its biological applications I must thank Dr Dmitriy Khodakov. A big thank you must also go to the staff of the faculty's technical services unit and in particular Wayne Peacock who was instrumental in building the electronic components of our system. It was a long process, but without your help I think we would still be trying to build it today!

I must thank my fellow PhD students that have been through this journey with me. To my office buddies Christine, Karen and Caitlyn, thanks for the many long lunches, tea breaks, conversations (both serious and not so serious!) and support. We have had many laughs and I could not have asked for a better environment and group of people to share a confined space with. To our honourary fourth office buddy Gos, I think you have single handonly kept me sane at times. Whether it be for a serious conversation about science or life, or a moment of fun and hilarity you always managed to bring perspective to uni life. Thanks also to Lachlan for the many football conversations, we are both still waiting for success to come to our respective teams and I hope it will become reality for us soon!

I want to thank the Lenehan, Popelka-Filcoff and Kirkbride research groups for listening to presentations and offering valuable feedback over the course. It's been an honour to be part of such a diverse research group and one that supports each other. Meetings were always constructive and finished with many delicious cakes!

To my mum and dad, I don't think words can express my gratitude for all you have provided me with over not just the last four years but my lifetime. I admire so much your determination and hard work to achieve your goals no matter what life throws at you. You have always believed in me and encouraged me in all of my endeavours. You are my inspiration and this thesis would not exist without you! To Chris, Megan, Lachlan, Caelan and Ella thank you for always being there. Family life has always provided a constant positive and happy environment full of laughs and fun. In many ways, and at many times, it was an escape from the world of science that I needed.

A massive thank you goes to all my extended family and friends. Thank you for your unconditional and ongoing love, support and encouragement throughout the last four years. I'm sure at times it felt like I was going to be a poor, struggling uni student forever and that I was never going to enter the 'real world'. Thankfully, it is coming to an end and I apologise for my grumpy responses every time one of you asked me when I was going to finish!

Finally, the biggest thank you goes to my fiancé Krysta. It's hard to believe that for the entire time we have known each other I have been doing my PhD and you have still found me tolerable. My love for you is infinite and I thank you for the enormous amount of love, support and patience you have shown especially through my many grumpy moods when things weren't going so well. Hopefully, this final result is proof that all the blood, sweat and tears were worth it.

Summary

Over the past two decades there has been an increasing trend towards miniaturised analytical systems. These so called 'Lab-on-a-Chip' (LOC) devices offer considerable advantages over traditional lab scale instrumentation in terms of greatly reduced manufacture and analysis costs (associated with decreased reagent and analyte consumption), improved analysis timeframes and increased instrument portability. Notably, one of the main driving forces for LOC production has been the development of simple, low cost fabrication techniques. Nevertheless, despite its great potential, there remains a considerable number of limiting factors in producing commercially viable portable LOC systems. These arise from the complex fabrication processes required to integrate commonly utilised detection systems with the microchip. Capacitively coupled contactless conductivity detection (C^4D) offers a readily miniaturised, potentially portable detection approach that is well suited to LOC systems. Whilst its integration with LOC systems has been well studied, most reported methods require cost (and time) intensive equipment and multi-step electrode patterning/fabrication processes to manufacture the devices. Furthermore the ex-situ manufacture of the detection system results in difficulty in consistently aligning the C^4D detection electrodes. These limitations have the potential to compromise analytical performance of the detection system and significantly increase the time and cost of device production.

This thesis reports the first successful use of injected gallium metal electrodes for C^4D in polymer microchips. The developed design and fabrication process is fast, simple (no complex instrumentation), highly reproducible, and eliminates difficulties with electrode alignment. Using this approach C^4D can be readily achieved in any microchip by simply adding extra 'electrode' channels to the microchip design. This design flexibility allowed for straightforward optimisation of electrode parameters to be performed; namely electrode geometry, distance from separation microchannel and length. Optimum values for each parameter were determined by evaluation of the peak heights and S/N ratios obtained for the model analytes lithium, sodium and potassium ions. This gave rise to optimised detection electrodes in anti-parallel geometry with a 75 μm electrode to separation microchannel distance and a 1000 μm electrode length.

The analytical performance of the injected gallium electrodes for C^4D was evaluated by the quantitative determination of the model analyte mixture containing small cations. Utilising the optimised electrode system produced detection limits ranging from 6.2 to 8.7 μM for lithium, sodium and potassium ions with linear calibration data between 100 to 700 μM. Furthermore, the repeatability of the method demonstrated its suitability for quantitative analysis with both the inter-day and intra-day percentage relative standard

deviation (%RSD) reported to be lower than 4% for both migration time and peak height.

To demonstrate the ability of the novel electrode system to perform sensitive and quantitative analysis it was applied to the detection of histamine in fish flesh samples. Histamine is a primary amine formed by the decarboxylation of the amino acid L-histidine and belongs to a group of compounds known as biogenic amines (BAs). Despite being present naturally in certain foods; BAs are normally formed as a result of uncontrolled microbial action which can lead to high levels upon food decomposition. Elevated histamine levels (> 200 mg/kg) have been reported as the cause for scombroid fish poisoning and therefore, simple and portable quantitative methods for the determination of histamine levels in such products are of importance to monitor the spoilage and quality during processing and storage. The first use of microchip electrophoresis with C^4D for the direct detection of histamine in fish flesh samples is reported here. After optimisation of the background electrolyte (BGE) conditions a competitive detection limit of 0.43 mg.L^{-1} was achieved. The developed method was successfully applied to the determination of spiked histamine in yellowfin tuna flesh samples with excellent recoveries. Further versatility was demonstrated through the analysis of a variety of fish products purchased from local supermarkets.

In summary, due to the expensive and complex fabrication approaches used to integrate C^4D electrodes with LOC devices, the development of an alternative simple and inexpensive method is required. The research presented here introduces a novel approach utilising molten gallium metal injected into electrode guide channels patterned during microchip fabrication. The development of this technique provides a significant advance and allows for consistently aligned electrodes to be produced without the need for costly instrumentation.

Publications

The published works originating from work contained in this thesis are as follows:

Leigh D. Thredgold, Amanda V. Ellis & Claire E. Lenehan
Direct detection of histamine in fish flesh using microchip electrophoresis with capacitively coupled contactless conductivity detection.
Analytical Methods, Vol. 7 (5), 2015, pp. 1802-1808

Leigh D. Thredgold, Dmitriy A. Khodakov, Amanda V. Ellis & Claire E. Lenehan
Optimization of physical parameters of 'injected' metal electrodes for capacitively coupled contactless conductivity detection on poly(dimethylsiloxane) microchips.
Proceedings of SPIE Micro/Nano Materials, Devices and Systems. Vol. 8923, (2013)

Leigh D. Thredgold, Dmitriy A. Khodakov, Amanda V. Ellis & Claire E. Lenehan
On-chip capacitively coupled contactless conductivity detection using "injected" metal electrodes.
Analyst, Vol. 138 (15), 2013, pp. 4275-4279

Additional publications arising from work related to this thesis are as follows:

Dmitriy A. Khodakov, Leigh D. Thredgold, Claire E. Lenehan, Gunther Andersson. Hilton J. Kobus & Amanda V. Ellis
DNA capture-probe based separation of double-stranded polymerase chain reaction amplification products in poly(dimethylsiloxane) microfluidic channels
Biomicrofluidics, Vol. 6 (2), 2012, pp. 026503-1-026503-11

Dmitriy A. Khodakov, Leigh D. Thredgold, Claire E. Lenehan, Gunther Andersson. Hilton J. Kobus & Amanda V. Ellis
Surface modification of poly(dimethylsiloxane) (PDMS) microchannels with DNA capture-probes for potential use in microfluidic DNA analysis systems
Proceedings of SPIE Micro/Nano Materials, Devices and Systems, Vol. 8204, (2011)

Dedicated to

My Parents
Nick and Julie Thredgold

For always inspiring, believing and encouraging
me to achieve

Contents

Figures

Tables

Equations

List of Acronyms

%RSD	Percentage Relative Standard Deviation
µEOF	Electro-osmotic Flow Mobility
BA	Biogenic Amine
BGE	Background Electrolyte
C^{4}D	Capacitively Coupled Contactless Conductivity Detection
CAPS	3-(cyclohexylamino)-1-propanesulphonic acid
CE	Capillary Electrophoresis
CHES	2-(cyclohexyl amino)ethanesulphonic acid
DDM	n-Dodecyl β-D-maltoside
EOF	Electro-osmotic Flow
FFT	Fast Fourier Transform
GC	Gas Chromatography
GC-MS	Gas Chromatography-Mass Spectrometry
HEPES	2-[4-(2-hydroxyethyl)piperazin-1yl] ethanesulphonic acid
His	Histidine
HPLC	High Performance Liquid Chromatography
HV	High Voltage
LOC	Lab-on-a-Chip
LOD	Limit of Detection
LOQ	Limit of Quantitation
MES	2-(N-morpholino)ethanesulphonic acid
PCB	Printed Circuit Board
PDMS	Poly(dimethyl)siloxane
RE	Receiving Electrode
S/N	Signal to Noise
SDS	Sodium Dodecyl Sulphate
SPE	Solid Phase Extraction
TE	Transmitting Electrode
Tris	2-amino-2-hydroxymethyl-propane-1,3-diol
UV-vis	Ultraviolet-visible

1. Introduction

1.1   Microfluidics

Microfluidics refers to the broad area of scientific research that examines systems that utilise microscale channels to process or manipulate small amounts of fluids (10^{-9} to 10^{-18} litres) [1]. In terms of scientific fields, microfluidics is relatively new and the full capability of its associated technologies has not yet been reached [2]. Between the years 2000 and 2012 there was a steady increase in publications containing references to microfluidic in their topic (Figure 1). Since this time publication numbers have remained strong demonstrating the increasing importance of this field to the scientific community and its potential for wide ranging applications.
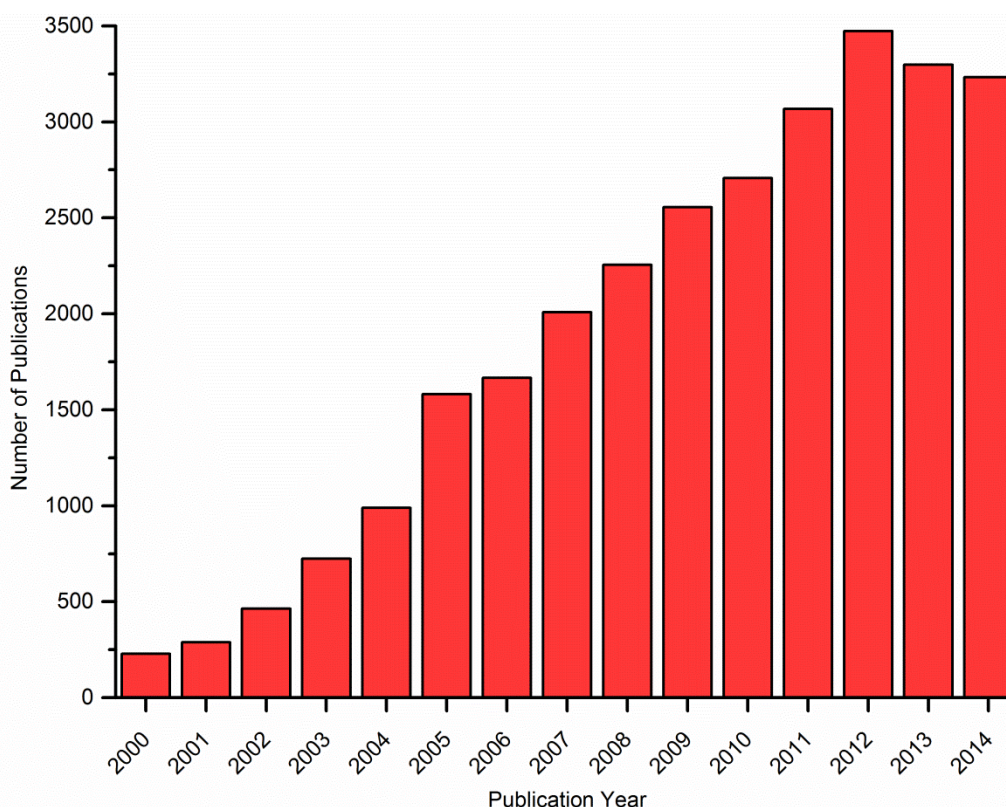
Figure 1   **Number of publications containing microfluidic as a topic**
Searched in the Web of Science™ database between the years 2000 and December 2014

The main application of microfluidics remains, as was originally intended, miniaturised analytical systems [3]. This is a direct result of its associated benefits in decreased manufacture costs, analysis times, reagent and analyte consumption coupled with increased separation efficiency and portability [1, 4-6]. However, it is these same benefits, along with the unique characteristics of fluid behaviour at the microscale, that have seen the extension of microfluidic applications into areas such as chemical synthesis, biochemistry, clinical diagnostics and pharmaceutical drug delivery [3].

Microfluidics sustained growth as an important area of research is underpinned by its commercial market value being estimated at \$1.59 billion in 2013 [7] which is expected to increase significantly to \$3.57 billion by 2018 and \$8.64 billion by 2023 [8]. The largest market share is currently occupied by point-of-care diagnostics due to the benefits of miniaturisation previously outlined, along with their disposability and potential for high-throughput processing in pharmaceutical research applications [2].

In terms of research based analytical applications; microfluidics has been reported for the analysis of a diverse range of samples and analytes addressing a variety of scientific challenges [1]. The main driving force behind this research has been the development of miniaturised versions of traditional systems including capillary electrophoresis (CE), high performance liquid chromatography (HPLC) and gas chromatography-mass spectrometry (GC-MS) which has led to analytical techniques with both enhanced portability and efficiency levels [3]. Such systems have been reported across scientific disciplines for high-throughput screening in drug development [9], bioanalyses [6], DNA analysis and sequencing [10-11], clinical diagnostics [12-13], protein analysis [13-15] and wastewater analysis [16] to name just a few.

1.1.1 Principles of microfluidics

The foundations of microfluidic technologies are based, almost entirely, on the fundamental differences observed between fluids moving in conventional 'large' channels, capillaries or columns and those moving in microscale channels [17-19]. The most significant of these differences is the presence of laminar flow in microfluidic channels. In larger scale systems fluid flow is considered turbulent leading to the assumption that inertia is commonly more important than viscosity in macroscopic fluids [1]. However, in microsystems, fluids do not mix convectively, resulting in the parallel flow of two fluid streams as they come together. This is known as laminar flow, which, by definition, is a condition in which the velocity of a particle in a fluid stream is not a random function of time [20]. An important outcome of laminar flow is that mixing of two fluid streams flowing in contact with each other only occurs through diffusion at the interface between the liquids, not through any other means (Figure 2) [17]. This characteristic has proven to be advantageous in many circumstances, particularly through the manipulation of surface gradients in the fields of molecular and chemical biology [6, 21]. In order to counter laminar flow in microfluidic systems, the development of specific devices or components to achieve mixing has been necessary. However these components are only required if convective mixing is required.
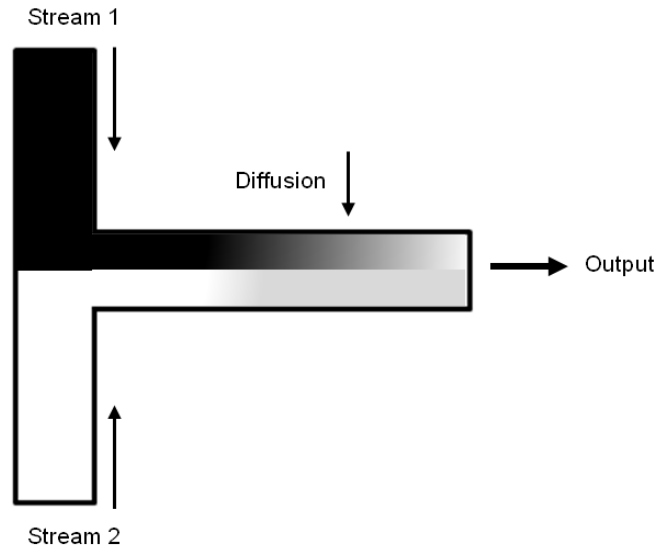
Figure 2   **Schematic of a two fluid stream flow in a microfluidic channel**

Demonstrating mixing only by diffusion.

Whether flow in a particular system is classified as laminar or turbulent, is determined by the calculation of the dimensionless parameter known as the Reynolds number (Re). Essentially the Reynolds number is the ratio of the inertial to viscous forces on fluids and can be calculated from the fluid density (ρ), characteristic velocity of the fluid (υ), fluid viscosity (μ) and hydraulic diameter (D_h) using Equation 1 [22].

Equation 1   **Determination of Reynolds number (Re)**

$$\text{Re} = \frac{\rho \upsilon D_h}{\mu}$$

The hydraulic diameter is a computed value that depends on the channels cross-sectional geometry [17] and is calculated from the cross sectional area (A) and the wetted perimeter of the cross section (P) according to Equation 2.

Equation 2   **Determination of hydraulic diameter**

$$D_h = \frac{4A}{P}$$

For fluid flow to be considered laminar it must have a calculated Re of less than 2300. Fluids begin to show signs of turbulence as the Reynolds number approaches 2300 and become turbulent above this value [17, 23].

As outlined previously, the mixing of two fluid streams flowing in contact with each other, in the absence of specific mixing devices or components, occurs only through diffusion. Diffusion is the process by which a concentrated group of particles in a volume spread, through Brownian motion, over time so the average concentration of particles throughout the volume becomes constant [17]. Diffusion typical for a simple microfluidic system can be observed in Figure 2. The one dimensional model of diffusion can be calculated using the distance a particle moves (*d*) in a time (*t*) and the diffusion coefficient of the particle (D) according to Equation 3 [17].

Equation 3   **One dimensional model of diffusion in a microchannel**

$$d^2 = 2Dt$$

Diffusion is an important parameter in microfluidic systems as distance varies to the square power in Equation 3. This translates to fluids taking significantly shorter times to diffuse over short distances. Therefore, given microchannels have dimensions on the microscale, the distance travelled due to diffusion becomes important.

A further consideration in microfluidic systems is the fluidic resistance, or the forces that oppose the relative motion of the fluid through the microchannel. This becomes important because of the relatively small amounts of fluids flowing through the microchannels in these systems. Fluidic resistance in microchannels is governed by the geometry of the given channel [17]. For example the fluidic resistance of rectangular microchannels with high aspect ratios (i.e. $h \ll w$) can be calculated from the fluid velocity (μ), the channel length (*L*), the channel width (*w*) and channel height (*h*) using Equation 4 [17].

Equation 4   **Fluidic resistance of a rectangular microchannel with high aspect ratio**

$$\text{R} = \frac{12\mu L}{wh^3}$$

As is evident in Equation 4, the fluidic resistance is proportional to the channel length and therefore becomes an important consideration when designing microfluidic networks. The equation for determining the fluidic resistance of rectangular microchannels with low aspect ratios ($h \approx w$) is considerably more complex than that for high aspect ratios but is also available in literature along with alternative channel geometries [17].

Surface area and surface tension forces are also factors that become important at the microscale. In the case of surface area; compared to macroscale systems the surface

area to volume ratios in microscale systems are commonly many orders of magnitude larger [24]. This large increase is associated with a number of significant effects on microfluidic systems. Beneficially this leads to increased efficiency of electrophoresis in microchannels due to the more rapid removal of excess heat [25]. However, increased surface area to volume ratios can result in macromolecules diffusing more rapidly to the microchannel surface subsequently leading to their adsorption to channel surfaces when using electrokinetic flow. This results in reduced pumping efficiency and should be considered when designing microfluidic devices for specific purposes [26-27]. In addition, surface tension is a property of liquids that arises from the unbalanced molecular cohesive forces at the liquid/gas interface resulting in the contraction of the surface [17]. In microfluidic systems where channels have dimensions in the order of microns, the extents liquids will travel based on capillary forces are significant. This is because the distance travelled by a liquid through a capillary is related to both the liquid's surface free energy and the radius of the capillary [17]. Surface energies of liquid's have been utilised in previous studies for multiple applications including the creation of virtual walls [28] and pumping mechanisms [29-30] within microfluidic networks.

1.1.2   Fluid transport in microfluidic channels

Although the specific characteristics of fluid flow in microfluidic systems are important considerations, also of equal importance when considering microfluidic design is the mechanism by which fluid transport is achieved. Fluid transport in microfluidic systems is commonly accomplished using either pressure driven flow or electroosmotic flow (EOF). The type of transport employed is dependent on the intended use of the device with both flow systems having features that make them unique from the other.

Pressure driven flow is most commonly produced 'off microchip' utilising positive displacement pumps, such as syringes or piston pumps. This type of fluid transport is applicable to a wide range of aqueous or non aqueous solvents. In addition the system is also compatible with microchannels made from a wide range of materials. However, pressure driven flow is largely reliant on both the fluid viscosity and microchannel geometry, resulting in predominantly laminar flow in such systems [31]. Although this type of fluid transport is easy to achieve, the characteristic flow profile of the fluid within the microchannel is parabolic as shown in Figure 3 [6]. For many applications a parabolic profile is not an issue, however is undesirable in systems requiring high resolution for quantitative analysis due to its detrimental effects on peak broadening [6]. Further, pressure driven systems also have high associated back pressures, which are unfavourable for many applications.

Profile for pressure driven flow
(parabolic)

Profile for electro osmotic flow
(EOF) (flat)
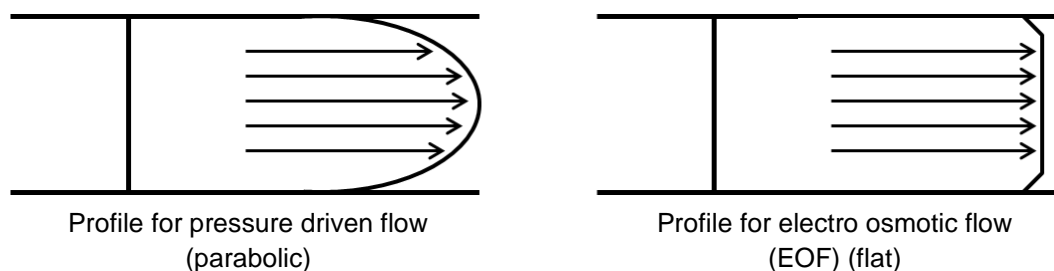
Figure 3   **Schematic of pressure driven and electroosmotic flow profiles**

Electroosmotic flow (EOF) is an alternative fluid transport mechanism based on the movement of molecules in an applied electric field. The movement of molecules is a result of their charges and typically arises in microfluidic systems due to the formation of an electric double layer of counter ions at negatively charged channel walls. On applying an electric field the positive counter ions accumulated adjacent to the channel walls migrate towards the negative electrode resulting in the bulk flow of solution [31]. The principles of EOF are discussed in more detail in Section 1.2.1. The characteristic result of this flow is a flat fluid profile (Figure 3). Therefore EOF driven devices are considerably better suited for quantitative analysis systems requiring high resolution as band broadening effects are significantly reduced. Further, EOF is easily controlled, does not contain the back pressure issues associated with pressure driven flow and is pulse free [6, 31]. However, EOF does have limited solvent compatibility, requires an off chip power supply and requires frequent changes in voltage settings. Additionally, solvent evaporation is an issue due to high voltages being applied to small amounts of liquid in solvent reservoirs [6]. Although EOF is the fluid transport mechanism of choice for quantitative analysis, careful selection of the correct mechanism for the desired application is critical when designing microfluidic devices.

1.1.3 Microchip fabrication methods

A wide variety of fabrication techniques for microfluidic devices have been developed over the years. These include; micromachining [32], micromoulding [33-34], embossing [35], lithography [36] and more recently 3D printing [37]. Each of these techniques has associated advantages and disadvantages depending on the required application for the end microfluidic device.

1.1.3.1 Micromachining

Microfluidic devices constructed using micromachining typically use silicon or glass substrates. The technique is a two-step process which first requires the physical etching of microchannels into the substrate followed by a wafer bonding process, such as anodic bonding or fusion bonding, to attach a top surface and create a sealed system [32]. Micromachining offers a high degree of precision, allowing for the manufacture of highly

complex channel networks or components within microfluidic systems to be achieved [38]. Despite the high degree of intricacy capable in silicon micromachined devices, they are restricted by their optical opacity, high cost, surface characteristics not suited to biological applications and requirement of highly specialised skills, equipment and facilities [17]. In addition, numerous microfluidic systems do not require the level of precision offered by micromachining. The technique is, however, suited to certain chemistry applications, in particular, chip based capillary electrophoresis, due mainly to the favourable surface properties of glass [17].

1.1.3.2 Micromoulding

The large scale production and usage of microfluidic devices within many fields is focused on developing disposable devices that can be manufactured at low costs and in high quantities. Due to the inherently high manufacture costs of glass and silicon based devices, research into alternatives has significanltly increased. On the other hand, polymers have been found to posses several advantageous characteristics for large scale production one of which is significantly reduced costs when compared to silicon and glass based devices [39]. Elders *et al.* reported a comparison between polymers and glass for manufacturing microfluidic devices which is summarised in Table 1 [40].

Micromoulding is a well researched technique for creating polymer based microfluidic devices. It involves the transfer of microstructured metallic moulds with micron precision to moulded polymeric products [39]. A number of micromoulding techniques are reported in the literature, with two of the most common being micro-injection moulding [41] and hot embossing [42]. Both techniques use polymers to create low cost, flexible and disposable microfluidic devices with the potential for large scale production.

Micro-injection moulding is a multi-step fabrication process where initially granulated thermoplastic materials are placed in a heated barrel to produce molten and/or soft products. The molten material is then pressure driven into a mould cavity where it is subsequently subjected to a holding pressure for a specified time. This allows for the compensation of material shrinkage. The material is then solidified by decreasing the temperature of the mould below the glass transition temperature of the specific polymer used. After sufficient time the material freezes into the mould shape and is ejected with the desired patterned surface. This process can therefore be repeated many times as desired offering the potential for automation [39].

Table 1   **Comparison of glass and polymer properties for microfluidic applications**

Table adapted from Elders et al. [40]

Comparative measure	Polymers	Glass
Properties	Large range of polymers with a wide selection of mechanical, optical, chemical and biological properties available	Considerably less variability in available properties compared to polymers
Manufacturing costs	Low, relative to glass	High overall costs that increase with increasing substrate area
Fabrication complexity	Simple and does not require wet chemistry. Clean rooms only required for certain applications	Time and cost intensive and requires wet chemistry. Clean rooms always required
Operation temperature	Limited by the glass transition temperature of individual polymers	Wide range of operational temperatures
Optical properties	Optical transparency good but lower than glass. Polymers tend to have higher background fluorescence signals	Excellent optical properties with very low background fluorescence signals
Bonding	Different options include using adhesives, thermal fusion, ultrasonic welding, covalent bonding and mechanical clamping	More time consuming than polymers, options include thermal, adhesive and anodic
Surface treatment	Methods available for surface modifications, but well established techniques are not widely available	Well established chemical modification procedures available.
Solvent compatibility	Generally not compatible with most organic solvents and in certain cases strong acids or bases	Compatible with organic solvents and strong acids and bases
Joule heating and gas permeability	Joule heating significant due to low thermal conductivity / higher gas permeability compared to glass	More resistant to joule heating however has a relatively low gas permeability
Electro-osmotic flow (EOF)	Smaller EOF than glass, due to lack of ionisable functional groups. Surface modification required	Higher EOF than polymers, surfaces easily modified.
Geometrical flexibility	Highly flexible geometric designs available	Limited geometrical flexibility due to isotropic nature of etching processes

Hot embossing is an alternative technique that also involves micromoulding. It is also a multi-step process requiring specialised equipment [42]. The process initially involves the fabrication of an embossing master, commonly achieved using photolithography whereby the patterned photoresist can be electroplated resulting in a nickel embossing tool [42]. Alternative techniques used to create embossing masters include the Dry Etching, Electroplating and Moulding (DEEMO) process [40], using silicon directly as an embossing master [43], advanced silicon etch processes [44] and the combination of laser micromaching and microwelding [45]. Once an embossing master has been obtained, it is placed in an embossing machine. A schematic of a typical embossing machine published by Becker and Heim is shown in Figure 4 [42]. Firstly, the embossing master and polymer substrate are heated separately, in a vacuum chamber, to a temperature just above the glass transition temperature of the polymer material. The embossing master is then brought into contact with the substrate and embossed with a controlled force. Whilst the embossing force remains applied the mould and substrate sandwich is then cooled to just below the glass transition temperature in order to stabilise the microstructure. To minimise thermally induced stresses in the polymer substrate, the thermal cycle is made as small as possible dependent on the polymer. After the lower cycle temperature has been reached the embossing master is mechanically forced apart from the substrate, which contains the required features and is ready for further processing [43].
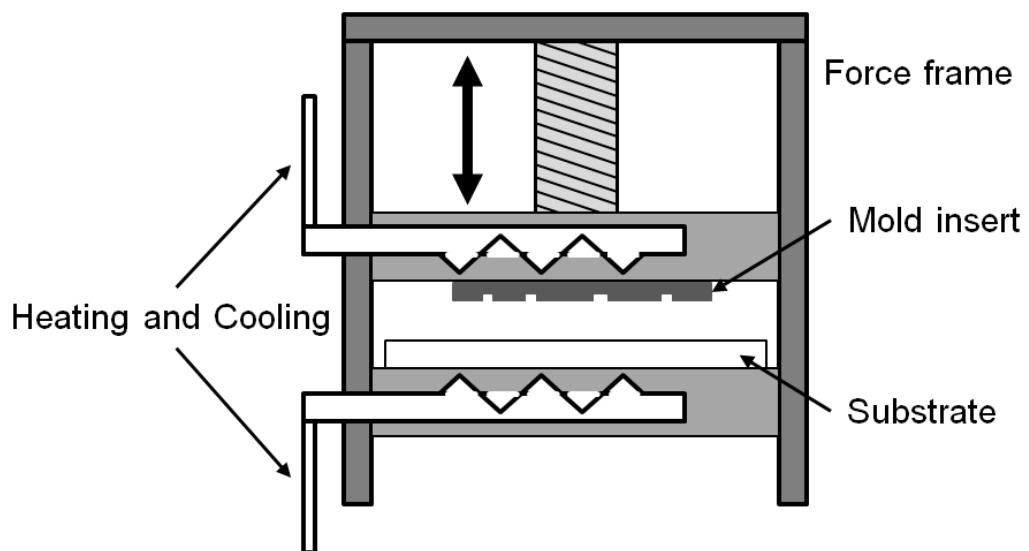
Figure 4   **Schematic of a typical hot embossing setup**

Micro-injection moulding and hot embossing have a number of advantages over traditional micromachined structures. These advantages include the wide range of available polymer substrates, potential automation of both processes, cost-effective production of potentially disposable devices, accurate shape replication, good dimension control and low maintenance costs of capital equipment [39, 42]. Both methods have

mainly been utilised for the fabrication of microfluidic devices related to medical and biological applications [45-47].

1.1.3.3 Lithography

The most commonly utilised fabrication technique for biological microfluidic systems is that of soft lithography. This is attributed not only to its convenient, effective and low-cost method but also to the wide variety of surface chemistries that can be applied to the most commonly employed polymer substrate poly(dimethylsiloxane) (PDMS) [48]. Therefore, since its discovery as a suitable technique, soft lithography has become the mainstream technique for microfluidic fabrication in many research laboratories.

There are multiple lithographic techniques designed for a number of different substrates and applications. However, the most common, and most applicable to the scope of the current project, is that of photolithography using transparency-based photomasks [4-5]. This process involves the production of a transparency photomask, fabrication of a photoresist template and finally transference of the template design to a flexible polymer. Initially, a transparent photomask containing the required microfluidic channel design is constructed using a computer aided design (CAD) program and high resolution printing technologies. Subsequently, fabrication of a photoresist template is achieved by first spin coating a thin layer of photosensitive polymer (photoresist) onto a substrate, commonly a silicon wafer. The thickness of this layer is dependent on the device being fabricated and corresponds to the required channel depth. After the photoresist layer has set the transparency mask is placed in contact with the photoresist coated substrate so that the mask is in good contact. The photoresist is then subsequently exposed using a UV light source, where the exposed areas either become more or less soluble in a developing solution, depending on the type of photoresist utilised [36, 49]. Finally the coated wafer is placed in development solution which washes away excess photoresist producing a template of the microfluidic channel network. An example of template production using photolithography is shown schematically in Figure 5.

1. Photoresist application and soft bake

Photoresist

Rotating sample chuck within spincoater

Soft bake on hotplate

2. Exposure

UV exposure through mask

3. Post exposure bake

Two step baking process on hotplate

4. Development

Beaker

Developer Solution
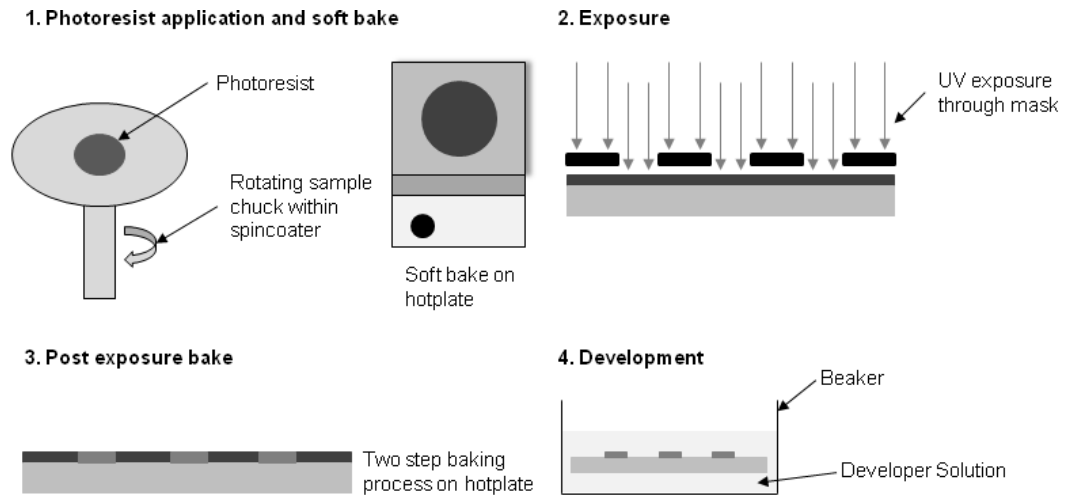
Figure 5   Photolithography template production using a negative photoresist

The photoresist template is then used to create the desired microfluidic channels in a polymer substrate. Poly(dimethylsiloxane) (PDMS) is the most commonly used polymer due to its flexibility, low cost, electro-osmotic flow compatibility and the ability to manipulate its surface chemistry [50]. The process of producing microchannels in PDMS is simple, and requires only for liquid PDMS to be poured over the photoresist template and cured, at a specified temperature. Once the polymer has cured the solid but flexible PDMS can simply be peeled away from the template (Figure 6). To complete the microfluidic device, the PDMS containing microchannels is then sealed using either another piece of solid PDMS or a glass slide. Sealing of the microfluidic device can either be reversible, by simply placing the two components together or irreversible by first oxidising the microchannel containing PDMS and flat PDMS or glass cover slide and then placing them together [36]. The latter produces reactive hydroxyl groups on the PDMS surface which form strong covalent bonds when brought into contact facilitating the irreversible sealing of the microchip.
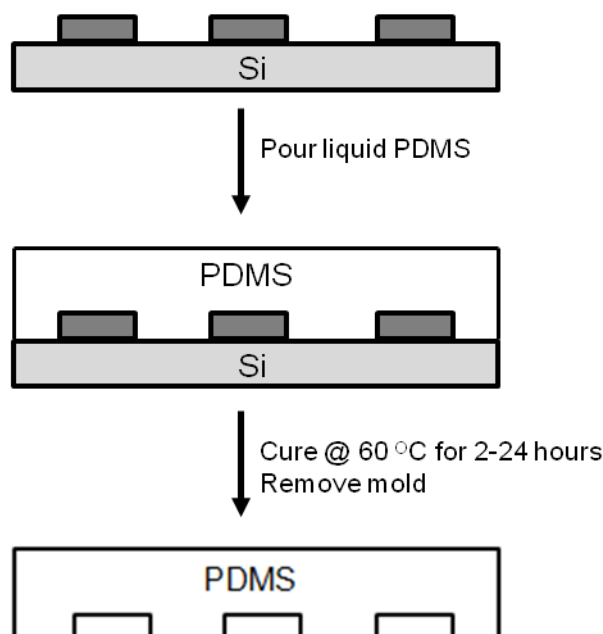
Figure 6   **Transferring template microchannels to PDMS**

As discussed previously PDMS is one of the most commonly used polymers for the fabrication of microfluidic devices in photolithography. This is due to its favourable optical and chemical properties that lend themselves to a wide range of applications [51]. Not only can PDMS devices be quickly and simply fabricated from its prepolymer, they also offer good optical transmittance, allowing for the incorporation of optical detection, have good electrical resistivity, supporting EOF necessary for electrophoresis, are biocompatible and their surface chemistry can be manipulated to allow for a wide range of potential applications [4-5, 52-53]. Therefore, a significant amount of current microfluidic research is based around PDMS devices and their potential applications, much of which focuses around the surface chemistry of PDMS [54-57] and microfluidic systems fabricated using PDMS [58-63]. Given the amount of research surrounding PDMS based devices there is a great deal of potential for this technology to offer a suitable platform for microfluidic devices with wide ranging applications.

1.1.3.4 3D Printing

As technologies advance, new and innovative ways are continually sought to more cheaply and simply produce microfluidic devices. 3D printing is a method that has the potential to achieve one-step microchip fabrication with such advantages. Despite the commercial availability of 3D printers since 1988 [64], a number of limitations have restricted their implementation for microfluidic device production until recently. These limitations have included the incapability of the technologies' resolution to produce usable microchips, incompatible resin substrates that do not have suitable mechanical, optical, electrical or chemical properties and the cost of printers with the required resolution to

produce less than 100 μm in all dimensions (approx. $20,000) [65].

3D fabrication can be achieved using either additive or subtractive methods where substrate is either added using techniques such as fused deposition modelling [66] and photofabrication [67] or removed using techniques such as femtosecond laser direct writing [65, 68]. Of these, additive methods have shown the most promise for microfluidic applications [67, 69]. More specifically, additive manufacturing is where substrate is deposited as layers to build up the device under construction. There are a number of available printing substrates including metal particles and plastics [70]. The most common substrates used are thermoplastics and photopolymers [71]. Thermoplastic 3D printers heat a thermoplastic substrate until it can be extruded from the printing nozzle whereas photopolymer 3D printers extrude a liquid photopolymer that is then cured by a light source. A three axis positioning system is used to position the device relative to the printing nozzle while the substrate is extruded in layers onto the printing surface [71].

In terms of 3D printing for fabrication of microfluidic devices relatively few systems have been reported to date. 3D printing has been demonstrated for the production of reactionware devices [72], modular microfluidic components for application to cancer diagnosis [73], analytical devices with electrochemical detection for bioanalytical investigations [74] and influenza antigens [75]. Promisingly, cost effective production of microchips for analytical applications have recently been reported using commercially available and affordable 3D printers [65, 76]. These reports provide great promise for the future of 3D printed microchips however; there exists a need for improved hardware and resin chemistry before its full potential can be harnessed for microfluidic electrophoresis [65]. Therefore, the use of 3D printing technology remains in its infancy and the reliability and robustness of such devices still requires thorough investigation. Whilst the technique offers great potential for the future fabrication of simple and cheap microfluidic devices in short time frames there is much research to be done before it reaches the same status as the more proven fabrication methods previously discussed.

1.2   Microfluidic devices for electrophoresis

The use of capillary electrophoresis (CE) as a mainstream technology during the 1990's brought with it the potential for greatly reduced analysis times and increased automation [10]. In comparison to its predecessor, gel slab electrophoresis, it offered a new level of analysis capabilities for advanced analytical applications. CE has been a powerful analytical technique over the last 25 years due largely to its ability to successfully analyse a wide range of charged analytes. It is particularly well employed in forensic laboratories for the analysis of negatively charged DNA. Despite this, there exists a desire to develop technologies that have the same analytical power but are cheaper, offer increased throughput capabilities and are portable. These have been the driving forces for research into developing portable microchip electrophoresis technologies.

1.2.1   Fundamentals of capillary electrophoresis

Separation in CE results from differences in analyte velocity under application of a high voltage across a microcapillary (typically 25 – 75 µm in diameter) and is based on each ions mass and charge [77-78]. The traditional setup for CE instrumentation is relatively simple and is shown schematically in Figure 7. The instrumental elements comprise of a sample vial, source and destination vials, a microcapillary, electrodes, a high-voltage power supply, a detector and data analysis software. As microchip electrophoresis is a technological advance of traditional CE, most of the concepts explained in this section for capillaries are also applicable to microchips.
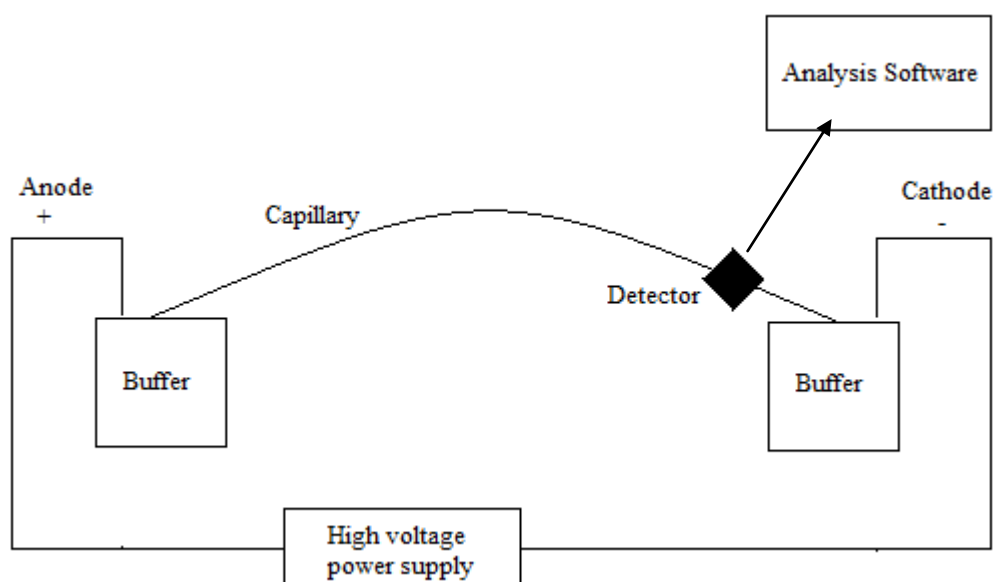
Figure 7   **Schematic of traditional CE instrumentation**

In operation the source and destination vials along with the microcapillary are filled with an aqueous electrolyte buffer solution and an electric field is applied across the capillary from the high voltage power supply. Upon application of the electric field the sample components migrate based on both their individual electrophoretic mobility and the electroosmotic flow (EOF) of the buffer solution [77, 79]. In the first instance the electrophoretic mobility (μ_{ep}) of an ion can be defined by Equation 5 when the electrical force is equal to frictional force [80].

Equation 5   Determination of electrophoretic mobility

$$\mu_{ep} = \frac{q}{6\pi\eta r}$$

In Equation 5 q is the ion charge, η is the viscosity and r is the ion radius. It is evident from this definition that an ion's mobility is proportional to its charge to size ratio (q:r). Whilst this is true, in reality it is the charge to solvated radius ratio that is important as the solvated radius governs the frictional force that in turn controls the mobility of an ion [80-81]. Further, Equation 5 indicates that the electrophoretic mobility is largest for highly charged ions and ions of smaller size. Finally, the nature of the charge (positive or negative) on an ion will influence the direction in which it moves, with neutral analytes having an electrophoretic mobility of 0. However, this is not the only phenomenon at play: the electroosmotic flow of the aqueous buffer solution under the applied electric field must also be considered.

A capillary that has fixed charges on its interior wall and is filled with a conductive solution will experience electroosmosis upon application of an electric field [80, 82]. Typically, fused silica capillary with ionisable surface silanol groups (SiOH) are used for CE. Silanol groups ionise at pH values greater than 4 resulting in a negatively charged silanoate (SiO$^-$) surface [80, 82]. This negative surface attracts positive counterions (cations) from the bulk solution in the capillary forming an electric double layer. As shown in Figure 8 this layer has two parts; a static layer closest to the capillary wall, known as the inner Helmholtz or Stern layer and a more diffuse layer known as the outer Helmholtz plane (OHP) [83-84]. When an electric field is applied, the cations in the diffuse layer migrate towards the cathode dragging their associated solvent molecules with them and giving rise to the electroosmotic flow (EOF). As the force driving the liquid originates at the capillary wall, the flow moves in a 'plug' fashion propelling the buffer and solvent towards the cathode with a characteristic flat fluid profile [77, 79, 84].
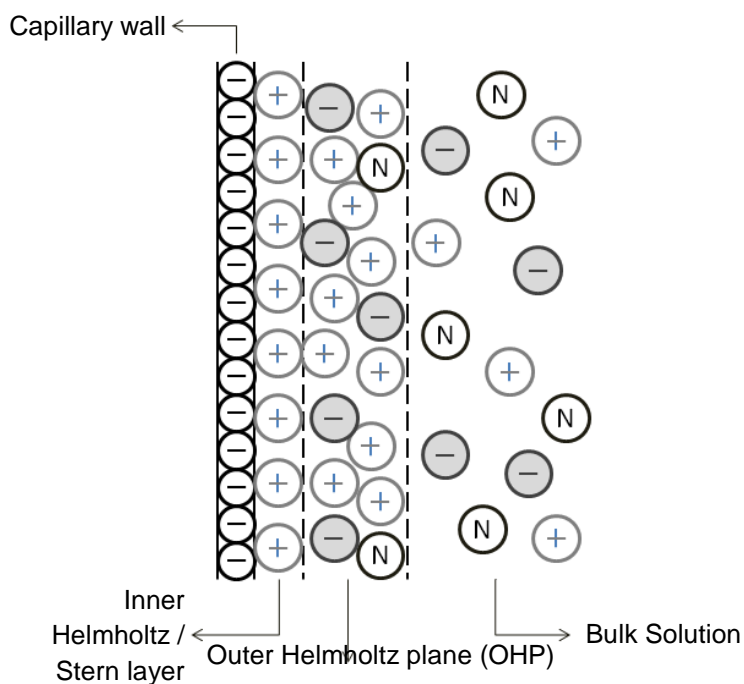
Figure 8   **Electric double layer in fused silica capillaries**

The bulk flow produced by the EOF propels all molecules; cationic, neutral or anionic towards the detector. Therefore separation is ultimately governed by differences in migration of the individual analytes and the total apparent mobility of each analyte (μ_{total}) can be calculated using Equation 6.

Equation 6   **Determination of analyte total apparent mobility**

$$\mu_{total} = \mu_{ep} + \mu_{EOF}$$

Applying this theory to fused silica capillaries, with EOF towards the cathode, it follows that analytes will migrate fastest to the detector in the order of cations followed by neutral molecules with the EOF and lastly anions [80]. Cations migrate fastest in the order of decreasing μ_{ep}, this is a result of their μ_{ep} being in the same direction as the EOF. Neutral analytes migrate with the EOF due to their uncharged nature and anions migrate in the order of increasing μ_{ep} as their mobility is in the opposite direction to the EOF. Any anions with a mobility greater than the EOF will not reach the detector but will instead migrate towards the capillary inlet.

Both the μ_{EOF} of buffer solutions and the μ_{total} of a given analyte can be determined experimentally from the CE electropherogram. The μ_{total} can be determined using the

migration time of the analyte and is expressed by Equation 7 [85]

Equation 7   **Experimental determination of analyte total apparent mobility**

$$\boldsymbol{\mu_{total}} = \frac{\boldsymbol{L_d L_t}}{\boldsymbol{t_m V}}$$

where L_d is the length to the detector, L_t is the total capillary length, t_m is the migration time of the analyte and V is the applied voltage. The μ_{EOF} can be determined similarly using the migration time of a neutral marker compound such as ethanol in place of the analyte migration time. Alternatively, the μ_{EOF} can be determined experimentally using two buffers of slightly differing concentrations [86]. After applying the voltage an electropherogram is collected and the migration time at which the lower concentration buffer passes the detector (point of inflection) is used in Equation 7 to calculate the μ_{EOF}.

After separation in capillary, the analytes pass through a detector, commonly UV-Visible absorbance or fluorescence, depending on the nature of the analytes. Detection systems for CE are generally incorporated onto the capillary itself resulting in high resolution electrophorograms. The most common types of detection systems for CE and microchip electrophoresis are discussed at length in Section 1.3. Given the fundamentals of CE, it is easily implemented on much smaller scales using microfluidic platforms. Whilst the theory remains similar there are distinct advantages to miniaturising this technology.

1.2.2   Microchip electrophoresis vs capillary electrophoresis

As previously mentioned, one of the main driving forces for the development of new microchip electrophoresis devices is the desire for increased portability of analytical techniques [13, 87]. Traditional CE instrumentation is bulky, laboratory based and not easily portable. To achieve CE analysis systems that can be implemented for point-of-care or on-site analysis there is a need to miniaturise the electrophoresis instrumentation to a scale that permits portability. Microchip electrophoresis has the potential to achieve this at a lower overall cost due to decreased consumption of reagents and analytes and cheaper fabrication and component costs. Table 2 further summarises the main differences between capillary and microchip electrophoresis.

Table 2   **Comparison of capillary and microchip electrophoresis properties**

Comparative measure	Capillary electrophoresis	Microchip electrophoresis
Fabrication	Well established, costly	Simpler and more time and cost effective
Reagent consumption	High	Low
Running cost	Intermediate	Lower than traditional CE
Analysis efficiency	High	Potential for greater than traditional CE, higher throughput capabilities
Portability	Not portable	Potential portability
Sample preparation	Performed separately before analysis	Potential for integration onto microfluidic platform connected to electrophoresis device

As can be observed, the benefits of miniaturising this technology are in fact not limited to increased portability alone. As early as 1994 Jacobson *et al.* [88] reported the ability for microchip electrophoresis devices to perform high speed separations with excellent efficiency. Indeed it has been demonstrated numerous times that microchip platforms have the ability to offer higher sample throughput capabilities than corresponding analyses on traditional CE instrumentation [89-91]. A further benefit of miniaturising or downscaling analytical processes is the reduction in the amount of consumables required. This is beneficial as it reduces the cost per analysis and can be further advantageous in forensic scenarios where the reduction in sample amounts required for testing are paramount [91]. Perhaps one of the biggest advantages of microchip CE over conventional CE is the potential for integration of miniaturised sample preparation devices with the electrophoresis chips to create what are commonly called micro total analysis systems (μTAS) [92]. The development of μTAS devices for applications spanning areas including environmental analysis, clinical diagnostics, forensic analysis and bioassays has been extensively reviewed over the years [93-98]. It is the combination of these favourable properties that make microchip electrophoresis devices so attractive for wide ranging applications. However, careful consideration must be given to both the substrate and design of each system before implementation.

1.2.3   Effect of microchip substrate on electrophoresis

As discussed in Section 1.1.3 microfluidic devices can be fabricated from glass or polymer substrates using a number of different methods. Glass and polymeric microchannels contain different surface properties which must be considered when developing a new device. Specifically, when implementing new electrophoresis systems it is essential to take into account the use of substrates that will support EOF. Traditional

fused silica capillaries contain surface silanol groups that are easily ionised to form a negatively charged surface capable of supporting EOF. Similarly, glass micochannels also contain surface silanol groups that can be easily ionised using sodium hydroxide solutions [86]. However, glass microchips are typically more cost and time intensive to produce than most polymeric microchips. Therefore, when disposable chips with faster fabrication times are required, polymer substrates are considered advantageous.

The most commonly reported polymer used within microfluidic platforms is PDMS. PDMS is a silicon-based rubber, which compared to other polymers has the advantages of gas permeability, optical transparency and biocompatibility [4-5]. These favourable properties have led to considerable research into PDMS based devices for biological electrophoresis applications [6, 99-100]. However, PDMS surfaces are also relatively unreactive and have poor EOF capabilities in their natural form. Consequently, PDMS surfaces must be modified before they become useful for reproducible electrophoretic separations. A significant amount of research on PDMS surface modification has focused on increasing its hydrophilicity. Both Makamba *et al.* [101] and Zhou *et al.* [55] published comprehensive reviews on the modification of PDMS surfaces for microchip electrophoresis devices. A common approach to PDMS surface modification is the plasma oxidation of its surface to form hydroxyl groups. However, PDMS readily undergoes hydrophobic recovery requiring further modification in order to produce a stable surface [55]. These modifications are usually performed via either permanent covalent attachment (traditionally employed in glass microchips) or dynamic adsorption of large molecules to the PDMS surface.

Dynamic PDMS surface modifications are the most commonly employed approach due to their inherent simplicity. A number of publications have investigated the use of various surfactants in dynamic surface coatings to produce stable EOF in PDMS microchip electrophoresis devices [102-104]. Specifically Guan *et al.* [103-104] have presented extensive studies on the effect on EOF and separation selectivity of using of ionic, non-ionic and zwitterionic surfactants in PDMS microchips. Examples of the surfactants used are shown in Figure 9.

(a)

(b)

(c)
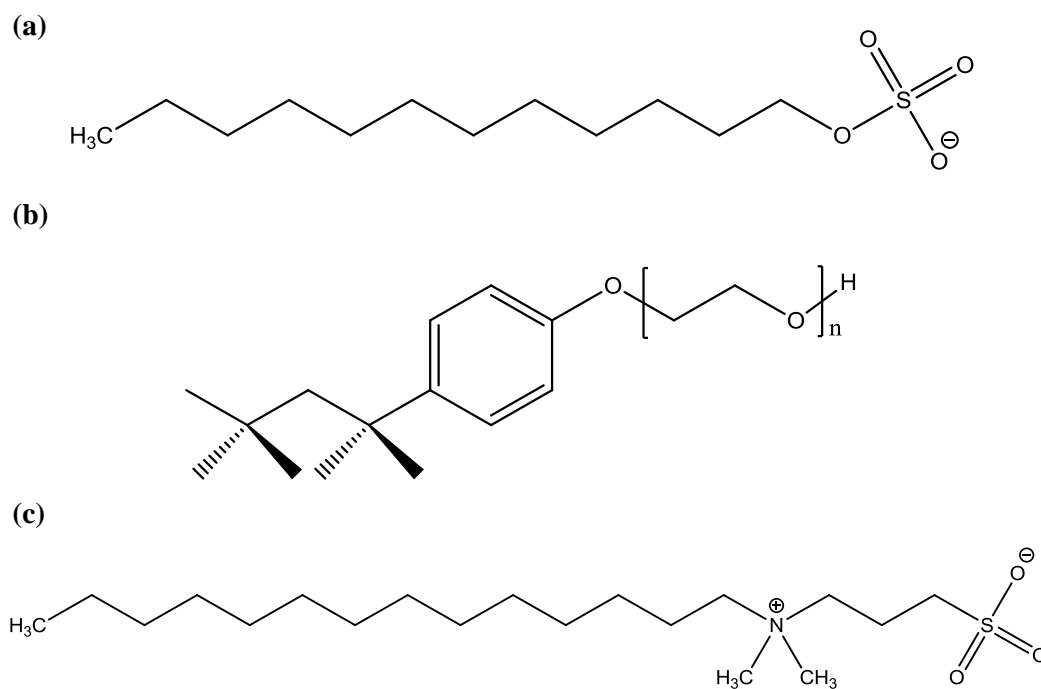
Figure 9   **Surfactants used for the dynamic surface modification of PDMS**

Including (a) sodium dodecyl sulphate (ionic), (b) Tween® 20 (non-ionic) and (c)
N-tetradecyl-N,N-dimethyl-3-ammonio-1-propane sulphonate (zwitterionic)

As a result of their work it was reported that non-ionic surfactants resulted in a decrease in the EOF as surfactant concentration was increased. Whereas the use of mixed surfactant systems produced higher EOF values and gave a wider tuneable range when compared to single non-ionic surfactants. Most importantly, they concluded that the correlation between EOF and surfactant concentration showed that EOF could be tuned over a range of values based on the surfactant ratio [104]. In another study, García *et al.* [102] investigated the use of the negatively charged surfactants sodium dodecyl sulphate, sodium deoxycholate and phosphatidic acid as BGE modifiers in PDMS microchips. They reported that all three resulted in increased EOF, enhanced detection signal using electrochemical detection and stabilisation of the run-to-run EOF. These reports indicate that EOF in PDMS microchips can be specifically tuned via the incorporation of selective surfactants to modify the microchannel surfaces which in turn also acts to increase the EOF repeatability in these devices.

1.2.4   Design of microchip electrophoresis devices

An important consideration when developing a microchip electrophoresis device is the design of the microchannel network. All practical components of a traditional CE system must be present to produce a microscale electrophoresis system with the same capability. The two most commonly reported microchannel networks for microchip electrophoresis devices are shown in Figure 10.
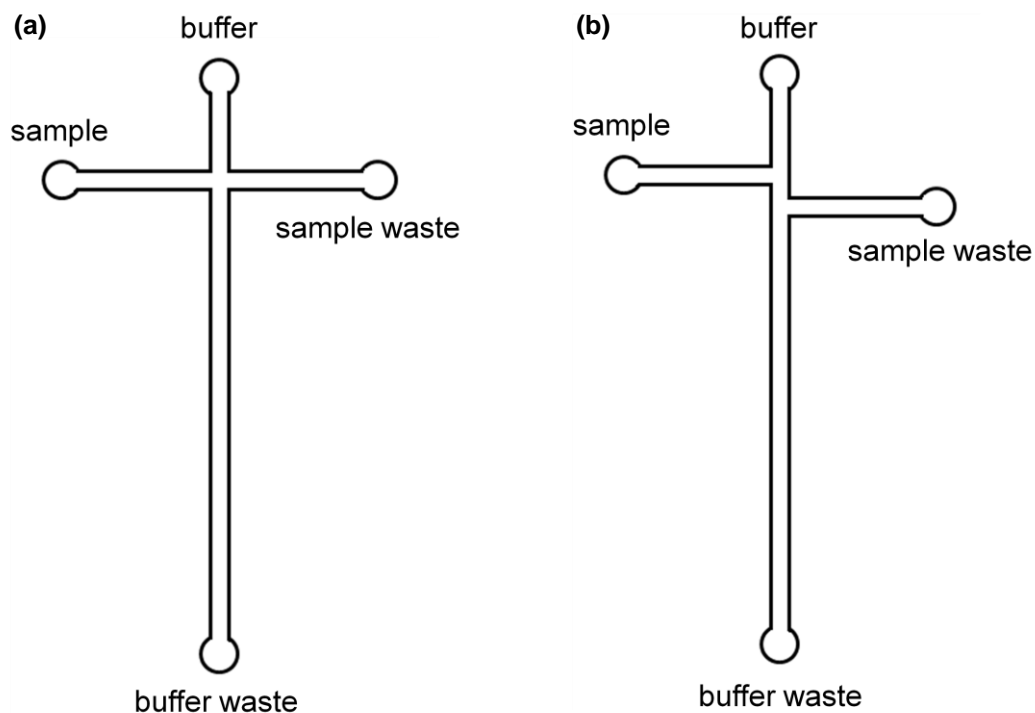
Figure 10   **Common microchannel networks for microchip electrophoresis**

Including (a) cross-channel injection and (b) double-T injection

The simplest design used for microchip electrophoresis is the cross channel injection design shown in Figure 10(a). This design allows for electrokinetic injection of the sample by first applying a voltage between the sample and sample waste reservoirs before switching the voltage to between the buffer and buffer waste reservoirs for separation. The key advantage of this design are its small injection volumes leading to smaller sample plugs which can enhance resolution in the short separation distances often employed in these devices. Alternatively, the double-T injection design shown in Figure 10(b) is often employed in microchip electrophoresis systems. It allows for electrokinetic injection in the same way as the cross channel design; however, it also results in the production of a larger sample plug. This is more commonly utilised for on-chip preconcentration using techniques such as field amplified sample injection (FASI) where larger injection plugs are advantageous [105-106]. Whilst both designs are simple to implement, consideration needs to be given as to the effective separation length of the

microchip before implementing the double-T design as the increased sample plug length can significantly reduce resolution in short separation channels. Once the microchip electrophoresis design is decided, the incorporation of effective detection systems must then be considered.

1.3 Portable detection systems for microchip electrophoresis

Despite significant research over the last decade into such devices, very few have transcended to commercial production [13, 107-108]. This is a result of a number of limiting factors in producing commercially viable LOC systems. These arise from the difficulty in producing miniaturised, cost effective detection components and the complex fabrication processes required to integrate detection systems, such as fluorescence and electrochemical techniques, with the microchip [108-110].

1.3.1 Common approaches

There are a number of potential detection systems that can be integrated with capillary/microchip electrophoresis platforms. The most commonly employed are compared in Table 3. These can either be performed on-chip or end-chip. On-chip methods involve the detection of analytes as they migrate through the separation microchannel. Typically, spectrophotometry or contactless conductivity detection are performed on-chip [80]. Alternatively, end-chip methods involve the use of the effluent of the separation microchannel, which is focussed or collected into the detector. On-chip detection is considered advantageous as it reduces peak distortion and loss of resolution that can arise using end-chip detection [80].

Table 3   **Common capillary/microchip electrophoresis detection systems**

Table adapted from [80]

Method	Detection limits (µM)	Advantages/disadvantages
UV-vis Absorption	$10 - 10^{-2}$	- Universal - Diode array offers spectral information - Difficult to employ in microchips
Laser Induced Fluorescence	$10^{-8} - 10^{-10}$	- Extremely sensitive - Usually requires sample derivatisation - Expensive
Mass Spectrometry	$10^{-2} - 10^{-3}$	- Sensitive and offers structural information - Interface to MS nontrivial
Amperometry	$10^{-4} - 10^{-5}$	- Sensitive - Selective, useful for electroactive analyses - Requires special electronics and integrated detection electrodes
Conductivity	$10^{-1} - 10^{-2}$	- Universal - Simple when implemented in contactless mode

1.3.1.1 Spectrophotometric methods

Spectrophotometric detection utilises a light source and monitors the change in light induced by the target analytes as they migrate through the detector. UV-vis absorption and laser induced fluorescence are the two most commonly reported spectrophotometric methods. UV-vis absorption is widely used for capillary electrophoresis [111]; however it is not routinely used in microchip electrophoresis devices. This is due to its incompatibility with many microchip materials and the difficulty in obtaining long pathlengths in microscale channels [110, 112].

The most commonly employed spectrophotometric technique for microchips is laser induced fluorescence (LIF). LIF's popularity is largely due to its high sensitivity and large range of potential analytes [110]. It typically involves the excitation of the target species with a laser of wavelength corresponding to the excitation maximum of the species. Within microseconds of excitation the species will de-excite with the corresponding emission of light of a longer wavelength than the excitation source. This light is known as fluorescence and is commonly measured using photomultiplier tubes (PMTs) or photodiode arrays. Despite a large range of potential analytes, most do not fluoresce well in their native state and must first be derivatised with fluorescent reagents to improve sensitivity [113]. This process can be time consuming and therefore imposes restrictions on the efficiency of such analyses.

Integration of LIF detection systems with microchips has been the subject of a number of review articles [113-114]. Initial investigations centred around the use of traditional LIF setups coupled with microchips [115]. However, despite its excellent sensitivity these detection systems were not portable, due to the size of their components and power requirements. One of the first truly portable microchip fluorescence detection systems was published in 2001 by Chabinyc *et al.* [116]. Their system employed a light emitting diode (LED) connected to an optical fibre imbedded into the PDMS microchip to supply the light source. This was coupled with a prototype microavalanche photodiode to detect the emitted light. This system reported good sensitivity and contained readily available and inexpensive components [116]. However, the main disadvantage of the system was the complexity of reproducibly incorporating optical fibres into PDMS moulds. More recently, the continued use of LEDs in place of conventional lasers has been explored. In 2011 Ryu *et al.* developed system using LEDs as an excitation source coupled with a combination of short and long pass filters, linear and reflective polarisers and a photodiode for detection in a microfluidic flow cytometry device [117]. The device was low cost and the simplicity of the optical components utilised were considerably advantageous. In the same year both Kettlitz *et al.* [118] and Yang *et al.* [119] used LEDs combined with simple focussing pin holes and photodiodes as components for portable detection on microchip electrophoresis systems. A schematic of the system implemented

by Yang *et al.* is shown in Figure 11.
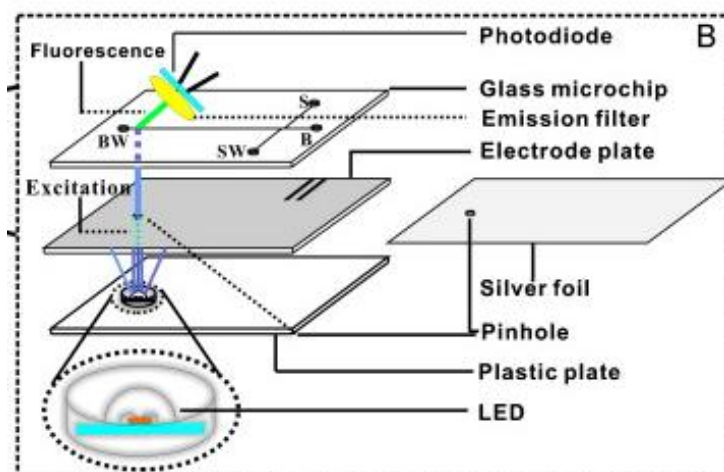
Figure 11   **Detailed configuration of an LED-IF detector**

Reported by and adapted from Yang et al. [119]

To date, this is one of the most promising developments for portable fluorescence detection in microfluidics. Their device consisted of four main elements: a fan-shaped LED, a focussing pinhole, a yellow filter and a flat photodiode. Significantly the design did not require focussing lenses, optical fibres, combined filters or a PMT [119]. The result of their simplified design was an easy to build, economic, compact and miniaturised system suitable for portable microfluidic devices. The detection system was successfully used in conjunction with a CE microchip to detect penicillamine enantiomers. These select examples of integrated microfluidic fluorescence detection systems demonstrate the advances that have been achieved in this field. However, the limitation of many analytes requiring derivatisation before analysis is still an issue with this method of detection.

1.3.1.2 Mass spectrometry

Mass spectrometric (MS) detection is the most powerful of the potential microchip detection techniques; however it is also one of the most difficult to integrate on the small scale [120-121]. It has been demonstrated as a powerful detection method when coupled with capillary electrophoresis particularly in the fields of metabolomics, peptidomics and proteomics [122-124]. The majority of recent developments in microchip-MS applications have centred on developing chips with single functional elements and/or optimising the MS interface [120, 125-128]. Conversely, there have been fewer reports of dedicated microchip electrophoresis devices coupled with MS detection.

Recent publications reporting the use of ME-MS devices are listed in Table 4. Of those that have been reported, Chambers *et al.* [129] detailed the integration of two dimensional reversed phase LC-CE with electrospray ionisation (ESI) for application to proteomics. Fritzsche *et al.* [130] coupled a microfluidic glass chip with an integrated

nanospray emitter to a fast time of flight (TOF) MS to achieve high speed separation and detection of model pharmaceuticals and peptides. Alternatively, Sikanen *et al.* [131] integrated a sheath-flow ESI interface in microchips which was coupled with an ion trap MS for the analysis of proteins. Most recently, Batz *et al.* [132] described the use of surface modified glass microchips with integrated nanoelectrospray ionisation for the analysis of peptides and proteins. Despite these promising demonstrations, of ME-MS systems, the bulky MS components seriously restrict the miniaturisation of such systems. Therefore, the advantages of reduced sample and reagent consumption are achieved but portability of these devices is no more practical than traditional lab based CE-MS or LC-MS systems.

Table 4   **Recent publications reporting integrated ME-MS devices**

Analyte	Chip Substrate	Mass Spectrometer	Reference
Peptides	Glass	Time of flight	[130]
Proteins	PDMS-Silicon	Ion trap	[131]
Drug metabolites	SU-8 photoresist	Triple quadrupole	[133]
Glycopeptides	Glass	Time of flight	[134]
Therapeutic drugs	Glass-PDMS	MS-MS	[135]
Peptides and proteins	Glass	Time of flight	[132]
Proteins	Glass	Time of flight	[129]

1.3.1.3 Electrochemical methods

Electrochemical detection utilising potentiometry, amperometry and conductometry has been extensively reported with both capillary and microchip technologies [136-137]. The instrumental simplicity of microchip electrophoresis matches well with these techniques. Potentiometry involves the measurement of voltage between a measuring and reference electrode. Whilst fundamentally simple, it is the least favourable electrochemical method due to the lack of availability of highly selective potentiometric electrodes [136]. Although it has been used with traditional CE [138-140], to our knowledge its application to microchip electrophoresis has not been reported.

Amperometric detection is more common than potentiometric detection and has been the subject of multiple reviews in recent years [141-142]. It involves the oxidation or reduction of analytes by applying a suitable potential at a working electrode. The resulting current is detected as the signal of interest. Due to this the method is very sensitive and selective; however it can only be used for the detection of electroactive species.

Traditionally, amperometric detection has been an end chip detection method, as the working electrode is placed in the waste reservoir, with analytes detected after being electrophoretically separated. This has been considered disadvantageous as mentioned previously and recent literature has outlined methods to integrate the method on-chip [143-144]. In addition, amperometric detection has been demonstrated for a variety of applications including neurochemical studies [145-146], biochemical studies [147] and environmental and food analysis [148-149]. Despite these advances and its broad application base amperometry is still limited by its requirement for analytes to be electroactive and often requires specialised electronics. It is for these reasons that research into conductometric detection methods has received significant attention.

Conductometry detection methods are of increasing interest due to their simplicity and relative ease of integration with microfluidic platforms compared to alternate methods [136]. Conductometric detection continuously monitors the conductivity during electrophoresis and records the change observed as charged analytes pass through the detection cell [150]. This setup requires the application of an alternating current (AC) at one electrode which is passed into the capillary/microchannel as an ionic current and picked up further downfield by a receiving electrode. A more in depth discussion on the setup of conductivity detection is provided in Section 1.3.2.

Conductivity detection can be performed in either contact or contactless mode. The former, known as contacted conductivity detection (CCD), is considered less advantageous. This is due to interferences that arise when integrating CCD with the high voltage electric field used for electrophoretic separation and issues with electrode fouling [141]. The preferred approach is known as capacitively coupled contactless conductivity detection (C^4D). In C^4D the detection electrodes are not in contact with the BGE avoiding the problems surrounding CCD. In addition, C^4D integration with portable microchip technologies is widely considered as the simplest of the detection methods presented [151-154] with a number of reviews assessing the advances in this area over the years [108, 155-157]. Therefore, C^4D is considered the detection method of choice for developing portable microchip electrophoresis devices for wide ranging applications to charged analytes. A thorough discussion of the literature surrounding C^4D integration with microchips is presented in Section 1.3.2.

1.3.2 Capacitively coupled contactless conductivity detection (C^4D)

1.3.2.1 Fundamentals of C^4D

Capacitively coupled contactless conductivity detection (C^4D) and its integration with microchip technologies has been the subject of multiple reviews [108, 156, 158]. The detection technique utilises integrated conductive electrodes, most commonly in the form

of metal, to continuously monitor the conductivity of a solution moving through a microchannel. More specifically, it works by utilising a transmitter electrode to subject a sample region to a large amplitude, high frequency AC electromagnetic signal. Another electrode termed the receiver electrode is placed downstream to register the corresponding attenuated AC signal as shown in Figure 12. This is possible as the electrodes form capacitors with the electrolyte solution which are transparent for AC signals [158]. The capacitances using contactless electrodes are much lower than traditional double-layer capacitances of non-isolated electrodes due to the insulating layer. Therefore, higher frequencies are a requirement using C^4D. As analytes pass into the detection region they cause small changes to the overall sample conductivity, therefore continuous monitoring of this signal produces a series of peaks, relative to the separated analytes and their concentration. An important consideration when integrating this method with microchips is the direct coupling between the two electrodes. This is otherwise referred to as stray capacitance, and can have a detrimental effect on the performance of the whole detection system if not accounted for [150].
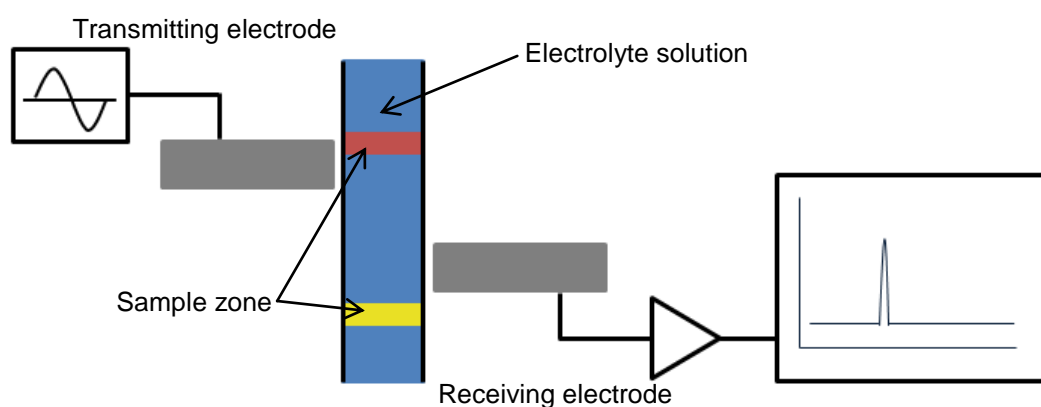
Figure 12   **Basic setup for C^4D detection in microfluidic devices**

C^4D has been used in electrophoretic separation systems for the detection of small inorganic ions as well as organic and biochemical species [158-160]. One of the most attractive features of this method is that the electrodes are electrically isolated from the electrolyte solution making it particularly applicable to microfluidic platforms. Interest in C^4D has grown significantly since 2004 as evidenced by the increase in publications referring directly to the topic seen in Figure 13. The bulk of research into C^4D detection on microfluidic chips has surrounded both electrode fabrication and integration techniques. These factors are critical in developing cost and labour efficient systems that are commercially viable. In addition to this, consistent electrode placement is a critical factor, especially when working on the microscale, to reduce possible variation in measurements. However, obtaining both precise and consistent placement of electrodes on the microscale can be a challenging task.
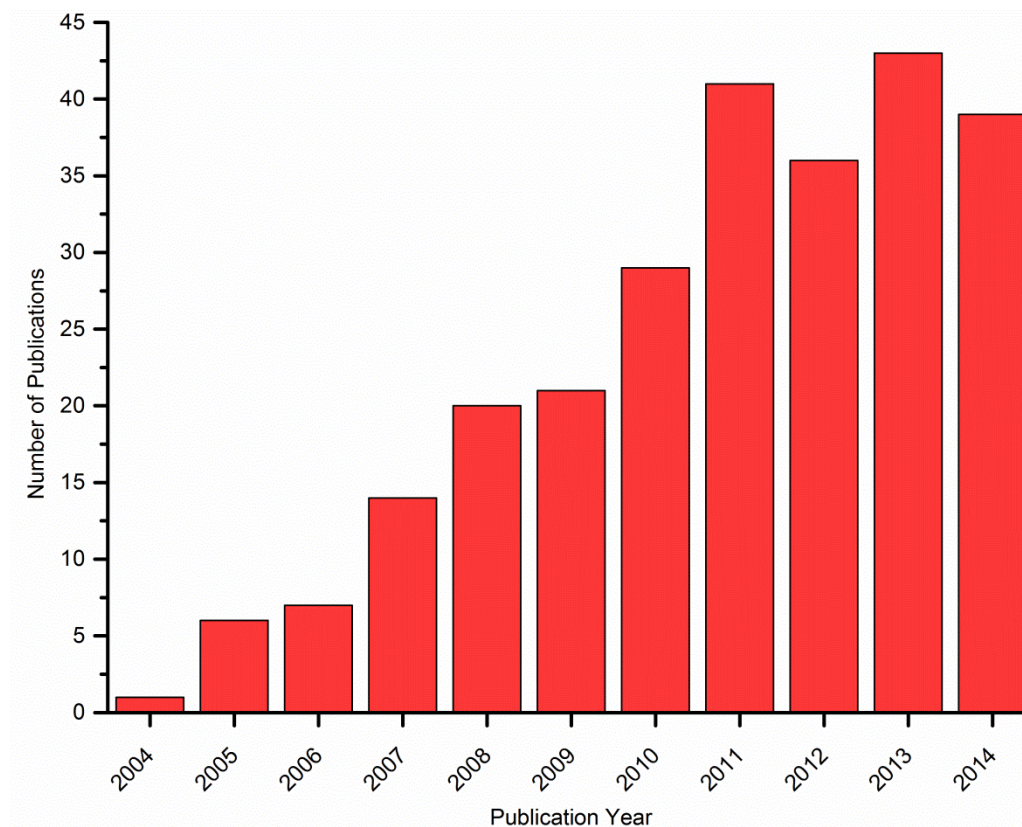
Figure 13   **Publications containing capacitively coupled contactless conductivity detection as a topic**

When searched in the Web of Science™ database between the years 2000 and 2014

1.3.2.2 Electrode fabrication and integration approaches

A number of approaches for fabricating and integrating contactless electrodes in LOC devices have been reported in the literature. These include the fabrication of microfluidic chips on top of printed circuit boards [151, 153, 161] and glass wafers [162-165] containing microscale electrodes. Alternatively, metal electrodes have been directly integrated into the polymer microchip during moulding [166], mounted in external housings [167-169] and deposited onto previously etched glass wafer surfaces to form electrodes in the same plane as the analysis channels [170-171].

The fabrication of microfluidic chips on top of printed circuit boards is found in the literature a number of times. This approach was first reported by Vazquez *et al.* [161] who implemented both amperometric and conductivity detection onto the same PDMS/glass hybrid microchip. C^4D electrodes were fabricated on PCB material by first copying the electrode design using a toner mask followed by etching away unwanted material resulting in microscale copper electrodes. The microchip was positioned on top of the PCB to allow detection. This method produced slightly lower sensitivity than previously reported methods attributed to the relatively large thickness of the glass

insulating layer. This was followed by further reports of copper PCB electrodes that utilised a much thinner insulating layer made up of dry film photoresist [151] or poly(ethylene terephthalate) [153] to form hybrid devices with microfluific channels cast in PDMS. These devices reported detection limits ranging from 6 μM to 30 μM for small inorganic cation model analytes with both reporting the thickness of the insulating layer as a limiting factor to higher LODs.

An alternative to integrating microscale electrodes on PCBs is the use of glass wafers with patterned electrodes. Shang *et al.* [162] formed microscale electrodes for C^4D by depositing chrome film on a glass wafer. A thin oxide insulating layer was employed and a microchannel fabricated on top using a sacrificial photoresist approach. The reported detection limits for sodium and calcium ions were both below 1 μM for this device. A further approach by Segato *et al.* [164] sputtered gold electrodes onto glass wafers that were incorporated for detection in PDMS microfluidic devices using a thin PDMS insulating layer spin coated on top of the wafer containing the microscale electrodes. However, the reported detection limits for small cations were quite high and ranged from 25 to 50 μM [164]. Liu *et al.* [163] also used this method to produce a PDMS microchip but coupled their device with a multiplier based readout system instead of the commonly reported rectifier circuits. Detection limits as low as 1.7 μM were achieved for the model analyte potassium using this approach. However, it was reported this was a direct result of the noise suppression associated with the multiplier circuit and not the electrode design [163]. Most recently, Coltro *et al.* [165] used sputtered electrodes on glass wafers in order to monitor binding events in real time. A silicon dioxide insulating layer was used and this device was successfully used to monitor biotin-avidin binding demonstrating the diversity of conductivity detection.

Another common electrode integration approach involves the use of housings to mount external electrodes in contact with the outside of the microfluidic chip. Multiple publications have investigated this approach in depth using a variety of techniques. It was first reported by Tanyanyiwa *et al.* [168] in 2003, who used copper tape adhered to a PMMA holder to implement C^4D detection electrodes. The housing also contained an in-built vertical earth plane to minimise direct capacitive coupling. Detection limits of 1-5 μM for inorganic ions were achieved using this device [168]. More recently, two examples of dual electrode C^4D arrangements have been proposed [167, 169]. This approach utilises electrode pairs both on top and below the microfluidic channel with the electrode setups encased in a shielded metal housing. In conjunction with thin electrophoresis microchips these designs reportedly doubled the total cell capacitance enabling an enhancement effect on the signal coupling into and from the detection volume [167]. This resulted in a significant improvement in analytical performance in terms of lower LODs ranging from 0.3 μM to 5 μM for small cationic species.

In addition to the above mentioned electrode system designs, the integration of in-plane electrodes for C^{4}D has also been examined. In 2002 Lichtenberg *et al.* [170] demonstrated the integration of platinum electrodes in recesses in plane with a microchannel network after initial glass etching. They claimed this design allowed precise electrode positioning and potential batch fabrication [170]. Despite this, a detection limit an order of magnitude higher (18 μM) than comparable capillary based systems was achieved for potassium ions [170]. Lee *et al.* reported a further novel in-plane electrode approach which involved the use of gold sputtering with a "lift-off" process to produce electrodes in pre-fabricated glass channels [171]. Due to the etching process used these electrodes were unique in their semi-circular nature and the detection limits achieved were claimed to be better than those reported with conventional planar electrode designs.

A number of other unique electrode integration approaches have also been described in the literature. Ding and Rogers [166] developed an approach involving the embedding of metal electrodes in PDMS during the fabrication process that resulted in in-plane electrodes. Their device was used for the detection of haloacetic acids in water samples with success, however the tedious nature of this methodology limits its practicality and no data on reproducibility is presented [166]. Henderson *et al.* [172] outlined the use of novel laser-patterned polymer electrodes on PMMA substrates as an alternative to conventional metal electrodes. They reported detection limits (~30 μM) on par with similar devices employing integrated C^{4}D without sample stacking and using similar conditions [172].

Despite low limits of detection achieved using the integration approaches discussed, typically in the 10^{-6} M range [158], each of these methods have practical limitations. These arise from the multi-step patterning/fabrication processes utilised that often require specialised equipment. In addition, many contain inherent difficulty in consistently aligning detection electrodes with the analysis microchannel. Furthermore, these fabrication techniques are often time consuming, for example Henderson *et al.* reported that their laser-patterned polymer electrodes required a 20 h timeframe to complete [172]. The overall result of these limitations are lengthy fabrication processes that often require cost intensive equipment and consumables [169]. Perhaps most importantly the analytical performance of these devices is potentially compromised due to the limitations in fabrication reproducibility [169]. Therefore the development of a simpler approach that is more time and cost effective whilst allowing consistent electrode alignment would be advantageous.

1.3.2.3 Alternative approach - injected metal electrodes

A potential alternative approach, for the fabrication of LOC devices with integrated contactless electrodes, is to use injected molten metal to form in-plane electrodes. Injected metal electrodes have been demonstrated in microfluidic applications for the production of in-plane on-chip electromagnets [173] and on-chip microplasma patterning of PDMS microchannels [174]. More recently, injected metal has been used to produce electrodes which are in direct contact with fluid in microchannels for mixing [175] and neural stimulation [176] applications.

Injected molten metal electrodes have the advantage that both electrode and analysis microchannels are patterned in the same lithographic process, whereby the electrode design is incorporated directly onto the mask template. This allows precise micron-scale electrode designs that can be simply and easily tailored to the microfluidic device under construction. Once the device has been assembled, the molten metal is then injected into the required microchannel where it either remains molten or solidifies to form a solid electrode.

A number of metals and alloys have been reported as substrates for molten metal electrodes. Namely, relatively low melting point alloys such as molten solder (In 52 %, Sn 48 % m.p $\approx$117 $^{\circ}$C) [173], eutectic gallium indium (Ga 75 %, In 25 % by weight m.p $\approx$ 15.7 $^{\circ}$C) [175-176] and indium alloy (In 51 %, Bi 32.5 %, Sn 16.5 % by weight m.p $\approx$ 60 $^{\circ}$C) [175]. The use of pure gallium (m.p 29.8 $^{\circ}$C) as an electrode material has been shown to be preferable over low melting point alloys due to its low toxicity, relatively low melting point and ease of handling [174-176]. However, despite its confirmed simplicity, the use of injected metal electrodes for C^{4}D detection on LOC devices had not been reported prior to its development and publication as a result of this thesis [177-178]. This was followed shortly after by an additional publication of a report on this topic by Gaudry *et al.* [179].

1.4   Application – determination of histamine

1.4.1   Background: food poisoning causative agent

Histamine is a primary amine formed by the decarboxylation of the amino acid L-histidine [180] and belongs to a group of compounds known as biogenic amines (BAs) (Figure 14). BAs are synthesised by microbial, vegetable or animal metabolisms and are known to be the causative agents in a number of food poisoning cases; which is due to their ability to initiate a variety of pharmacological reactions [180-181]. As a result, high levels of BAs during food intake are unable to be metabolised by the body, to sufficiently eliminate the toxins, leading to conditions ranging from migraines to hypertension [182-183].
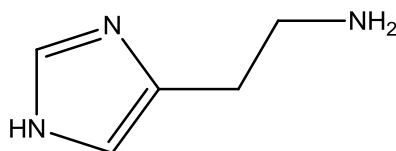
Figure 14   **Structure of the biogenic amine histamine**

BAs can be present in certain foods, such as some fruit and vegetables (e.g. spinach and bananas) with concentrations dependant on maturity [184]; however they are normally formed as a result of uncontrolled microbial action [184], resulting in elevated levels in food and beverage products after degradation. This is usually as a result of poor quality raw materials, contamination or unsuitable conditions during food processing and storage [184]. Typically, elevated levels of BAs above safe limits can be found in fish and fish products, dairy products, meat and meat products as well as fermented products such as vegetable, soy and alcoholic beverages [181-182]. The maximum limits are BA dependant with important BAs present in food and beverages including histamine, β-phenylethylamine, tyramine, tryptamine, putrescine, cadaverine, spermine and spermidine [182, 185].

In particular, histamine has been reported as the toxin responsible for scombroid fish poisoning [186-188] a type of food poisoning arising from the incorrect handling and storage of scombroid fish products [189]. The current maximum limit for histamine in fish and fish products ranges from 50 ppm (mg.kg^{-1}) in the United States [190] up to 200 ppm in Australia and New Zealand [191]. Elevated levels of histamine have also been reported in fermented wines [185, 192]. Therefore, simple portable quantitative methods for the determination of histamine levels in food and beverage products are of increasing interest to allow monitoring of food spoilage and quality during processing and storage.

1.4.2 Quantification methods

Numerous quantification methods for biogenic amines, including histamine, have been developed and are the subject of multiple reviews [193-195]. The most common approaches to BA detection have been coupling fluorescence or UV based detection with analytical separation methods such as high performance liquid chromatography (HPLC) [196-198] and capillary electrophoresis (CE) [199-201]. The lack of chromaphore in histamine is the major drawback of these methods which means derivatisation with other highly fluorescent or UV active compounds is required to achieve adequate sensitivity [194-195]. Often this results in time intensive, indirect analysis methods. LC methods have also been coupled with mass spectrometric (MS) detection [202-203] for the analysis of histamine but this still required histamine derivatisation. CE has also been coupled with chemiluminescence [204], amperometry [205] and conductivity [206] detection systems. Whilst providing sensitive detection, CE techniques are restricted to laboratory settings and cannot be deployed for simple in-field analysis in their traditional format.

Further analytical methods that have been reported for the determination of histamine include thin layer chromatography (TLC) [207-208], gas chromatography-mass spectrometry (GC-MS) [209-210] and biosensor/assay based techniques [211-212]. Of these methods TLC is simple and does not require complex instrumentation but is often time consuming and only semi-quantitative [194]. GC is not commonly applied for BA analysis with only one example not requiring derivatisation [209]. Biosensors are simple, portable, low cost and have inherently short analysis times; however, most only produce semi-quantitative determinations. Ideally, the timely and efficient monitoring of food quality and spoilage would be done using a simple portable technique that negates the need for derivatisation.

More recently, the use of portable analytical devices coupled with different detection techniques have been reported for the quantification of a range of BAs including histamine. Microchip electrophoresis with indirect fluorescence detection has been reported for the detection of histamine and other common BAs in fermented beverages [213-214], fish products [215] and standards [216-217]. A novel chemiluminescene detection system has also been used with microchip electrophoresis for the indirect detection of BAs including histamine in urine samples [218]. Whilst the reported systems symbolise a shift towards the desire to achieve greater portability most still contained laboratory scale detection components and required a derivatisation step. There remains a need for the development of a truly portable device with miniaturised detection components for quantitative determination of histamine.

1.5   Conclusions and project premise

In view of the limited truly miniaturised, cost-effective and portable detection platforms for microchip electrophoresis systems, there is a need to further develop sensitive miniaturised detection systems that can be simply and cheaply fabricated. In particular, one of the detection approaches most commonly utilised to achieve this is capacitively coupled contactless conductivity detection (C^4D). However, the fabrication approaches employed to produce these devices involve numerous steps, require costly instrumentation and posses inherent difficulties in maintaining consistent electrode placement. The development of a microchip electrophoresis device with C^4D capability that can be quickly and cheaply built whilst providing reliable electrode alignment may lead to improved analytical performance and reduced costs. Hence, the research in this thesis is focussed on developing and optimising a novel approach for C^4D detection on polymer microchips based on liquid gallium electrodes injected into prefabricated guide channels.

Therefore the aims of this research are:

1.   To integrate injected gallium electrodes with a microchip electrophoresis device for C^4D using electrode guide channels fabricated during microchip fabrication.

2.   Optimise the electrophoresis conditions for the analysis of a model analytical system.

3.   Investigate and optimise C^4D electrode parameters including geometry, distance from separation channel and length to achieve sensitive detection of model analytes.

4.   Demonstrate the ability of the novel electrode system to perform sensitive and quantitative analysis through the application of the microchip electrophoresis device to the detection of the food poisoning causative agent histamine.

2. General Experimental: Instrumental Design and Setup

2.1   Chapter overview

The microfluidic channel network design, electrode integration approach and electronic setup are integral to the successful implementation of a microchip-C^4D system. Careful consideration must first be given to the electrophoresis microchannel design for the desired application. Subsequently, considerable thought must also be given to the integration of the C^4D electrodes and the electronic setup associated with this. In the presented work the C^4D electrodes are incorporated onto the microfluidic chip using specially designed guide channels to allow for the injection of molten gallium electrodes and so must be considered as part of the microchannel design process. Additionally, it is of utmost importance to design and implement an electronic setup that is robust due to the many potential interferences associated with this detection method.

In this chapter the general chemicals and consumables used throughout this work are outlined and the microchip design for both electrophoresis and C^4D electrodes is both outlined and discussed. Moreover, the integration of the injected gallium electrodes is explained along with the incorporation of the detection electronics and how the components are housed to produce a stable and robust separation and detection platform for further optimisation and investigations.

2.2   General experimental

2.2.1   Chemicals

The chemicals used in this study are shown in Table 5, with 18.2 MΩ cm deionised water (Millipore, Australia) utilised for the preparation of aqueous solutions.

Table 5   **List of chemicals used throughout this study**

Chemical	Supplier	Grade	Concentration/Purity
Gallium metal	Sigma-Aldrich	Analytical	99.99%
2-(N-morpholino)ethanesulphonic acid	Sigma-Aldrich	Analytical	>99%
DL - histidine	Sigma-Aldrich	Analytical	>99%
n-dodecyl β-D-maltoside	Sigma-Aldrich	Analytical	>98%
Sodium dodecyl sulphate	VWR International	Analytical	>99%
Lithium chloride	Sigma-Aldrich	Analytical	>99%
Sodium chloride	Sigma-Aldrich	Analytical	>99%
Potassium chloride	Sigma-Aldrich	Analytical	>99%
2-amino-2-hydroxymethyl-propane-1,3-diol	Sigma-Aldrich	Analytical	>99%
2-(cyclohexyl amino)ethanesulphonic acid	Sigma-Aldrich	Analytical	>99%
3-(cyclohexylamino)-1-propanesulphonic acid	Sigma-Aldrich	Analytical	>98%
2-[4-(2-hydroxyethyl)piperazin-1yl] ethanesulphonic acid	Sigma-Aldrich	Analytical	>99%
Isopropanol	Chem-Supply	Analytical	99.5%
Histamine	Sigma-Aldrich	Analytical	>99%
Tyramine	Sigma-Aldrich	Analytical	>99%
2-phenylethylamine hydrochloride	Sigma-Aldrich	Analytical	>99%
Methanol	Chem-Supply	Analytical	99.8%
Ammonia solution	Merck	Analytical	28% - 30%

2.2.2 Background electrolytes and standards

Background electrolyte (BGE) solutions for electrophoretic separations were prepared by dissolving the relevant BGE components in Milli-Q water (18.2 MΩ cm). Sample stock solutions were prepared by dissolving their ionic salts in Milli-Q water (18.2 MΩ cm). Working standards were prepared by dilution of the stock solutions in BGE. All solutions were degassed by ultrasonication prior to use. The type of BGE used differed depending on the study and therefore BGE components and specific concentrations are detailed at the start of subsequent chapters discussing individual studies.

2.2.3 Analytical samples

Frozen fish samples used in this study were obtained from local supermarkets and underwent an extraction and cleanup method prior to the analysis of the analytes of interest. The extraction process comprised of four main steps, the first step involved extraction of histamine into alkalised methanol. This was followed by evaporation under nitrogen, reconstitution in water and then extract cleanup using C18 SPE (Phenomonex, Australia). Full details of the extraction and cleanup procedures are described in the text where they are applied.

2.2.4 Microfluidic chip design

In this work, two separate design elements were required to develop a microchip electrophoresis device with integrated injected conductivity electrodes. These elements were i) the electrophoresis microchannels and ii) the C^4D electrode microchannels.

The computer automated design software package Solidworks® was used to create electronic versions of all microchip designs. Initially, a standard elongated cross configuration was created for the electrophoresis microchannel design that consisted of a 57 mm separation channel and an 18 mm injection channels shown in the schematic in Figure 15. These dimensions were chosen due to the size limitation of the silicon wafers (diameter 75 mm) used for patterning the microchannel designs and the desire to keep the resulting microchips as compact as possible. Electrophoresis microchannels were fabricated with a width of 100 μm and a depth of between 40 - 45 μm. Width and depth dimensions were chosen to fit within the accepted range for fabrication using photolithography [4-6, 36]. Two commonly utilised channel configurations for microchip electrophoresis are the cross channel and the double T junction. In this study the cross channel configuration was chosen for implementation due to its design simplicity and to improve electropherogram resolution by reducing the sample plug size during electrokinetic injection.
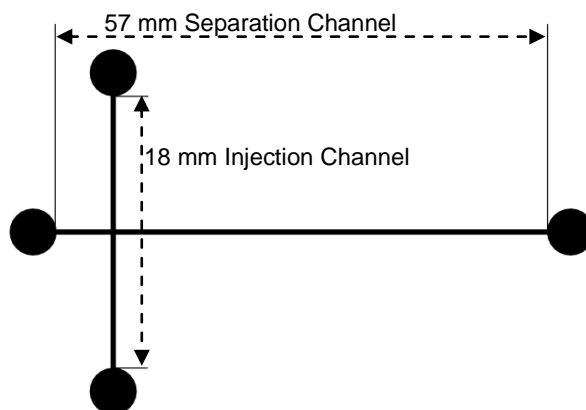
Figure 15   **Schematic diagram of electrophoresis microchannel design employed**

The second part of the microfluidic chip design phase was the integration of guide channels for the eventual injection of metal electrodes for C^4D. At the time of development the use of injected electrodes for C^4D on microchips had not been reported. Therefore, the design chosen for implementation was similar to that of Priest *et al.* [174] who used injected gallium electrodes to produce microplasmas in PDMS microchannels. The design took into consideration allowing maximum flexibility of the electrode setup whilst still containing design elements that reflected existing C^4D electrode setups external to the microchip. Designs reported in the literature contain up to four electrodes for conductivity measurements and a grounded shielding plane between transmitting and receiving electrode components. To best emulate this design integrated into a microchip the developed design consisted of four conductivity electrode guide microchannels and two shielding plate guide microchannels as shown in Figure 16. This facilitated the investigation of different detection electrode geometries namely parallel, anti-parallel and quad (4-electrode) during the optimisation process. The C^4D electrode microchannel arrangement was positioned 37 mm from the separation/injection channel cross over to allow room for all of the guide channels to be patterned on the silicon wafer. The integration of four electrode guide microchannels onto the one photolithographic template was designed to allow flexibility for the transmitter and receiver electrodes to be setup in multiple geometries permitting testing and optimisation using the one template, something which cannot be achieved with the same simplicity using traditional electrode integration approaches.
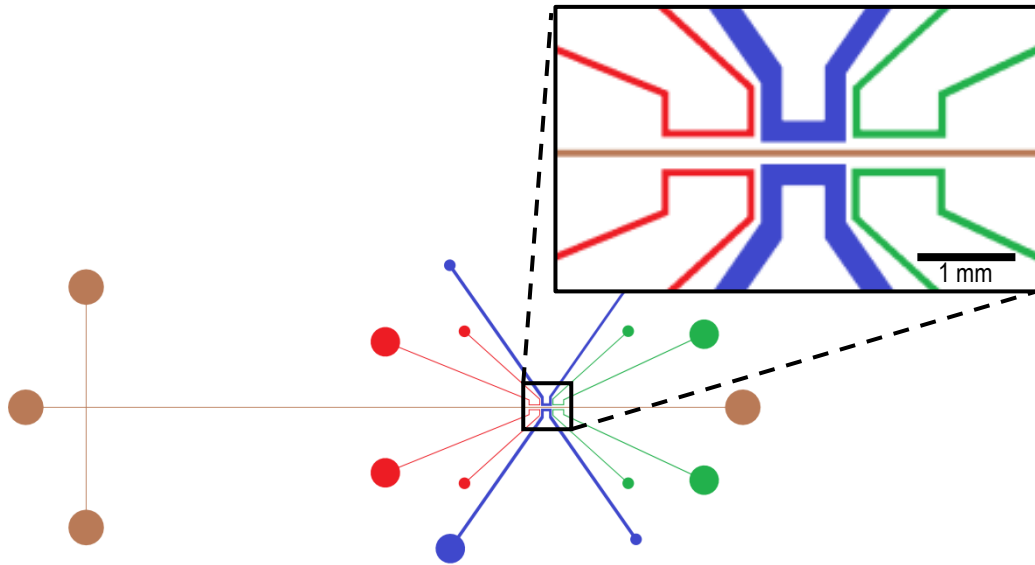
Figure 16   **Schematic of microfluidic chip design**

Containing zoomed in (inset) C^4D guide microchannels showing transmitting electrodes (−), receiver electrodes (−) and grounded shield plates (−) guide microchannels

The C^4D transmitting and receiving electrode guide microchannels were offset by 1 mm along the length of the separation channel with the two ground plane shield plates situated between them. The offset distance of 1 mm was chosen due to its use in a similar microchip C^4D system [167]. The ground shielding plates were incorporated to reduce direct coupling between the transmitting and receiving electrodes, consistent with previous systems reported in literature [141]. Injected electrode guide microchannels were fabricated with a width of 100 µm and a depth of 40 µm, whereas the ground shielding plate guide microchannels has a width of 200 µm and a depth of 40 µm. The ground shielding plate guide channels had a larger width in an attempt to reduce the amount of stray capacitance reaching the receiving electrodes as much as possible. To facilitate electrode design optimisation (Chapter 4) multiple chip designs were produced with varying electrode lengths (750 – 125 µm) and distances between electrode and separation microchannels (50 – 100 µm). The ground shielding plate channels were held at a constant distance of 50 µm from the separation channel for all designs as this was the closest to the separation channel they could be without compromising the integrity of the microchannel walls.

2.2.5 Microchip fabrication

As previously discussed (Chapter 1) silicon, glass and polymers are conventional substrates used in the fabrication of microfluidic devices. Due to high manufacture costs associated with silicon and glass devices, polymers are an attractive option for the

fabrication of microfluidic devices for commercial production. One commonly reported polymer used within microfluidic platforms is poly(dimethylsiloxane) (PDMS). PDMS is a silicon-based rubber, which is gas permeable, optically transparent and biocompatible [4-5]. These favourable properties combined with its significantly lower comparative manufacture costs make PDMS an attractive substrate for microchip production. It was for these reasons that PDMS was chosen as the microchip substrate for this work.

PDMS microfluidic chips were fabricated using standard soft lithography techniques [6]. Initially, the electrophoresis and electrode microchannel designs outlined in Section 2.2.4 were printed on transparent film (JD Photo-Tools, UK) to create high resolution masks of the required designs. Subsequently, a master mould of the patterned microchip electrophoresis and electrode channels was prepared on non-porous, polished Silicon (100) wafers (p^{++} type, boron doped, 0.0008 – 0.0012 Ω cm) purchased from Siltronix, France, with SU-8 photoresist (MicroChem Corp., USA) according to the schematic in Figure 17. Specifically, silicon wafers were first cleaned using acetone and iso-propanol solutions, before being dried for 10 mins on a 120 ^{o}C hotplate. Photoresist was then spin coated onto the silicon wafer to the desired 40 μm thickness using a spin program of 500 rpm for 10 s followed by 2000 rpm for 30 s. The applied photoresist then underwent a soft bake procedure first on a 65 ^{o}C hotplate for 3 mins followed by 6 mins on a 95 ^{o}C hotplate. After cooling to room temperature, the printed photomask was placed on top of the photoresist layer before exposing to 340 nm UV light with an exposure energy of 160 mJ/cm^2. Immediately after exposure the wafer with photoresist underwent a post exposure bake procedure first on a 65 ^{o}C hotplate for 1 min followed by 6 mins on a 95 ^{o}C hotplate. After cooling the exposed microchannel design was developed by submerging in a developing solution of propylene glycol monomethyl ether acetate (PGMEA) for 6 mins with constant swirling. Remaining developer was washed from the master mould using acetone followed by isopropanol before drying with air. To complete master mould fabrication a hard bake procedure was performed by placing first on a 65 ^{o}C hotplate for 1 min followed by 4 mins on a 95 ^{o}C hotplate, 6 mins on a 120 ^{o}C hotplate, a further 4 mins on the 95 ^{o}C hotplate and finally a further 1 min on the 65 ^{o}C hotplate. After this master moulds were ready for use in fabricating PDMS microchips.
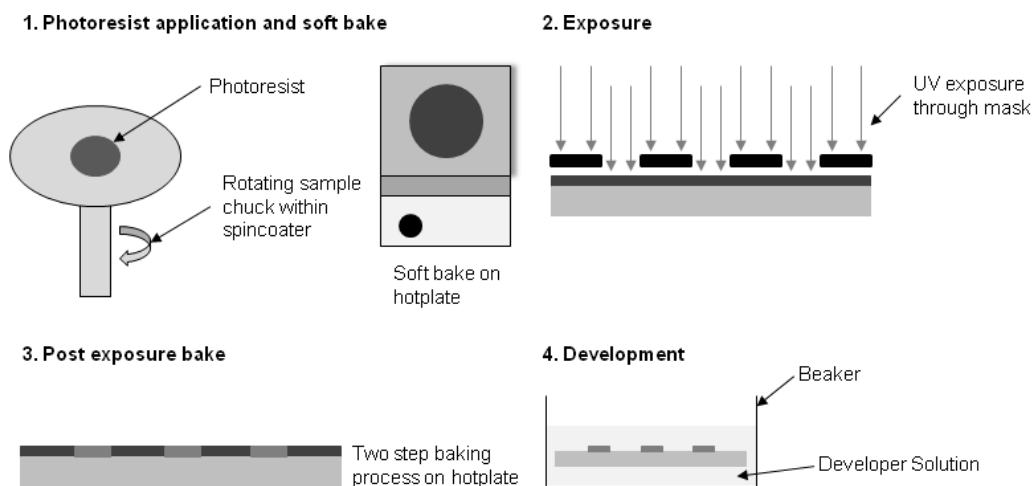
Figure 17   **Schematic representation of the soft lithography process**

Employed for the fabrication of master moulds for PDMS microchip production

PDMS replicas of the master mould were made using a Sylgard® 184 silicone elastomer kit (Dow Corning, USA). A mix of PDMS base and curing agent in a ratio of 10:1 (%w/w) was first poured on top of the master mould. PDMS replicas were then cured on a 90 $^{\circ}$C hotplate for approximately 30 mins. After cooling the replicas were removed from the master mould by cutting around the microchannel designs with a scalpel and peeling off the PDMS with imprinted channels. Holes were then punched where required for later integration of reservoirs for fluid introduction. Finally the resulting PDMS replicas were cleaned by sonication in isopropanol. Replicas, along with a flat sheet of PDMS were then oxygen plasma treated (PDC-32G-2 Plasma Cleaner, Harrick Plasma, USA) at 0.2 Torr of O_2 at 18 W for 45 s. The replica and flat sheet of PDMS were then brought into contact with each other within 10 s of plasma treatment. This resulted in irreversible covalent bonding [36] creating a sealed microfluidic chip containing both electrophoresis and electrode microchannels.

2.2.6 Electrode integration

As discussed in the Introduction (Chapter 1) many approaches to integrating contactless conductivity electrodes with microfluidic devices have been explored. In this work a novel integration approach using molten metal injected into pre-fabricated electrode guide microchannels was used. Injected metal electrodes have previously been demonstrated for a range of different microfluidic applications [173-176]. The major advantage of this approach is that both electrode and analysis microchannels are patterned in the same lithographic process, whereby the electrode design is incorporated directly onto the mask template (Section 2.2.4). Substrates used for molten metal electrodes previously included a range of low melting point alloys [173, 175-176]. However, the use of pure gallium (m.p 29.8 $^{\circ}$C) as an electrode material was considered preferable for the integration of C^4D

electrodes in this work due to its low toxicity, relatively low melting point and ease of handling [174-176].

To integrate the C^4D electrodes molten gallium (99.99%) was injected into the electrode microchannels according to Figure 18 and using a previously described method by Priest *et al.* [174]. Initially, solid gallium was warmed to 50 $^{\circ}C$ on a temperature controlled hotplate to produce the molten metal. Subsequently, the molten gallium was drawn into narrow bore plastic laboratory tubing using a 1 mL syringe. A plastic pipette tip, attached to the end of the tubing, was then placed into an electrode channel inlet and gallium was injected by suppressing the syringe until it protruded into the reservoirs at the opposite end of the channel.
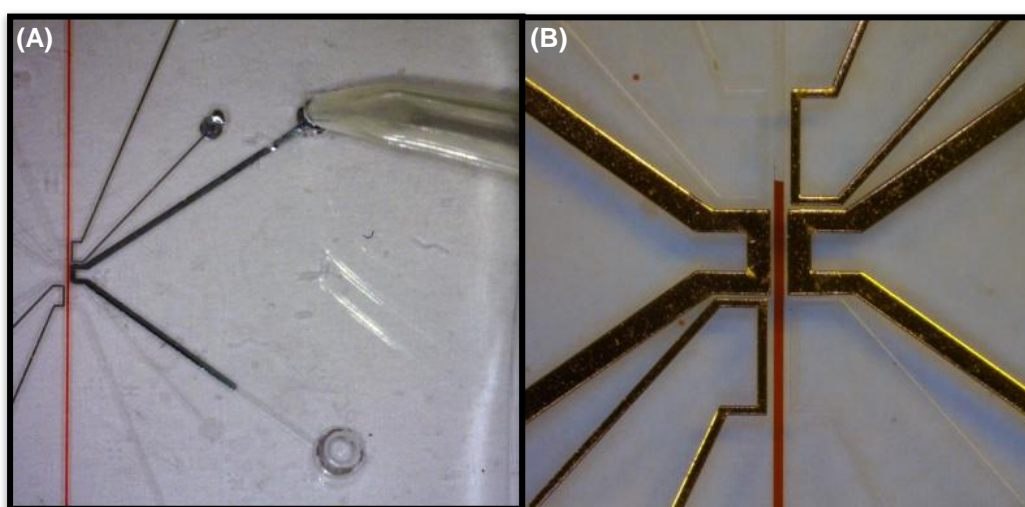
Figure 18   **Photos of injected gallium electrodes**

Indicating (A) the injecting of molten gallium into pre-fabricated electrode guide channels via pipette and (B) the injected electrode system in anti-parallel configuration with separation microchannel highlighted using a red dye

Reservoirs were placed at one end of each electrode microchannel to facilitate the connection of the metal electrodes to external electronic circuitry. To achieve this connection a custom designed printed circuit board was developed in house and is shown in Figure 19. The circuit board contains milled tracks that lead to a circular pad corresponding to all electrode and ground shielding plane reservoirs. Tin plated copper pins were then placed into the middle of each circular pad so that they protruded into each reservoir. Connection between the circuit board and injected electrodes was obtained by filling each reservoir with more molten gallium which was then solidified using a seed crystal to create a rigid and stable connection. The same circuit board also contained milled tracks and circular pads to allow the integration of the high voltage platinum electrodes required for electrophoretic separations and an in-built amplifier for the signal from the receiving electrode(s). Further explanation of the electronic setups for

electrophoretic separations and C^{4}D detection is provided in Section 2.2.7.
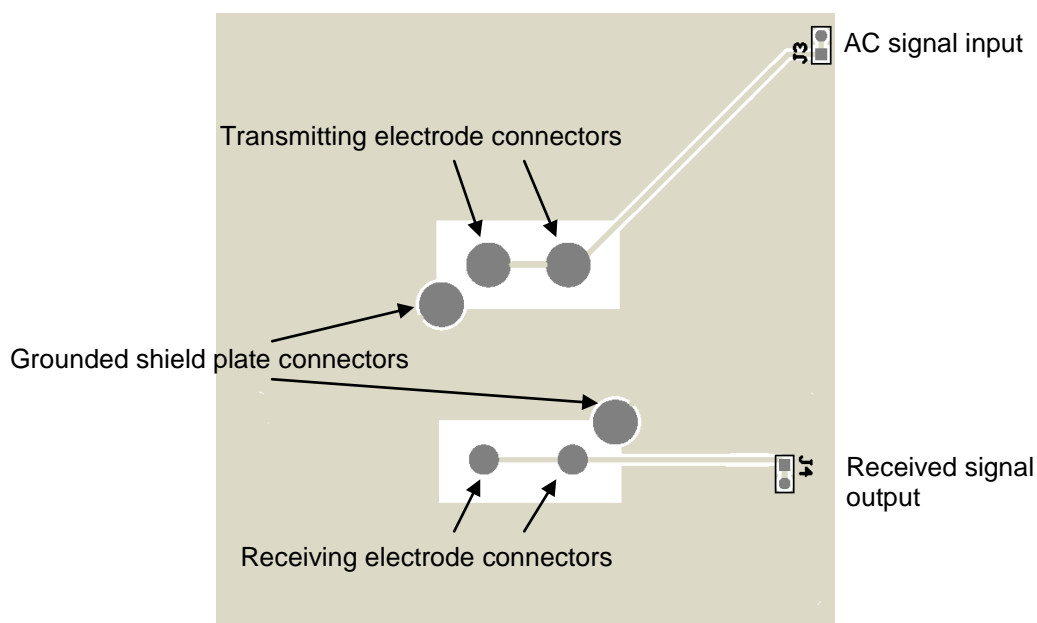
Figure 19   **Schematic of printed circuit board design**

Implemented for the connection of injected gallium electrodes to external electronic components

2.2.7 Electronic setup

To successfully implement a portable microchip electrophoresis system with injected metal C^{4}D electrodes the accompanying electronics needed to be small scale and compact enough to allow the final device to be easily transported and setup. Two main electronic components were required to implement the microchip C^{4}D system. These were the electrophoresis electronics and the detection electronics. In addition, the electronic components required a suitable computer program to control both systems in tandem. Each of the components, their design and implementation are discussed at length in proceeding sections.

2.2.7.1 Microchip electrophoresis

Injection and separation voltages were generated using a high-voltage (HV) power supply (Bertan PMT-50A/P) which were controlled by a purpose built interface connected to a NI USB-6009 DAQ unit (National Instruments). The HV power supply and associated electronics were housed in a 24 x 16 cm plastic housing with insulated leads from the box facilitating connection with platinum electrodes contained inside the microchip housing as shown in Figure 20. Connection of the platinum electrodes to the BGE and sample solutions was achieved by simply resting them in the respective microchip reservoirs during the electrophoresis procedure.
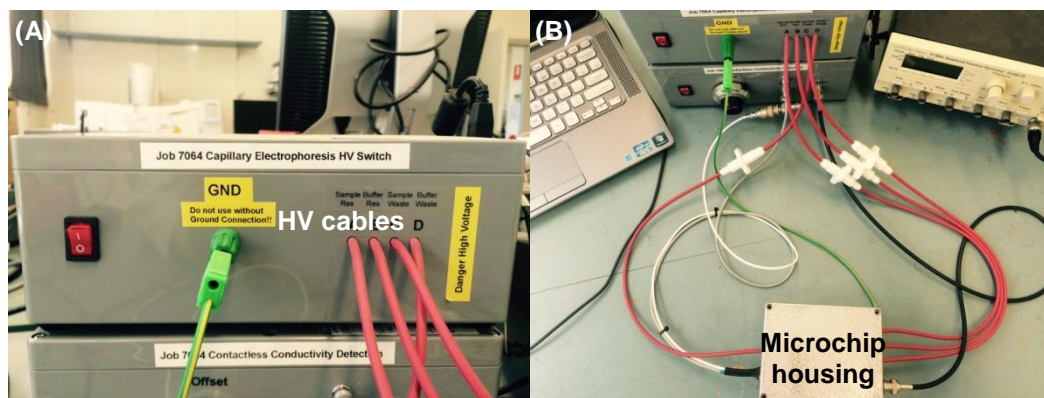
Figure 20   **Photos of electronic components**

Indicating (A) high voltage (HV) box with leads exiting and (B) HV cables running from the HV box to microchip housing.

Electrophoretic separations were performed in PDMS microchips by applying a HV ranging from 1200 – 1400 V across the separation channel. A fixed 25 µL volume of BGE and sample solutions were dispensed into their respective reservoirs using a micropipette. Sample plugs were injected into the separation microchannel using an electrokinetic injection procedure. Specifically, a standard unpinched cross-channel injection was performed by applying an optimised injection voltage (800 – 1000 V) to the sample reservoir, whilst the sample waste reservoir was grounded and the BGE and BGE waste reservoirs were floated. This allowed the sample solution to fill the sample loading microchannel, creating a sample plug at the cross-over with the separation microchannel. After a standardised period of time the voltage was switched and an optimised voltage was subsequently applied to the BGE reservoir (anode) whilst the BGE waste (cathode) was grounded and sample and sample waste reservoirs were floated. This produced a cathodic EOF facilitating the separation of the cationic analytes. This was the general method used throughout this study; however specific details on the optimised electrophoresis conditions are discussed at length in Chapter 3.

2.2.7.2   C^{4}D using injected electrodes

On-chip detection of electrophoretically separated analytes was performed using the previously outlined injected electrode arrangement (Figure 15). To achieve this an excitation signal in the form of sine waves sourced from a function generator (Wavetek 11 MHz stabilised, model 21), with an optimised frequency and amplitude, was transferred to the transmitter electrode (TE). This signal produced an induced alternating current that passed through the microchannel detection cell area and was subsequently picked up down field by the receiver electrode (RE). The shielding plates between the transmitting and receiving electrodes remained grounded throughout to minimise direct coupling caused by stray capacitance. After the signal was received at the RE the current was converted to a voltage using an OPA827A receiver operational amplifier (Texas

Instruments, 2.2 MΩ feedback resistor). The receiver amplifier was positioned on the printed circuit board base encased inside the microchip housing to achieve minimal signal loss. The output signal of the amplifier was then transferred to the signal processing circuit encased in a grounded housing external to the microchip housing. The amplified signal was then full wave rectified, further amplified using an AD744 operational amplifier (Analog Devices) before being passed through a low pass filter with a time constant of 30 ms to remove unwanted high frequency noise. The implemented electronic design was based on a system described previously in the literature [167]. The resulting signal was then collected using a NI USB-6009 DAQ unit (National Instrument) controlled by a custom designed LabVIEW$^{®}$ program written in-house and run on a portable laptop computer.

2.2.8 Microchip housing

C^4D is inherently susceptible to external electrical noise which can have a direct negative impact on detector sensitivity [167]. To minimise the influence of electrical noise, the printed circuit board electronics, high voltage electrodes and microchip needed to be shielded from these sources. This was achieved by housing these components in a 12 x 9.5 cm die cast box as shown in Figure 21(A). The key features of the die cast box housing included a removable lid to facilitate external access to the microfluidic chip for sample introduction, drilled access holes to allow for the introduction of high voltage cables for electrophoresis and two external electrical plugs allowing for the AC electrical signal to be delivered to the injected electrodes and the corresponding received signal to be carried to the external electronics. In addition to these features the housing also contained an additional recessed ground plane inside the box between the transmitting and receiving electrodes to further minimise direct coupling between electrodes. The housing and shielding plane were grounded to eliminate interferences from external noise sources.
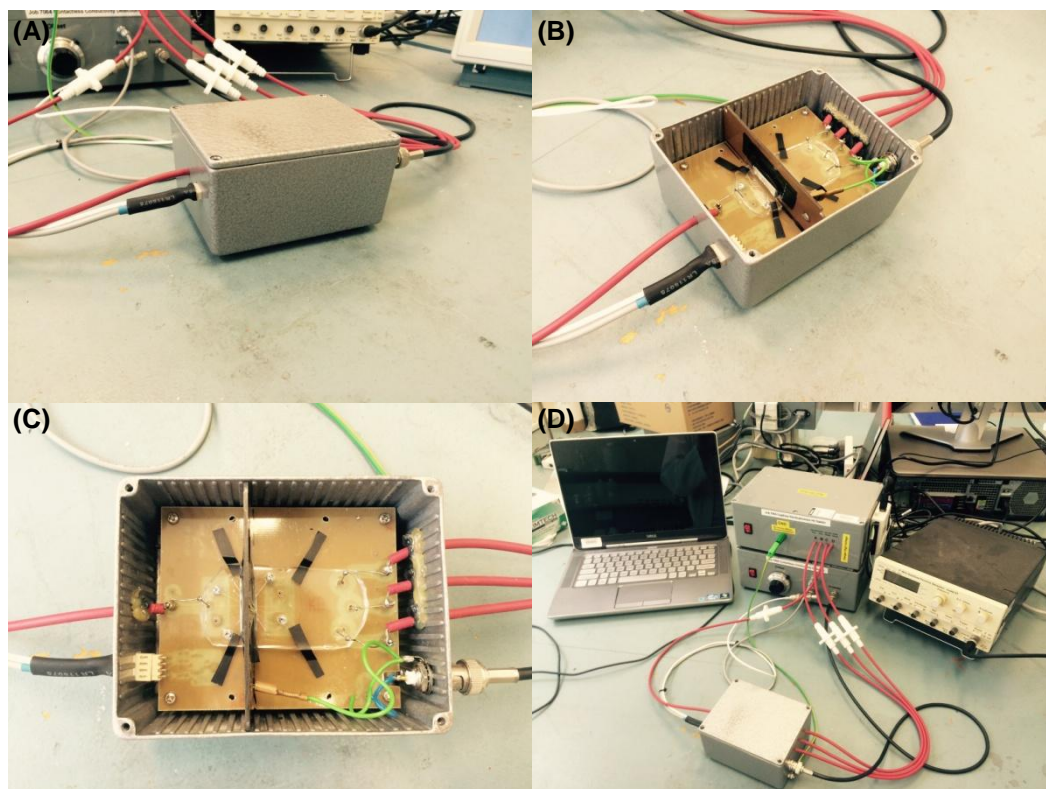
Figure 21   **Photos of complete microchip-C^{4}D system**

Indicating (A) microchip die cast box housing, (B) microchip housing with lid removed, (C) microchip housing showing recessed ground plane inside and (D) complete microchip-C^{4}D setup

2.2.9 Data processing

As mentioned previously, raw data was collected using a NI USB-6009 DAQ unit (National Instrument) controlled by a custom designed LABVIEW$^®$ program. All collected raw data was first exported into Microsoft Excel for further analysis and review before exporting into OriginPro 9.0 (OriginLab, Northhampton, MA, USA) to produce electropherograms for presentation. Baseline subtraction, peak height and peak area determination were performed using the peak analyser function in OriginPro 9.0

Linear regressions were performed using Origin's least-squares method and the obtained regression equations were used to estimate limits of detection (LOD) and limits of quantification (LOQ) for the analytes studied. Furthermore, repeatability within data sets were reported using the percentage Relative Standard Deviation (%RSD) calculated from the standard deviation and mean of each data set. Full details of the equations used to determine these parameters are described in the text where they are applied.

3. Development and Optimisation of Microchip Electrophoresis Conditions

3.1   Chapter overview

Microchip electrophoresis devices require careful optimisation of operating conditions in order to achieve reproducible quantitative analytical data. Optimum conditions vary from microchip to microchip depending on i) electrophoresis microchannel design, ii) sample introduction method and iii) microchip substrate. Here, the effect of BGE composition on the EOF in PDMS microchips is explored with a view to increased reproducibility of the separation of sodium, lithium and potassium ions. Moreover, electrophoresis parameters such as separation voltage, injection conditions and BGE concentration are carefully optimised to obtain an adequate separation of the sodium, lithium and potassium cations.

3.2 Introduction

In this work PDMS is used as the microchip substrate due to its ease of fabrication and ability to integrate injected gallium electrodes. PDMS is a silicon-based rubber, which compared to other polymers has the advantages of gas permeability, optical transparency and biocompatibility [4-5]. However, PDMS surfaces are also relatively unreactive and have poor EOF capabilities in their natural form. Consequently, PDMS surfaces must be modified before they become useful for reproducible electrophoretic separations. Both Makamba *et al.* [101] and Zhou *et al.* [55] have published comprehensive reviews on the modification of PDMS surfaces for microchip electrophoresis devices. A common approach to PDMS surface modification is the plasma oxidation of its surface to form hydroxyl groups. However, PDMS readily undergoes hydrophobic recovery requiring further modification in order to produce a stable surface [55]. These modifications are usually performed via either permanent covalent attachment (traditionally employed in glass microchips) or dynamic adsorption of large molecules to the PDMS surface.

Dynamic PDMS surface modifications are the most commonly employed approach due to their inherent simplicity. Previous publications reported the use of various surfactants as dynamic surface coatings to produce stable EOF in PDMS microchip electrophoresis devices [102-104]. Specifically Guan *et al.* [103-104] have presented extensive studies on the effect of using of ionic, non-ionic and zwitterionic surfactants in PDMS microchips on EOF and separation selectivity. They showed that non-ionic surfactants resulted in a decrease in the EOF as surfactant concentration was increased. Whereas, the use of mixed surfactant systems produced higher EOF values and gave a wider tunable range when compared to single non-ionic surfactants. Most importantly, they concluded that the correlation between EOF and surfactant concentration showed that EOF could be tuned over a range of values based on the surfactant ratio [104]. In another study, García *et al.* [102] investigated the use of the negatively charged surfactants sodium dodecyl sulphate, sodium deoxycholate and phosphatidic acid as BGE modifiers in PDMS microchips. They reported that all three resulted in increased EOF, enhanced detection signal using electrochemical detection and stabilisation of the run-to-run EOF. These reports indicate that EOF in PDMS microchips can be specifically tuned via the incorporation of selective surfactants to modify the microchannel surfaces which in turn also acts to increase the EOF repeatability in these devices.

Careful consideration of the type and concentration of background electrolyte (BGE) to be used in PDMS microchips with conductivity detection is essential. During electrophoretic separations analyte ions displace BGE co-ions equivalent to their charge. Therefore, detection signal responses arise from the difference in conductivity between

analytes and BGE co-ions. In order to achieve the best S/N ratios the difference in conductivity of the analytes and electrolyte should be as large as possible [219]. Two sets of conditions are able to satisfy this criteria being (i) the sample analyte zones exhibit conductivities that are larger than the BGE co-ions or (ii) the sample analyte zones and BGE co-ions exhibit matching equivalent conductivities. However, higher ionic strength of the sample analyte zone compared to the BGE is required to obtain a positive signal response. This contradicts general capillary electrophoresis principles which require the use of BGEs that have a higher ionic strength compared to the sample zone to employ electrostacking effects. In order to overcome this issue the use of amphoteric buffers in microchip electrophoresis is widely reported [219-220].

Amphoteric buffer systems are made up of electrolytes with low background conductivities allowing them to be used at high ionic strengths. This allows considerably high concentrations to be employed increasing the ionic strength and electrostacking effects reducing peak broadening. A commonly utilised amphoteric buffer for the separation and detection of model cationic systems with C^4D is a combination of 2-(N-morpholino)ethanesulphonic acid (MES) and histidine (His) in equal concentrations at a pH of approximately 6 [161, 221]. The structures of these two compounds are shown in Figure 22. In this system histidine acts as an ampholyte to keep background conductivity low whilst providing an adequately high ionic strength for current transport.
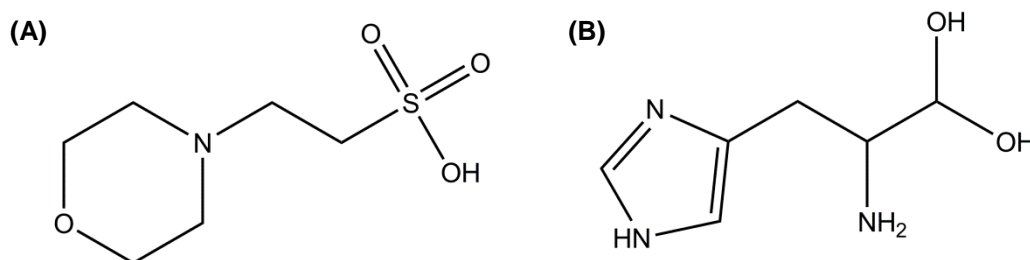
Figure 22   **Structures of background electrolyte components**

(A) 2-(N-morpholino)ethanesulphonic acid (MES) and (B) Histidine (His)

In addition to EOF reproducibility and BGE composition, the electrophoretic analysis conditions for individual microchip designs must also be optimised to perform reliable analytical measurements. In this work a cross channel electrophoresis design is used which allows for electrokinetic injection of the sample by applying a voltage between the sample and sample waste reservoirs before switching the voltage to between the buffer and buffer waste reservoirs for separation. The key advantage of this design is its smaller injection volume compared to a double-T injection design. However, it is important to consider both the electrokinetic injection voltage and time in order to prevent excess leakage of the sample into the separation microchannel resulting in large sample plugs and decreased resolution [222-223]. In a similar manner careful consideration must be

given to the optimisation of the separation voltage used for analysis in microchip electrophoresis devices. Low separation voltages can lead to broad, poorly resolved analyte peaks whereas high separation voltages can lead to the co-migration of sharper analyte peaks, due to the short migration distances in microfluidic setups, and excessive joule heating [80, 82]. Therefore, a compromise between the two is often required whereby an intermediate voltage is applied to produce sharp analyte peaks that are sufficiently resolved.

This chapter focuses on the development of a stable and reproducible PDMS electrophoresis microchip for quantitative analysis. In particular, detailed investigations into microchannel surfactant modification to achieve stable electro-osmotic flows are reported. In addition optimisation of the electrophoresis parameters i) separation voltage, ii) electrokinetic injection conditions and iii) background electrolyte are discussed at length.

3.3   Experimental

3.3.1 Instrumentation

All experiments in this chapter were performed using the purpose designed microchip electrophoresis instrument with injected metal electrodes for capacitively coupled contactless conductivity detection as described previously in Chapter 2. In order to evaluate and optimise the electrophoresis conditions for the PDMS microchip a set of standard detection electrode parameters was chosen and held constant throughout all experimental work. The C^4D design contained transmitting and receiving electrodes 1 mm in length arranged in an anti-parallel configuration with a 1 mm offset. Further, the distance between the detection electrodes and the electrophoretic separation microchannel was set at 75 μm. The C^4D excitation signal employed for optimisation experiments was sinusoidal with a peak to peak voltage of 5 V and frequency of 240 kHz, unless stated otherwise.

3.3.2 Chemicals

Unless otherwise specified, all chemicals were of analytical grade, purchased from Sigma-Aldrich (Australia) and used as received. Microchannel modification experiments were performed using solutions prepared by dissolving 2-(N-morpholino)ethanesulphonic acid (MES) and histidine (His) with the addition of the non-ionic surfactant n-dodecyl β-D-maltoside (DDM) or the anionic surfactant sodium dodecyl sulphate (SDS) according to the concentrations in Table 6. Background electrolyte solutions for electrophoretic separations were prepared by dissolving the required mass of 2-(N-morpholino)ethanesulphonic acid (MES) (10 - 20 mM) and histidine (His) (10 - 20 mM) in Milli-Q water (18.2 MΩ cm). Sample stock solutions (100 mM) of aqueous lithium, sodium and potassium ions were prepared by dissolving their chloride salts in Milli-Q water (18.2 MΩ cm). Working standards (0.1 mM – 1 mM) of lithium, sodium and potassium ions were prepared by dilution of the stock solutions in MES/His background electrolyte. All solutions were degassed by ultrasonication prior to use.

Table 6   **List of buffers used for surfactant effect on µEOF study**

Buffer	Background electrolytes	Electrolyte concentration (mM)	Surfactant added	Surfactant Concentration (mM)
1a	MES/His	18/18	-	-
1b	MES/His	20/20	-	-
2a	MES/His	18/18	SDS	1
2b	MES/His	20/20	SDS	1
3a	MES/His	18/18	SDS	2
3b	MES/His	20/20	SDS	2
4a	MES/His	18/18	SDS	5
4b	MES/His	20/20	SDS	5
5a	MES/His	18/18	SDS	10
5b	MES/His	20/20	SDS	10
6a	MES/His	18/18	DDM	0.1
6b	MES/His	20/20	DDM	0.1
7a	MES/His	18/18	DDM	0.2
7b	MES/His	20/20	DDM	0.2
8a	MES/His	18/18	DDM	0.4
8b	MES/His	20/20	DDM	0.4
9a	MES/His	18/18	DDM	0.8
9b	MES/His	20/20	DDM	0.8
10a	MES/His	18/18	DDM	1.5
10b	MES/His	20/20	DDM	1.5

3.3.3 Determination of electro-osmotic flow

The use of buffers with differing concentrations for the determination of electro-osmotic flow mobility (µEOF) of buffer solutions using C^4D has been described previously [86]. This method was used in this study to characterise the effect of modifying PDMS microchannels with surfactants. Multiple concentrations of each of the surfactants n-dodecyl β-D-maltoside (DDM) and sodium dodecyl sulphate (SDS) were used as outlined in Table 6. The experimental setup for µEOF determinations is shown in Figure 23. Firstly, 20 mM BGE solution was placed in the buffer and buffer waste reservoirs and the separation microchannel filled by applying a voltage. The 20 mM BGE was then removed from the buffer reservoir and replaced with 18 mM BGE. A voltage was then applied across the channel and the electropherogram recorded, a signature 'drop' in C^4D signal is observed as the lower concentration BGE passes through the detection cell.
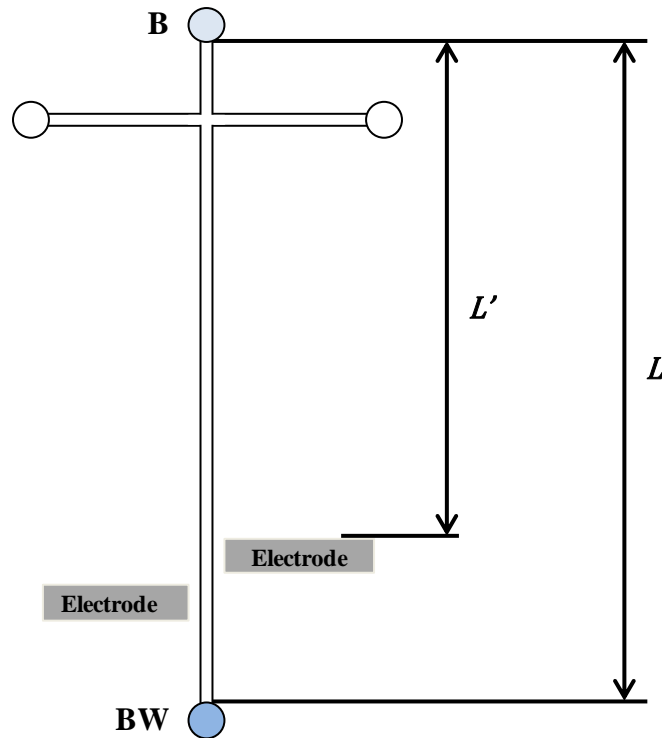
Figure 23   **Schematic diagram of microchip setup used for determination of µEOF**

Illustrating B as buffer reservoir and BW as buffer waste reservoir, L as the total length of separation channel and L' as the distance between the buffer reservoir and detection point

The time to inflection from the electropherograms were then used to calculate the µEOF according to Equation 8, where *L* is the total length of the separation channel (cm), *L'* is the distance between the buffer reservoir and the detection point (cm), V is the voltage applied across the microchannel (V) and t is the time to inflection (s).

Equation 8   **Equation for the calculation of µEOF**

$$\mu EOF = \frac{LL'}{Vt}$$

All values reported are the average of ten replicates and uncertainties were determined as the standard error calculated from the corresponding standard deviations of each data set.

3.4 Results and discussion

3.4.1 Investigation of PDMS microchannel modification with surfactants

As discussed in Chapter 1, native PDMS microchannels are known to produce unstable EOFs due to both its hydrophobic nature and ability to adsorb a large range of hydrophobic molecules. [55] The model analytes used for optimising both electrophoresis and electrode parameters were lithium, sodium and potassium cations. For these analytes an efficient and reproducible electrophoretic separation was required. In order to achieve this, a stable µEOF was essential. Due to its widely accepted use for cation separations in PDMS microfluidic chips, it was decided that for the current investigation a BGE containing a MES/His combination would be used with a starting concentration of 20 mM. It has been previously reported that the interaction of surfactant molecules with PDMS microchannel surfaces can have a significant impact on both the magnitude and stability of the µEOF in BGE systems [102]. For this reason the effect of the two different surfactants sodium dodecyl sulphate (SDS) and n-dodecyl β-D-maltoside (DDM), shown in Figure 24, on the µEOF of BGE in the developed PDMS microchip was investigated.
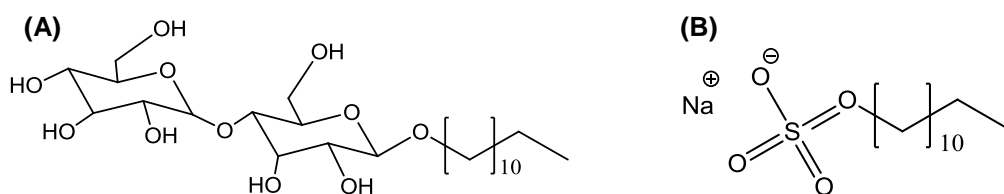
Figure 24   **Structures of surfactants studied**

(A) n-dodecyl ß-D-maltoside (DDM) and (B) sodium dodecyl sulphate (SDS)

SDS is an anionic surfactant which is commonly used to achieve desired separations by manipulating the EOF of electrophoretic systems [103]. In order to study the effect of adding SDS to the BGE in the presented system, increasing concentrations of SDS were added to BGE solutions (see Table 6 in Section 3.2.2) and the µEOF obtained for each. Figure 25 illustrates the resultant effect on the µEOF as the concentration of SDS was increased. A sharp rise in the measured µEOF was observed when 1 mM and 2 mM of SDS were present in BGE before a plateau of the data above 5 mM SDS. Above this concentration a stable µEOF of $2.96 \pm 0.07 \times 10^{-4}$ cm^2 V^{-1} s^{-1} was achieved.
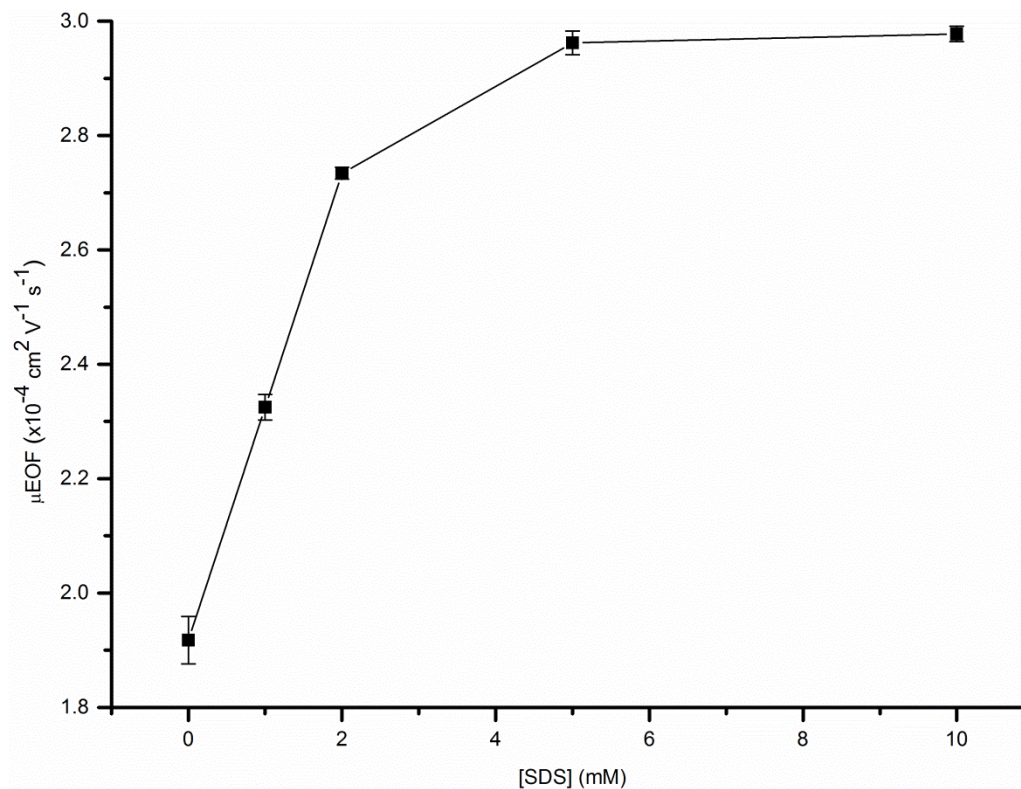
Figure 25   **µEOF as a function of concentration of SDS**

Using MES/His background electrolyte (20 mM and 18 mM) at pH 6

The increase in EOF associated with larger concentrations of SDS in the BGE is a result of the dynamic interaction of SDS molecules with the PDMS surface [55]. Zhou *et al*. have previously reported that this dynamic interaction arises from the hydrophobic tails of SDS being physisorbed onto the PDMS surface [55], a simplified schematic of this interaction is shown in Figure 26. This effectively exposes the negatively charged sulphate headgroups to the solution resulting in an increased zeta potential and consequently a higher EOF. An increase in the stability of the measured µEOF's obtained upon the addition SDS was also attributed to this interaction of the surfactant with the PDMS surface. Increased stability was confirmed by the reduction in the standard error associated with the experimental replicates shown in Figure 25.
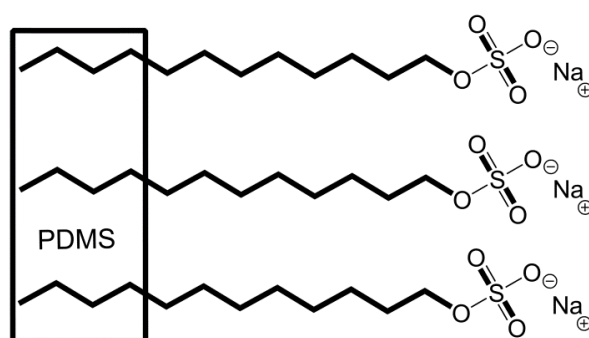
Figure 26   **Simplified representation of SDS interaction with PDMS**

As the separation microchannel in the developed microchip electrophoresis device was relatively short (effective length: 37 mm) an increased µEOF was considered unfavourable as it could potentially result in insufficient time for separation of the model analytes. Therefore it was determined that SDS was unsuitable for the current study. It was proposed that an alternative non-ionic surfactant be trialled in order to achieve a reduced and stable µEOF allowing greater separation times and improved reproducibility.

DDM is a non-ionic surfactant that's use has been demonstrated previously for the stabilisation of µEOF in PDMS electrophoresis microchannels [163]. In this study the effect of adding increasing amounts of DDM to BGE was studied on a new microchip using the same method outlined for SDS (See Table 6 in Section 3.3.2). Figure 27 shows the resultant effect on the µEOF as the concentration of DDM was increased. A larger initial µEOF was observed, compared to SDS (Figure 25), due to the use of a new PDMS microchip and the previously outlined inconsistencies with this material. Significant reductions in the measured µEOF were observed for the BGE solutions containing 0.1, 0.2 and 0.4 mM DDM respectively when compared with those containing SDS. Above 0.4 mM DDM the measured µEOF remained consistent at $0.84 \pm 0.03 \times 10^{-4}$ cm^2 V^{-1} s^{-1}. As previously observed with SDS, the addition of DDM to the BGE resulted in an increased stability of the measured µEOF, demonstrated through the reduction of the standard error associated with the experimental replicates (Figure 27).
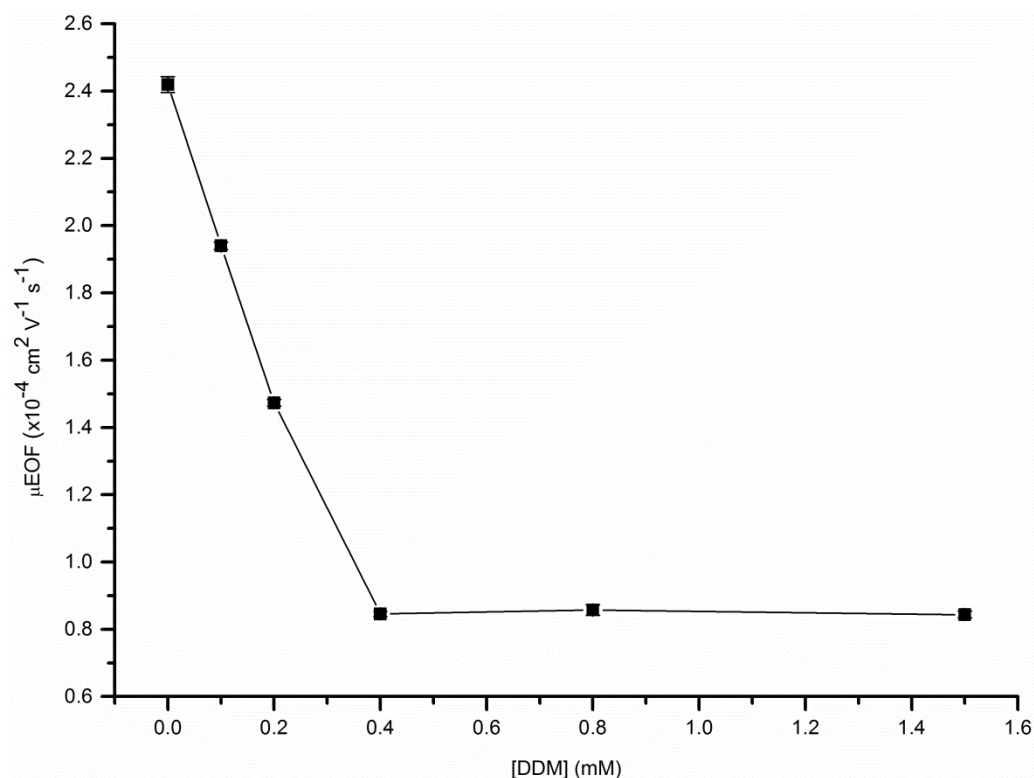
Figure 27   **µEOF as a function of concentration of DDM**

Using MES/His background electrolyte (20 mM and 18 mM) at pH 6

The decrease in measured µEOF associated with the larger concentrations of DDM in the BGE was again the result of the dynamic interaction of DDM molecules with the PDMS surface. As was the case with SDS, the large hydrophobic tails of DDM were physisorbed onto the PDMS surface effectively exposing the non-ionic maltoside headgroups to the solution. Huang *et al.* previously reported that the formation of such a DDM coating reduces the EOF by effectively covering the charges on the PDMS surface [224]. It follows that the reduced surface charges lead to a decreased zeta potential and consequently the lower measured µEOF values. Based on these results it was determined that a DDM concentration of 0.4 mM be used for further analysis experiments. It was postulated that the decreased magnitude and increased stability of the µEOF in PDMS microchannels associated with these conditions would allow the efficient and reproducible separation of the model cation system for further optimisation experiments.

3.4.2 PDMS modification approaches: continuous vs intermittent

PDMS microchannel surface modification using surfactant is traditionally achieved by the addition of surfactant to BGE for preconditioning and/or throughout analysis experiments. Both of these approaches are considered dynamic systems as they allow either continuous, when the surfactant is used in preconditioning and analysis experiments, or intermittent, when the surfactant is used only in preconditioning, replenishment of the surface coating. Alternatively, static surface modification, where the microchannel is only treated once with the modifying agent before analysis experiments, is also a common approach for the modification of both polymer and glass surfaces. However, it is primarily used when a covalent bond forms between the surface and modifying agent giving rise to a highly stable surface coating. Given the non-covalent nature of the interaction between DDM and PDMS the static modification approach is unfavourable for the presented system. Therefore in this study only the continuous and intermittent dynamic surface modification approaches were examined.

In order to examine the effect of using the continuous and intermittent dynamic surface modification approaches on the PDMS microchip electrophoresis device, both approaches were tested by separating a 0.5 mM mixture of Li^+, Na^+ and K^+ cations. Continuous modification experiments were performed by adding DDM to the BGE for preconditioning and electrophoretic separations. As opposed to intermittent modification experiments which were performed by adding DDM to the BGE for the preconditioning step only. Comparison of the effect on analytical performance was done using peak height divided by concentration ratios (P_H/Conc ratio) for each of the three cations. These values were plotted with their associated standard deviation (n=5) as shown in Figure 28.
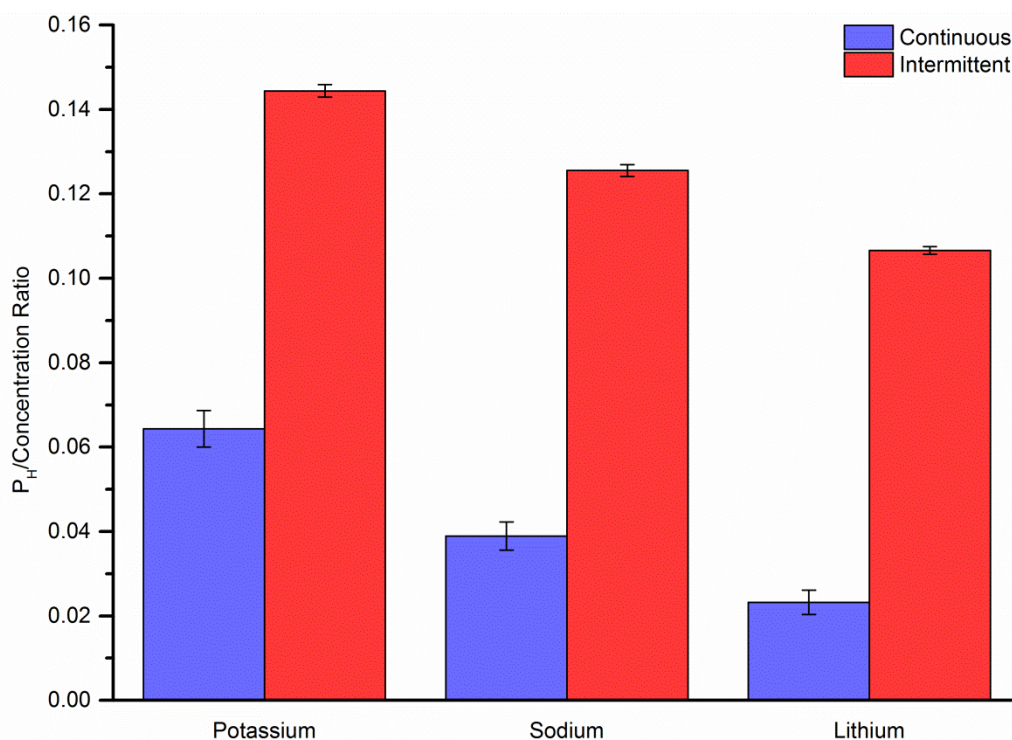
Figure 28 **Continuous and intermittent dynamic surface modification approaches**

Comparison of analytical performance of PDMS microchips

A significant increase in the P_H/Conc ratio coupled with a reduction in the standard deviation was observed using the intermittent surface modification approach (Figure 28). These results suggested that the intermittent approach resulted in more sensitive and reproducible detection of the potassium, sodium and lithium cations. This lead to the conclusion that the presence of DDM during analysis, in the continuous approach, interfered with the conductivity detection resulting in suppression of the analytical signal obtained. It was postulated that this was the result of increased background conductivity and/or the formation of micelles during electrophoresis (CMC_{DDM}=0.16 mM) changing the electrophoresis conditions. As a result of these findings it was determined that an intermittent dynamic surface modification approach using DDM be used for all further electrophoretic analysis.

3.4.3 Stability of microchannel EOF when using intermittent dynamic coating

After the selection of the intermittent approach for the dynamic modification of PDMS microchannels using DDM, the electro-osmotic flow mobility (μEOF) using this approach was determined. In addition, its stability over a number of days was examined as it was important that the μEOF be reproducible over a number of days to allow for its eventual use for quantitative analysis. The μEOF was determined, as previously described in Section 3.2.3, by performing five replicate analyses on three separate days (n=15). The

final μEOF is reported as the mean of the values over all three days. The intermittent dynamic surface modification approach was found to have a μEOF of 2.00 $\pm$ 0.11 x 10^{-4} cm^2 V^{-1} s^{-1}. The repeatability of the measured μEOF was determined by calculating the relative standard deviation (%RSD) of the means obtained from each of the three days. The %RSD was found to be 5.3, meaning the reported intermittent approach had a high degree of repeatability. %RSD values below 5 are often considered ideal for analytical systems and given the issues previously described surrounding PDMS microfluidic devices, an %RSD value of 5.3 was acceptable.

3.4.4 Optimisation of microchip electrophoresis parameters for the separation of a model analyte system

In order to evaluate the performance of injected gallium electrodes for analytical detection capabilities it was essential to first develop a standard PDMS microchip electrophoresis procedure. This was achieved by optimising the parameters separation voltage, injection voltage and injection time and further assessing the reproducibility of the developed procedure. After the establishment of a reproducible electrophoresis method further optimisation of the electrode arrangement and analysis of detection limits could be performed. During optimisation experiments it is essential to utilise model analytes to evaluate each parameter investigated. Model analytes are employed to provide a system that mimics a potential real sample that would be analysed by the device being developed. In this case, using capacitively coupled conductivity detection, a mixture of the cations lithium (Li$^+$), sodium (Na$^+$) and potassium (K$^+$) was chosen as the model analyte system due to the analytes high conductivity in solution and the previous reporting of such ions as standards for testing conductivity detectors [167, 172].

In order to perform accurate optimisation experiments it was important to initially determine the migration order of the model analytes in the developed PDMS electrophoresis microchip. To determine the migration order an electrophoretic separation of a 0.4 mM mixed standard followed by subsequent separations of individual standards was performed. The electrophoresis conditions utilised an electrokinetic injection voltage of 500 V for 5 s with a separation voltage of 1000 V for 80 s. The resulting electropherograms are shown in Figure 29. The cations migrated in the order K$^+$, Na$^+$ and Li$^+$. This is consistent with the theory of electrophoretic separations where the migration velocity is proportional to the effective charge to solvated radius ratio of each ion [81]. Therefore as the charge to solvated radius ratio for the three cations decreases in the order Li$^+$, Na$^+$, K$^+$ the migration velocity increases allowing for faster migration times and the order observed. This allowed for the easy identification of the model analyte peaks in subsequent electrophoresis optimisation experiments.
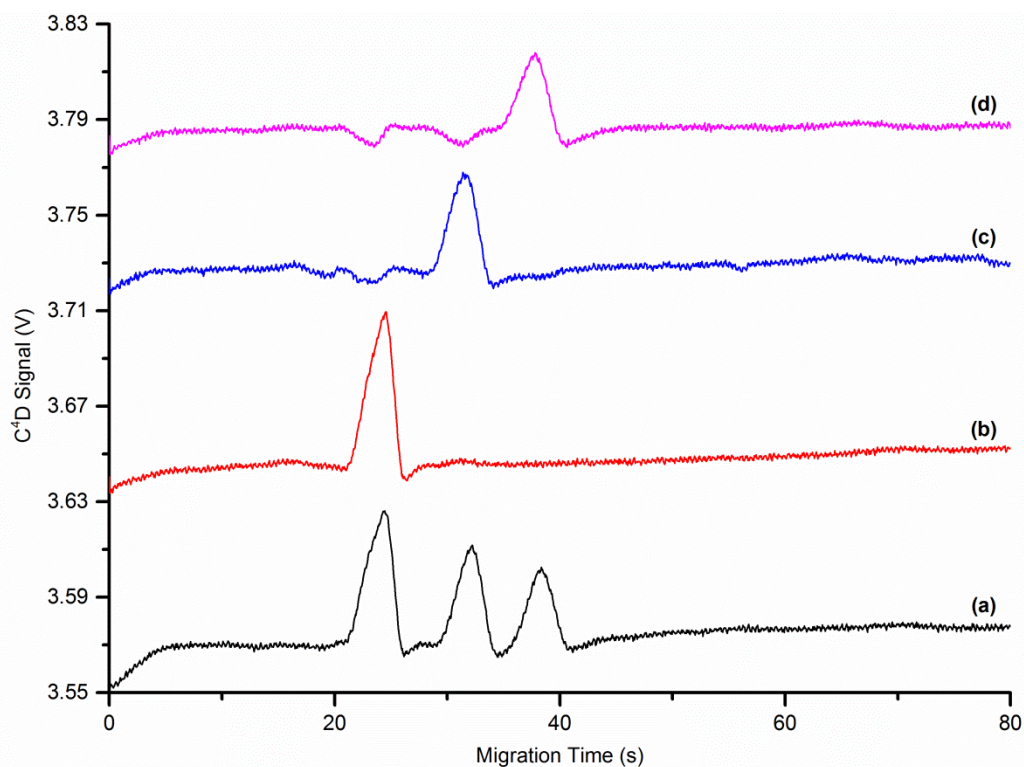
Figure 29   **Confirmation of model analyte migration order**

Offset electropherograms obtained for (a) 0.4 mM mixed Li^+, Na^+ and K^+ standard, (b) 0.4 mM K^+ standard, (c) 0.4 mM Na^+ standard and (d) 0.4 mM Li^+ standard

3.4.4.1 Optimisation of separation voltage

Initial microchip electrophoresis experiments were focussed on the optimisation of the separation voltage. Optimised separation conditions allow for the effective separation of analytes in the shortest timeframe possible without sacrificing analytical performance. In addition, there are a number of important factors to consider when determining an optimal separation voltage for electrophoretic separations on PDMS microchips with C^4D. Joule heating is one such factor and arises as a result of the heating of a conductive solution due to the passage of an electric current through the solution. As PDMS has a low thermal conductivity (~0.15 $W.m^{-1}.K^{-1}$) compared to other microchip substrates such as glass (~1 $W.m^{-1}.K^{-1}$), joule heating is an important consideration resulting in a lower separation voltage being favourable [225]. Further increased noise associated with using higher separation voltages with conductivity detectors is also an issue, which again favoured a lower separation voltage for our developed device. With these factors in mind, a 0.5 mM standard mixture of model analytes was separated using voltages in the range 1000 – 1800 V (175 - 316 $V.cm^{-1}$) with electrokinetic injection conditions held constant at 700 V for 10 s. The resulting electropherograms are displayed in Figure 30.
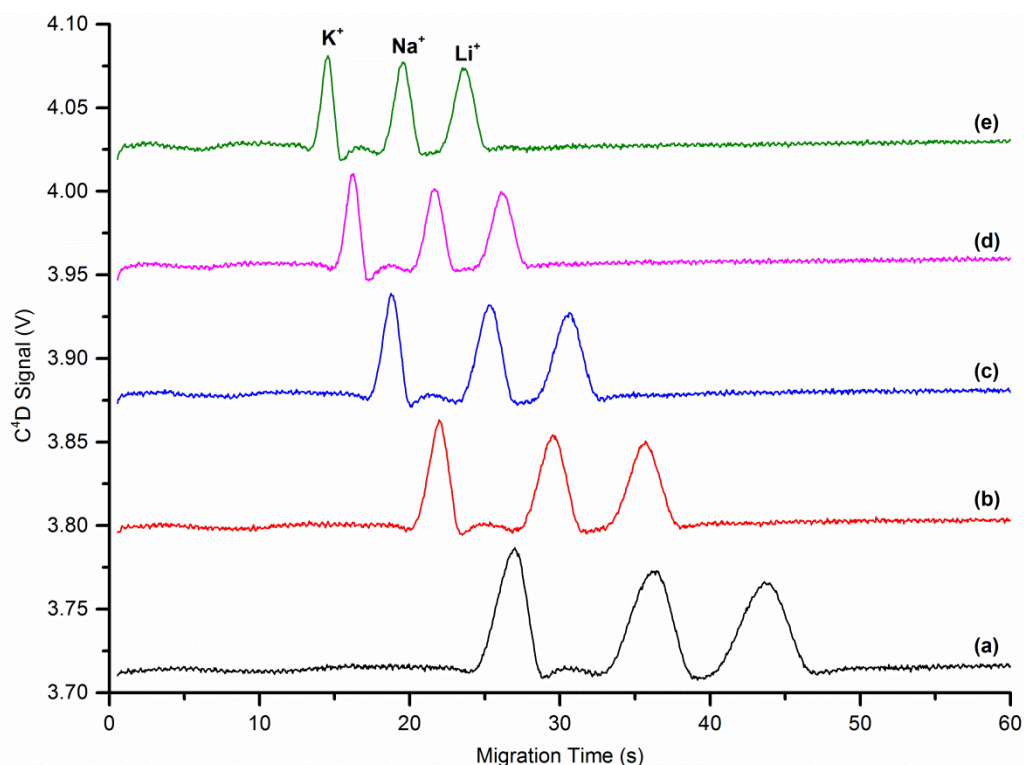
Figure 30   **Optimisation of microchip electrophoresis separation voltage**

Offset electropherograms obtained using separation voltages (a) 1000 V, (b) 1200 V, (c) 1400 V, (d) 1600 V and (e) 1800 V

As displayed in Figure 30 no significant increase in detector noise was observed at any of the separation voltages trialled. Additionally, all three model analytes were well resolved from each other at each voltage. Therefore, for all further optimisation experiments an intermediate separation voltage of 1400 V was chosen as a precaution to minimise any potential effect of joule heating during prolonged use of the device.

3.4.4.2 Optimisation of electrokinetic injection conditions

Following the optimisation of the separation voltage, a study to determine the optimum electrokinetic injection voltage was performed. Electrokinetic injections are performed in microchip electrophoresis devices by applying a voltage across an injection channel that intersects the separation channel. The application of a voltage results in the movement of ions effectively forming an injection plug at the injection/separation channel intersection that, upon switching to the voltage along the separation channel, is effectively introduced for separation and detection. Electrokinetic injections are favoured in microchip electrophoresis devices over hydrodynamic injections as it is an easily integrated method for sample injection under non-stacking conditions.

The electrokinetic injection conditions optimised in this study were injection voltage and time. Both of these factors are important as excessive voltage can result in joule heating

as previously mentioned when optimising the separation voltage. In addition, lengthy injection times can result in diffusion of sample at the injection/separation channel intersection effectively overloading the microchannel and resulting in the loss of peak resolution in the final electropherogram. Firstly, the electrokinetic injection voltage was optimised by performing a separation of a 0.5 mM mixture of the model analyte system using injection voltages ranging from 500 - 1000 V (333 – 667 V cm^{-1}) with a standard injection time (10 s). The previously optimised 1400 V separation voltage was used and all experiments were performed in triplicate with representative electropherograms for each voltage displayed in Figure 31.
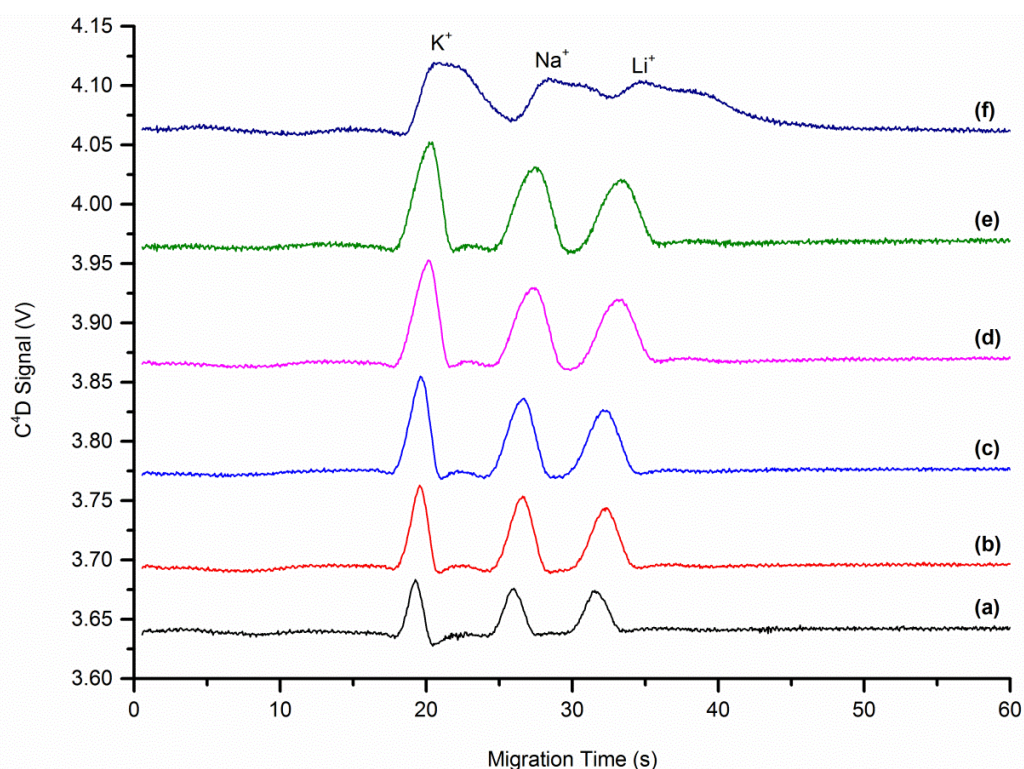
Figure 31   **Optimisation of electrokinetic injection voltage**

Offset electropherograms obtained using injection voltages (a) 500 V, (b) 600 V, (c) 700 V, (d) 800 V, (e) 900 V and (f) 1000 V

Baseline resolution of the three analyte peaks was achieved for all injection voltages trialled with the exception of 1000 V leading to its exclusion as a potential option. Consequently, the peak heights (P_H) and signal to noise (S/N) ratios at each of the remaining injection voltages were calculated to determine the optimum value. Peak heights and S/N ratios are important measures to consider when optimising a system to achieve the best possible analytical performance. Higher values of both parameters will allow for lower detection limits to be achieved after all other optimisation experiments have been completed. These values were determined as the average of three replicates performed at each injection voltage and are presented in Figure 32 with their associated standard deviation (n = 3).

Figure 32   **Effect of electrokinetic injection voltage on model analyte peaks**

Effect of electrokinetic injection voltage on the peak height (P_H) and S/N ratio of Li$^+$ ($-\blacktriangle-$), Na$^+$ ($-\bullet-$) and K$^+$ ($-\blacksquare-$) peaks (0.5 mM)

A general trend of increasing peak height with increasing injection voltage was observed until an apparent plateau in the data between 800 and 900 V for all three model analytes (Figure 32). This was expected due to the increased mobility of the cations under higher applied voltages resulting in a more concentrated sample plug at the injection/separation channel intersection. The plateau of the data is a result of the maximum number of cations in the channel intersection being reached at higher voltages. This was also observed in the electropherograms in Figure 31 except for the 1000 V injection which combined with the set injection time of 10 s resulted in diffusion of sample at the intersection as previously explained. Further examination of the data obtained indicated that the S/N ratios also steadily increased as the injection voltage was increased before dropping sharply at 900 V (Figure 32). Despite similar peak heights being obtained for the 900 V injection, compared to the 800 V injection, increased baseline noise accounted for the decreased S/N ratio. Given that higher S/N ratios produce lower limits of detection for analytical devices it was decided to continue further optimisation experiments of injection time using an optimised injection voltage of 800 V.

As previously mentioned, injection time is also an important parameter to optimise when implementing a new microchip electrophoresis device. Injection times that are too short can lead to insufficient sample loading into the injection plug, whereas lengthy injection times can result in overloading of sample in the injection plug, both of which have a

detrimental effect on the resulting electropherogram. The electrokinetic injection time was optimised by performing a separation of a 0.5 mM mixture of the model analyte system using injection times ranging from 2.5 – 12.5 s with a standard optimised injection voltage (800 V). The previously optimised 1400 V separation voltage was used and all experiments were performed in triplicate with representative electropherograms for each injection time displayed in Figure 33.
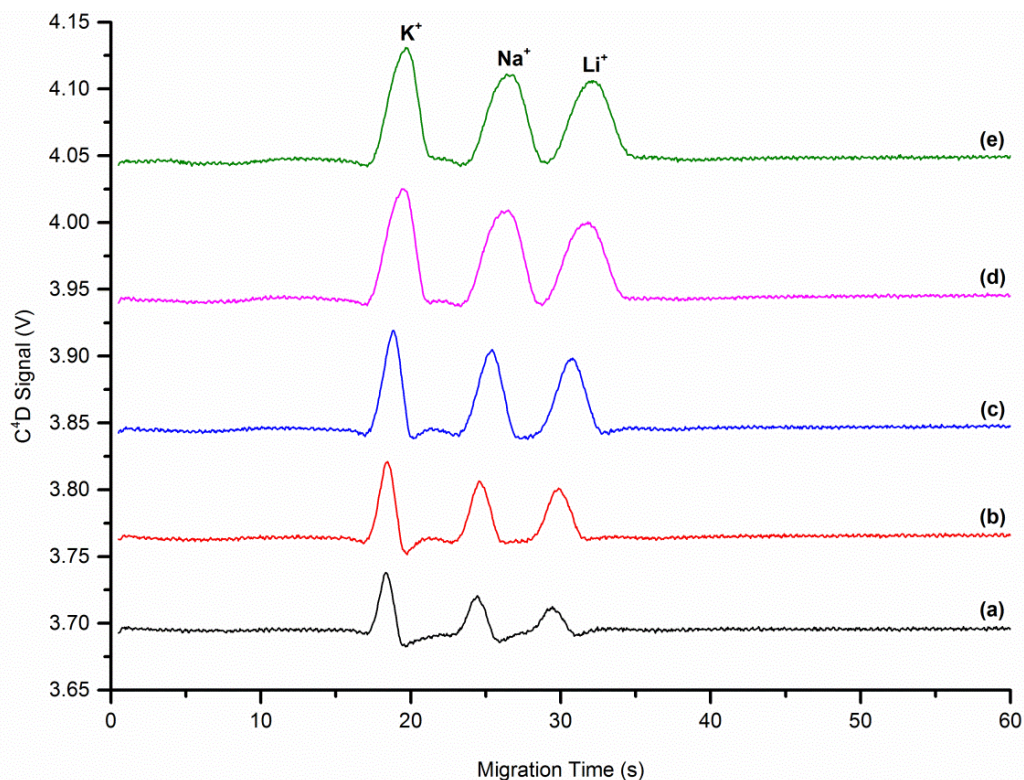
Figure 33   **Optimisation of electrokinetic injection time**

Offset electropherograms obtained using injection times (a) 2.5 s, (b) 5 s V, (c) 7.5 s, (d) 10 s and (e) 12.5 s

Baseline resolution of the three analyte peaks was achieved for all injection times trialled. As previously discussed, peak heights and S/N ratios are important measures to consider when optimising a new detection system as higher values of both parameters will allow for lower detection limits to be achieved. Therefore both values were calculated at each injection time in order to determine the optimum injection conditions. These values were determined as the average of three replicates performed at each injection time and are presented in Figure 34 with their associated standard deviation (n=3).
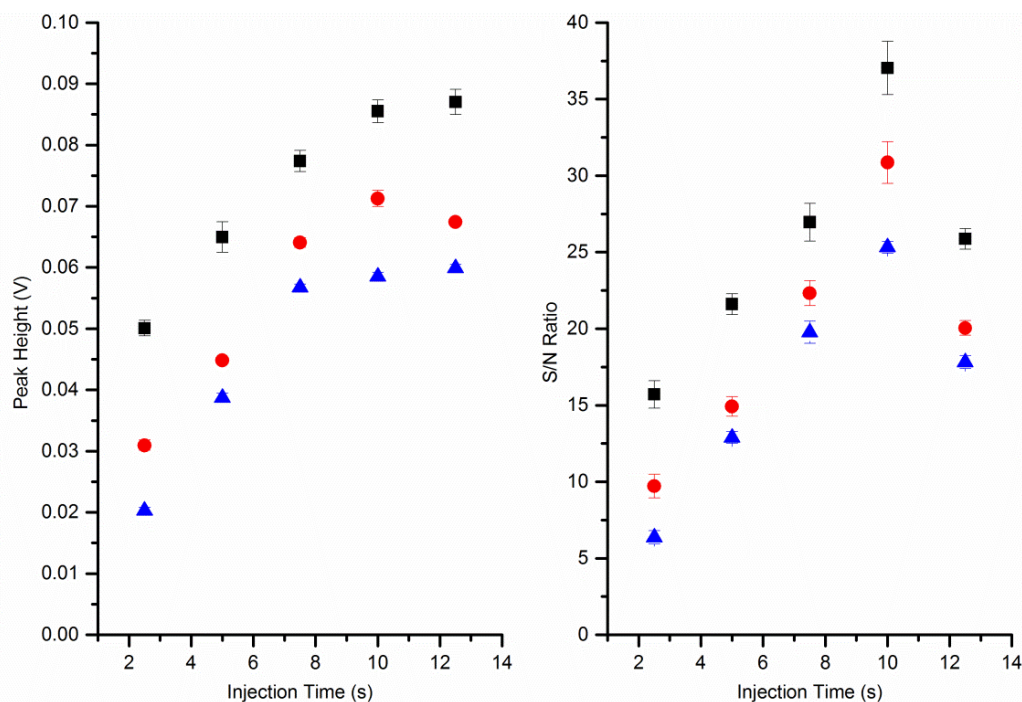
Figure 34   Effect of electrokinetic injection time on model analyte peaks

Effect of electrokinetic injection time on the peak height (P_H) and S/N ratio of Li^+ ($-\blacktriangle-$), Na^+ ($-\bullet-$) and K^+ ($-\blacksquare-$) peaks (0.5 mM)

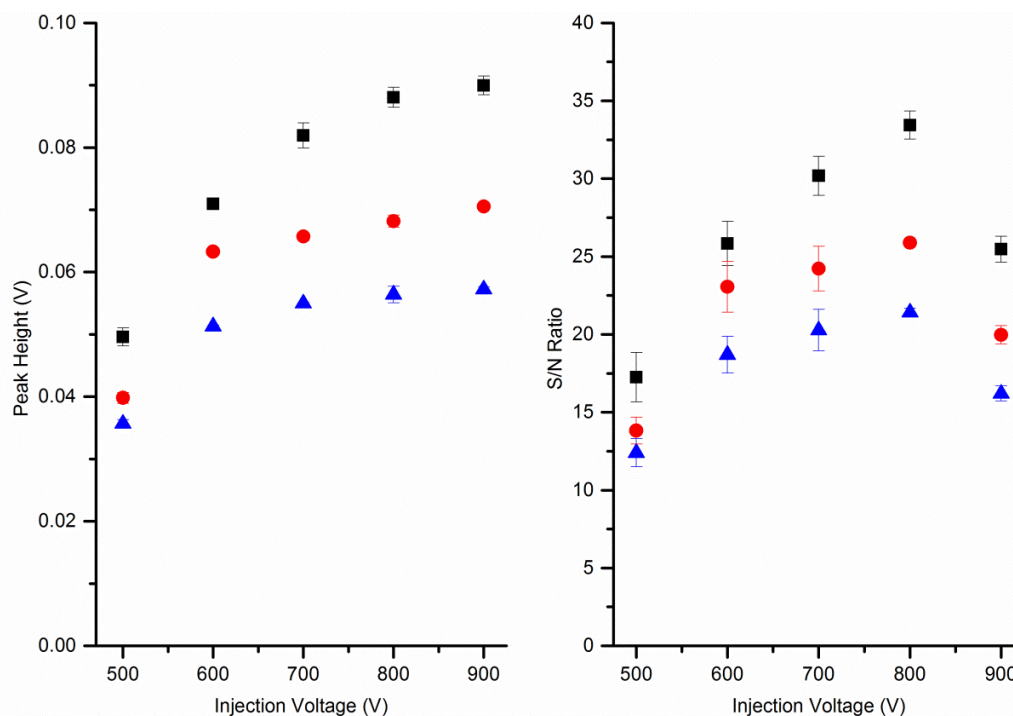Increasing the electrokinetic injection time progressively from 2.5 s to 10 s was associated with an increase in the peak heights for K^+, Na^+ and Li^+. Increasing further beyond 10 s to 12.5 s did not result in any further significant increase in the peak heights obtained for the three cations (Figure 34). The same increasing trend was also observed for the S/N ratios of the three cations between 2.5 s and 10 s. However, increasing the electrokinetic injection time to 12.5 s resulted in significantly reduced S/N values for each of the cations, similar to those observed for the 7.5 s injection time (Figure 34). The associated increase in both peak heights and S/N ratios between 2.5 s and 10 s with increasing electrokinetic injection times was a result of extra time allowing for a sequentially more concentrated sample plug being injected for electrophoretic separation. The plateau in peak height and significant drop off in S/N ratio observed for the 12.5 s electrokinetic injection time occurred as the optimum injection time had been exceeded. This resulted in broader cation peaks (see Figure 33) and an increased background noise level, both of which are unfavourable for sensitive and efficient separation and detection of analytes. As a result of this investigation it was decided to perform further experiments with an optimised electrokinetic injection time of 10 s.

3.4.4.3 Optimisation of background electrolyte (BGE) concentration

To achieve optimum detection the effect of using the BGE concentrations 10, 15 and 20 mM on the performance of the C^4D system was explored by separating a 0.5 mM K^+, Na^+

and Li$^+$ sample using an excitation voltage of 5 V$_{p-p}$ and frequency of 220 kHz. The optimum electrophoresis conditions determined in preceding sections were used for this study. In order to determine the optimum BGE concentration the resulting electropherograms and subsequent analytical performance were evaluated. Representative electropherograms obtained using each of the BGE concentrations are shown in Figure 35.
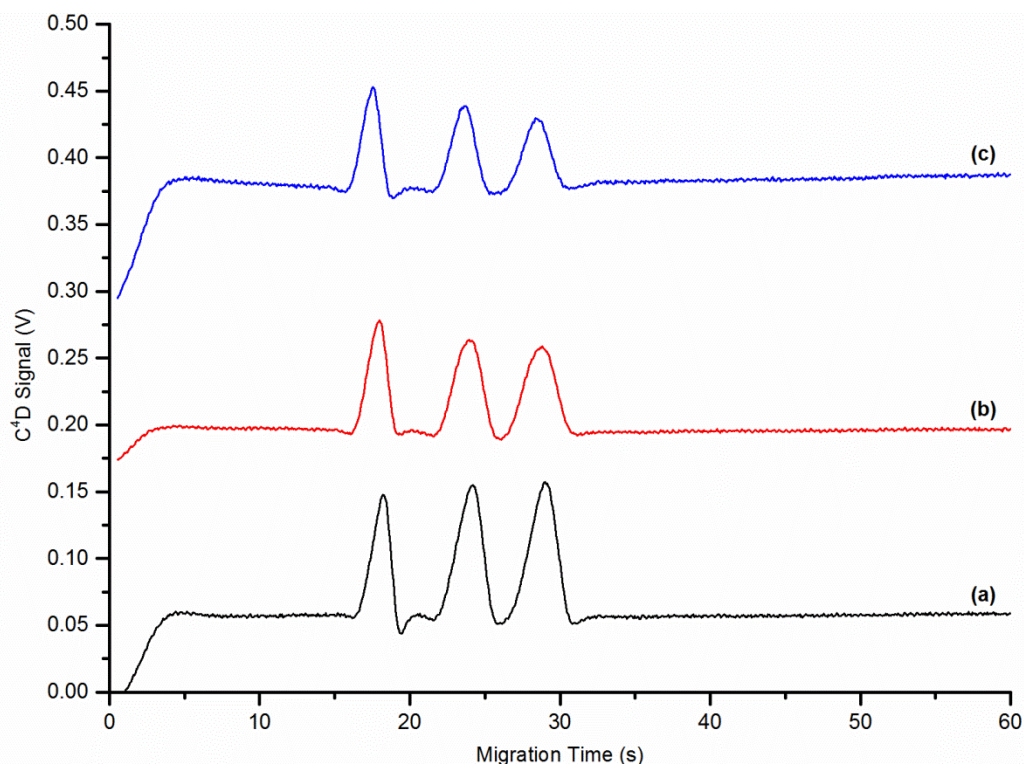
Figure 35 **Optimisation of BGE concentration**

Offset electropherograms obtained using BGE concentrations (a) 10 mM, (b) 15 mM and (c) 20 mM

Figure 35 shows baseline resolution was achieved for all analyte peaks using all three BGE concentrations trialled. Further, no significant change in the migration time was observed for the K$^+$, Na$^+$ and Li$^+$ peaks with the relative standard deviations (%RSD) for each over all replicates (n=8) calculated to be 1.4, 1.2 and 1.1 respectively. To determine the optimum BGE concentration in terms of analytical performance the peak height and S/N ratio of each of the ions was determined. For this analysis four sample runs were performed in duplicate (n=8) at each BGE concentration and the resulting peak heights and S/N ratios are presented in Figure 36 and Figure 37 respectively along with their associated standard deviations (n=8).
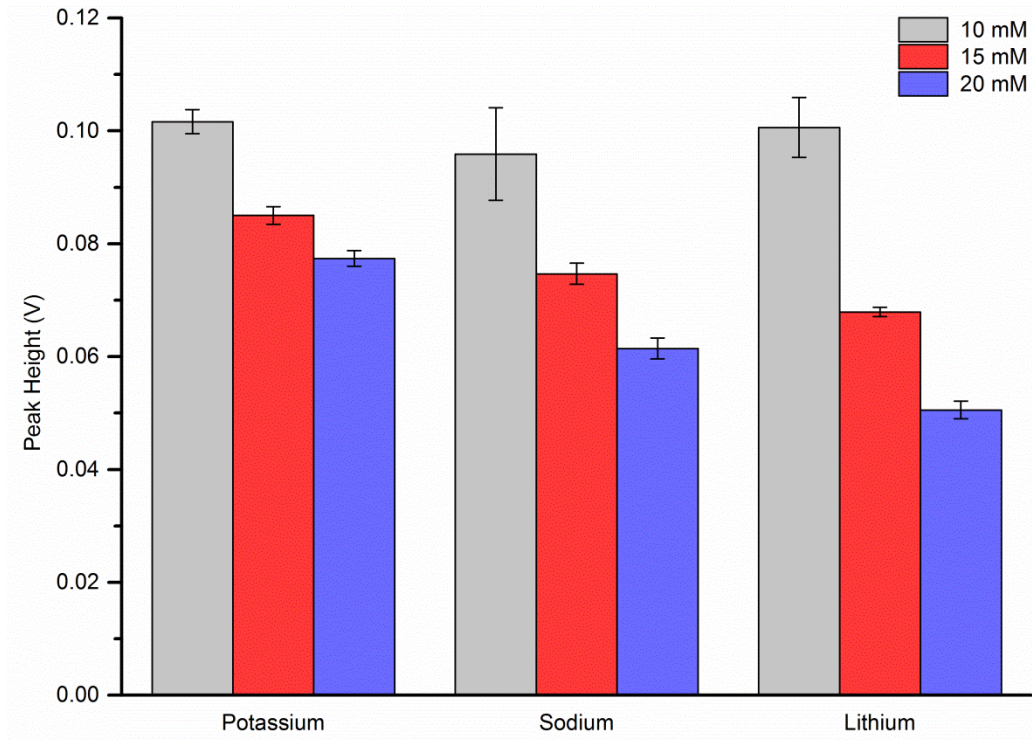
Figure 36   **Effect of BGE concentration on model analyte peak height**

Effect of BGE concentration on the peak heights of Li^+, Na^+ and K^+ peaks (0.5 mM)
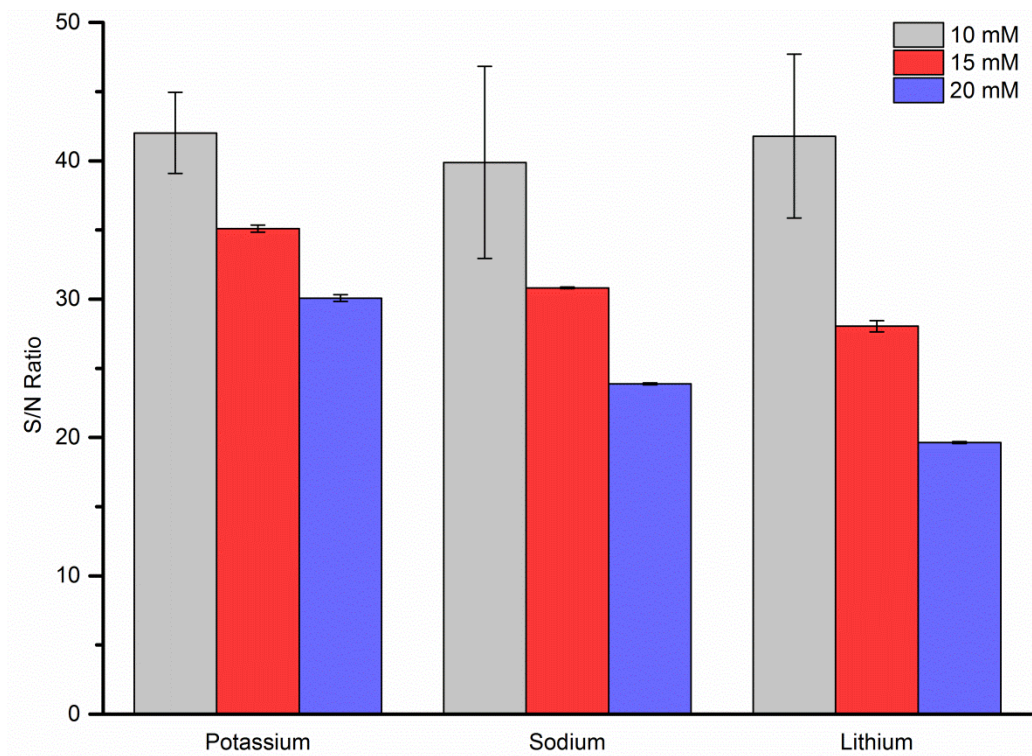
Figure 37   **Effect of BGE concentration on model analyte S/N ratio**

Effect of BGE concentration on the S/N ratios of Li^+, Na^+ and K^+ peaks (0.5 mM)

As the concentration of BGE was increased from 10 mM to 20 mM both the peak heights and S/N ratios for each of the K^+, Na^+ and Li^+ were observed to decrease (Figure 36 and Figure 37). Despite 10 mM BGE producing the largest peak height and S/N values the reproducibility obtained was significantly poorer than for 15 mM and 20 mM BGE, as is evidenced by the large standard deviations, for all analytes, in both Figure 36 and Figure 37. Furthermore, the use of 10 mM BGE resulted in a change in the ratio of the peak heights (Figure 36) which could have arisen due to the poor reproducibility mentioned. For these reasons the 10 mM BGE was considered unsuitable for analysis of the model analytes in the current system. The reproducibility of both the 15 mM and 20 mM BGE was observed to be much better. The standard deviations for each analyte over the duplicate analyses (n=8) for the 15 mM BGE peak heights were calculated to be 1.6×10^{-3} V, 1.9×10^{-3} V and 8.5×10^{-4} V for K^+, Na^+ and Li^+, respectively, while for the 20 mM BGE they were calculated to be 1.4×10^{-3} V, 1.8×10^{-3} V and 1.6×10^{-3} V for K^+, Na^+ and Li^+ respectively. Taking into consideration the presented data the 15 mM BGE was chosen for all further optimisation experiments as it gave the best peak heights and S/N ratios without compromising reproducibility.

3.4.5 Analytical repeatability of optimised electrophoresis procedure

Analytical methodologies and instrumentation need to be able to perform replicate analyses with a high degree of repeatability in order to report quantitative results. A traditional way of determining both the precision and repeatability of an electrophoretic analytical method is to calculate the percentage relative standard deviation (%RSD) of migration times and peak heights. The %RSD can be calculated using Equation 9 where s is the standard deviation and X is the mean of the data set.

Equation 9   **Calculation of the percentage relative standard deviation (%RSD)**

$$\%\text{RSD} = \frac{s}{X} \text{ x } 100\%$$

A higher percentage indicates a larger degree of variability in the data set, whereas a lower percentage indicates a lower variability. Percentages below 5% are considered highly repeatable and acceptable for quantitative analytical determination of standard concentrations.

To evaluate the overall analytical detection performance of the optimised electrophoresis procedure a sample comprising 5×10^{-4} M of the model analytes K^+, Na^+ and Li^+ was analysed. The intra-day and inter-day repeatability of analysis were determined by

relative standard deviations (%RSD) of migration times and peak heights. Both the intra-day and inter-day repeatability are important measures as the ability to perform consistent analysis over a number of days on the same microchip is advantageous. The intra-day repeatability of migration time and peak height for each analyte was determined by performing repeat analyses (n = 30 over a single day) of the same sample using the optimised standard protocol. Whereas the inter-day repeatability of migration time and peak height for each analyte was determined by performing repeat analysis (n = 5) on the same microchip over a five day period using the optimised standard protocol. The %RSDs obtained for both the intra-day and inter-day analyses are presented in Table 7.

Table 7   **Repeatability of the optimised electrophoresis procedure**

Analyte	Migration time %RSD		Peak height %RSD	
	Intra-day	Inter-day	Intra-day	Inter-day
K+	0.9	2.9	1.6	1.0
Na+	1.2	3.4	2.1	2.2
Li+	1.1	3.9	2.5	2.6

All determined %RSD values for intra and inter-day analyses were below 4% (see Table 7). A small increase in the %RSD for migration times was observed for the inter-day analysis compared to the intra-day. This was due to the migration times increasing slightly over the five day period which was attributed to the build-up of the surfactant modification on the PDMS surface employed to achieve a more stable electroosmotic flow. However, these values were still below 4% and were more than acceptable. The inter-day %RSDs for peak heights were better, in the case of K^+, or virtually unchanged when compared to the intra-day analysis. These values reflect the excellent repeatability of the optimised electrophoresis procedure for quantitative on-chip analysis.

3.5   Concluding remarks

The optimisation of electrophoresis conditions for the PDMS microchip with injected gallium electrodes has been shown. Stable electro-osmotic flows (μEOF) of 2.00 ± 0.11 x 10^{-4} cm^2 V^{-1} s^{-1} were achieved via an intermittent dynamic surfactant modification of the microchannel surfaces using an optimised solution of 15 mM MES/His BGE with 0.4 mM DDM. The μEOF repeatability (%RSD) using this approach was determined over three days to be 5.3 (n=15). Further, the optimised electrophoresis BGE, separation and injection conditions were as follows; BGE contained 15 mM MES/His, separation voltage: 1400 V, electrokinetic injection voltage: 800 V and an electrokinetic injection time: 10 s. The analytical repeatability of the optimised electrophoresis method was evaluated by determining the intra-day and inter-day %RSD of both migration time and peak height for the three model analytes K$^+$, Na$^+$ and Li$^+$. The intra-day %RSDs for migration time and peak height were below 1.2 and 2.5 respectively for all analytes. The inter-day %RSDs for migration time and peak height were below 3.4 and 2.6 respectively for all analytes. These results indicated the suitability of the optimised PDMS microchip electrophoresis method for analytical applications. In the proceeding chapter the developed method is used for the optimisation of the novel injected gallium electrode system.

4. Optimisation of Injected Gallium Electrode Parameters for C^{4}D

4.2   Chapter overview

Capacitively coupled contactless conductivity detectors require careful optimisation of operating conditions in order to achieve the best overall analytical performance of the device [226-227]. Here, a comprehensive study into i) electrode orientation (configuration), ii) distance between electrodes and the separation microchannel and iii) electrode length is presented for the developed injected electrode system. Furthermore, the optimised parameters are then used to determine instrument detection limits for each of the model analytes sodium, lithium and potassium ions.

4.1   Introduction

Lab-on-a-Chip (LOC) production has been significantly propelled by the development of simple, low cost fabrication techniques. One of the most prominent of these techniques is the use of poly(dimethylsiloxane) (PDMS) for producing microchannel networks from structured templates using photolithography for device fabrication [6]. Despite significant research over the last decade into such devices, very few have transcended to commercial production [13, 107-108]. This is a result of a number of limiting factors in producing commercially viable LOC systems. These arise from the complex fabrication processes required to integrate commonly utilised detection systems, such as fluorescence and electrochemical techniques, with the microchip [108-110].

Capacitively coupled contactless conductivity detection (C^{4}D) and its integration with microchip technologies has been the subject of multiple reviews [108, 156, 158]. The detection technique utilises integrated conductive electrodes, most commonly in the form of metal, to continuously monitor the conductivity of a solution moving through a microchannel. A number of approaches for integrated contactless electrodes in LOC devices have been reported. These include the fabrication of microfluidic chips on top of printed circuit boards [151, 161, 228-229] and glass wafers [162] containing microscale electrodes. Alternative methods have mounted the electrodes in external housings [167-168] and others have reported the deposition of metal layers onto previously etched glass wafer surfaces to form electrodes in the same plane as the analysis channels [170-171]. Each of these methods have practical limitations including multi-step patterning/fabrication processes often requiring specialised equipment and/or difficulty in consistently aligning the detection electrodes with the microchannel. Furthermore, these fabrication techniques are often time consuming, for example Henderson *et al.* reported the production of laser-patterned polymer electrodes that required a 20 h timeframe to complete [172]. All of these limitations have the potential to impact on analytical performance due to fabrication reproducibility or increase the overall time and cost associated with device production [169].

An alternative approach for the fabrication of LOC devices with integrated contactless electrodes is to use injected molten metal. Injected metal electrodes have been demonstrated in microfluidic applications for the production of in-plane on-chip electromagnets [173] and on-chip microplasma patterning of PDMS microchannels [174]. More recently, this approach has been used to produce electrodes which are in direct contact with fluid in microchannels for mixing [175] and neural stimulation [176] applications. Injected molten metal electrodes have the advantage that both electrode and analysis microchannels are patterned in the same lithographic process, whereby the electrode design is incorporated directly onto the mask template. This allows precise

micron-scale electrode designs that can be simply and easily tailored to the microfluidic device under construction. Once the device has been assembled, the molten metal is then injected into the required microchannel where it either remains molten or solidifies to form a solid electrode. Substrates for molten metal electrodes include relatively low melting point alloys such as molten solder (In 52 %, Sn 48 % m.p $\approx$117 ^{o}C) [173], eutectic gallium indium (Ga 75 %, In 25 % by weight m.p $\approx$ 15.7 ^{o}C) [175-176] and indium alloy (In 51 %, Bi 32.5 %, Sn 16.5 % by weight m.p $\approx$ 60 ^{o}C) [175]. The use of pure gallium (m.p 29.8 ^{o}C) as an electrode material has been shown to be preferable over low melting point alloys due to its low toxicity, relatively low melting point and ease of handling [174-176]. Despite its confirmed simplicity, the use of injected metal electrodes for C^{4}D detection on LOC devices has yet to be reported.

This chapter focuses on studies into the optimisation of physical electrode parameters of the in-plane injected gallium electrode C^{4}D system. Particularly, detailed investigations of the optimisation of i) electrode geometry, ii) electrode distance from separation microchannel and iii) electrode length are reported.

4.3 Experimental

4.3.1 Instrumentation

All experiments in this chapter were performed using the purpose designed microchip electrophoresis instrument with injected gallium electrodes for capacitively coupled contactless conductivity detection as described previously in Chapter 2. In order to evaluate and optimise the electrode parameters of geometry, length and distance from analysis microchannel a number of microchips were fabricated with varying electrode microchannel design features depending on the parameter under optimisation. Each of the microchip designs used in this study are outlined in Table 8. The C⁴D design parameters held constant throughout all optimisation experiments included the placement of the detection cell at 37 mm from the separation/injection channel cross over and a 1 mm distance between transmitting and receiving electrodes along the separation microchannel.

Table 8   **List of microchip design parameter variables**

Used to optimise the C⁴D injected electrode parameters geometry, length and distance from analysis microchannel

Optimisation Parameter	Geometry	Length (µm)	Distance from analysis microchannel (µm)
Geometry microchip 1	Quad (4-electrode)	1000	75
Geometry microchip 2	Parallel	1000	75
Geometry microchip 3	Anti-parallel	1000	75
Electrode length microchip 1	Anti-parallel	500	75
Electrode length microchip 2	Anti-parallel	750	75
Electrode length microchip 3	Anti-parallel	1000	75
DFAM microchip 1	Anti-parallel	1000	50
DFAM microchip 2	Anti-parallel	1000	75
DFAM microchip 3	Anti-parallel	1000	100

At each variation of the physical electrode parameters investigated the C⁴D excitation signal employed was sinusoidal. Optimisation of the peak to peak voltage and frequency of the excitation signal was performed for each design variation.

4.3.2 Chemicals

Unless otherwise specified, all chemicals were of analytical grade, purchased from Sigma-Aldrich (Australia) and used as received. Background electrolyte solutions for electrophoretic separations were prepared by dissolving 2-(N-morpholino)ethanesulphonic acid (MES) (15 mM) and histidine (His) (15 mM) in Milli-Q water (18.2 MΩ cm). Sample stock solutions (100 mM) of aqueous lithium, sodium and potassium ions were prepared by dissolving their chloride salts in Milli-Q water (18.2 MΩ cm). Working standards (0.1 mM – 1 mM) of lithium, sodium and potassium ions were prepared by dilution of the stock solutions in MES/His background electrolyte. All solutions were degassed by ultrasonication prior to use.

4.3.3 Electrophoresis procedure

Electrophoretic separations were performed in PDMS microchips using the optimised conditions determined in Chapter 3. Specifically, the microchips were first flushed with Milli-Q water for 2 min followed by BGE solution (15 mM) with n-dodecyl β-D-maltoside (DDM) (0.4 mM) for a further 20 min. After flushing, all reservoirs were filled with the running buffer solution (15 mM BGE). The microchip was rinsed with both the BGE containing DDM and running buffer between analysis runs to ensure reproducibility and maintain a stable baseline. The buffer and sample solutions were dispensed into the respective reservoirs using a fixed volume of 25 µL. Sample introduction was performed electrokinetically using a voltage of 800 V applied to the sample reservoir (S) for 10 s, whilst sample waste (SW) was grounded and BGE (B) and BGE waste (BW) reservoirs were floated. Separations were performed by applying a voltage of 1400 V to the B reservoir (anode) for 60 s whilst the BW (cathode) was grounded and S and SW were floated, producing a cathodic EOF. Voltage switching was carried out by the custom designed LabVIEW® program outlined in Chapter 2.

4.3.4 Excitation frequency and voltage optimisation procedure

The determination of optimum electrode frequency and voltage involved the repetitive separation of a mixed standard (0.5 mM) of the model analyte system (lithium, sodium and potassium ions) using the electrophoresis procedure outlined in Section 4.3.3 above. Optimum values for both excitation frequency and voltage were determined by evaluating the peak heights and S/N ratios of the three model analytes sodium, lithium and potassium ions. Initially, the frequency of the transmitting electrode was set at 100 kHz. This was increased by 20 kHz for each subsequent separation up to 300 kHz. For voltage optimisation experiments, the initial excitation voltage varied depending on the electrode configuration under investigation. The voltage was then steadily increased for each subsequent separation until the maximum level, allowed by the electronic setup (without saturating the detector), was reached.

4.3.5 Model analyte calibration experiments

Evaluation of the optimised C^{4}D electrode parameters was conducted by performing an external calibration of the model analytes lithium, sodium and potassium. Standard curves for all analytes were obtained by injecting (in triplicate) four working standards containing Li$^+$, Na$^+$ and K$^+$ at concentration levels ranging from 0.1 to 0.7 mM with final standard concentrations determined gravimetrically (Table 9). Each standard was analysed using the optimised C^{4}D injected gallium electrode system, outlined in this chapter and previously optimised electrophoresis conditions (Chapter 3). The analyte peak areas from the resulting electropherograms were determined and plotted versus analyte concentration. A linear regression was performed on the standard curve using the least-squares method and the obtained regression equations were used to estimate the limits of detection (LOD) and limits of quantification (LOQ) for each analyte. Peak integration and statistical analysis were carried out with the software OriginPro 9.0 (OriginLab, Northhampton, MA, USA).

Table 9   **Concentration ranges used for model analyte calibration**

Standard	Concentration (mM)			Gravimetrically determined concentration (mM)		
	Li$^+$	Na$^+$	K$^+$	Li$^+$	Na$^+$	K$^+$
1	0.10	0.10	0.10	0.11	0.11	0.11
2	0.30	0.30	0.30	0.31	0.30	0.31
3	0.50	0.50	0.50	0.51	0.51	0.51
4	0.70	0.70	0.70	0.71	0.70	0.71

4.4 Results and discussion

4.4.1 Optimisation of electrode geometry

Detection electrode geometry is an important consideration when designing and implementing new C^4D systems. This is because electrode geometry can have a significant impact on both the level of signal attenuation (coupling) through the fluid in the microchannel and the amount of stray capacitance between the transmitting and receiving electrodes. Traditionally, three different electrode configurations have been utilised for microchip C^4D. These are four-electrode (quad), two-electrode parallel or two-electrode anti-parallel (shown in Figure 38). Most commonly two-electrode anti-parallel configurations are implemented for microchip C^4D analysis [156]. However, four-electrode systems have recently been shown to produce more sensitive integrated C^4D systems on microfluidic chips, due to the increased signal attenuation capability permitted as a result of the extra transmitting and receiving electrode present [167, 169].
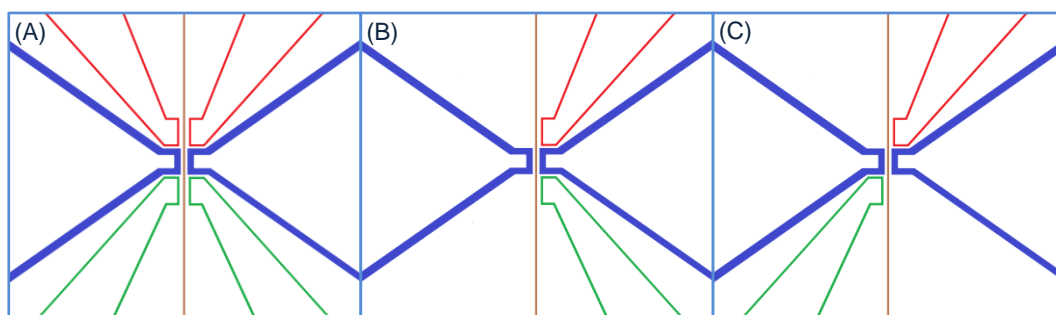
Figure 38   **Schematic of injected gallium electrode geometries**
Illustrating (A) four-electrode (quad), (B) two-electrode parallel and (C) two-electrode anti-parallel with transmitting electrodes (−), receiving electrodes (−), grounded shielding plates (−) and analysis microchannel (−)

In order to determine the optimum geometry for the developed injected gallium electrode system, the three electrode orientations quad, parallel and anti-parallel (Figure 38) were investigated for their effect on the analytical performance of the C^4D system. As described previously (Chapter 3) analytical performance was evaluated by comparing the peak heights and S/N ratios obtained for electrophoretically separated lithium, sodium and potassium cations. For this study a constant electrode length (100 μm) and electrode distance from analysis microchannel (75 μm) was utilised for each of the configurations.

For reliable operation, contactless conductivity detection requires careful optimisation of the excitation voltage and excitation frequency of the input signal (from the transmitting electrode) to achieve the best analytical performance possible [226, 230]. Optimum values for these variables are dependent on both the electronic setup of the C^4D system

and the geometry and layout of the integrated metal electrodes. As the electronic setup of the presented system was held constant throughout all experimental work, optimisation of the excitation frequency and voltage were only considered when altering electrode design parameters. Initially the excitation frequency and voltage of the three electrode geometries was optimised to allow accurate evaluation of the analytical performance of each. The first geometry investigated was the four-electrode quad design and the peak heights and S/N ratios obtained at the different frequencies and voltages trialled are presented in Figure 39 and Figure 40.

As evidenced in Figure 39, low input excitation frequencies result in a decreased signal response as the impedance of the microchannel wall is relatively high; leading to only a small current passing into the electrolyte inside the microchannel [226]. In contrast, at high frequencies the signal can be influenced by both increased stray capacitance and, in certain cases, poorer performance of the current to voltage convertor. Both of these factors account for the trend of increasing peak heights and S/N ratios upon increasing the excitation frequency up to a maximum optimum value followed by decreasing values beyond the optimum as observed in Figure 39. Further, it has been reported that that increasing excitation voltages in microfluidic C^{4}D systems can result in improved analytical performance [170, 226]. However, in the presented system, at high excitation voltages the associated high level of stray capacitance results in an increased background current that overloads the feedback resistor, resulting in the complete loss of signal. This effectively imposed a maximum excitation voltage which must be determined for each electrode design implemented.

On analysis of the peak data presented in Figure 39, the maximum peak heights and S/N ratios for the lithium, sodium and potassium cations were obtained using an excitation frequency of 220 kHz. Furthermore, the maximum peak heights and S/N ratios for all three cations were achieved using an excitation voltage of 1.5 V (Figure 40). Beyond 1.5 V no signal response was recorded due to the limitations of the feedback resistor outlined. Therefore, it was determined that an excitation signal with a voltage of 1.5 V and a frequency of 220 kHz was the optimum for the injected gallium electrode system in quad configuration.
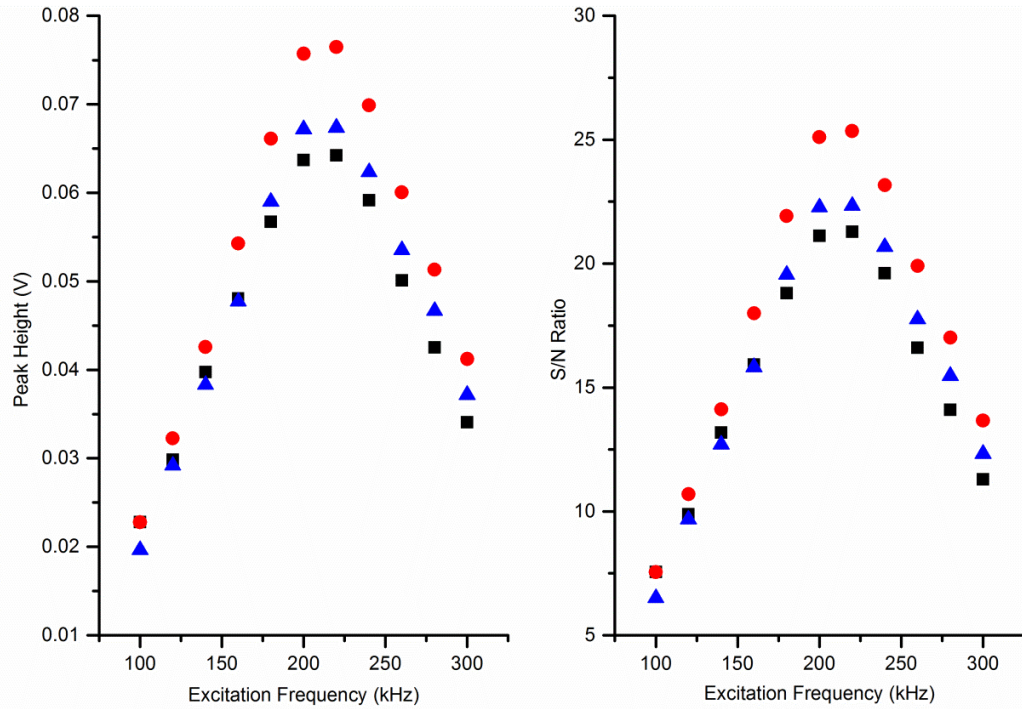
Figure 39   **Effect of excitation frequency on model analyte peaks using quad geometry**

Effect of excitation frequency on the peak height and S/N ratio of Li⁺ (−▲−), Na⁺ (−●−) and K⁺ (−■−) peaks (0.5 mM) obtained using injected gallium electrodes in quad geometry with an excitation voltage of 1.5 V
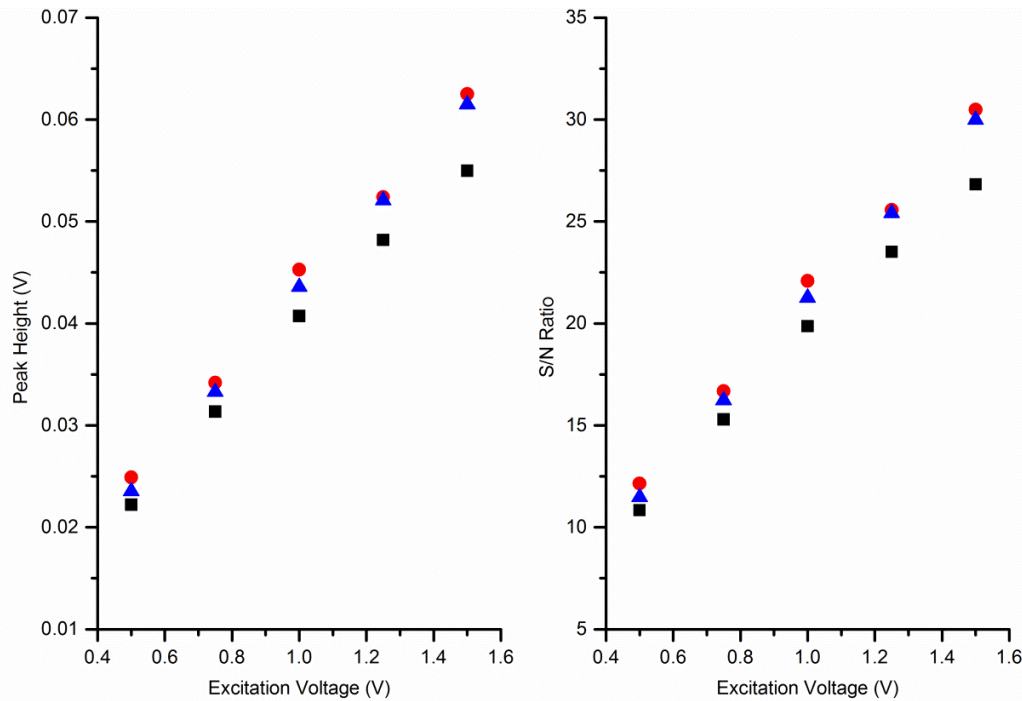
Figure 40   **Effect of excitation voltage on model analyte peaks using quad geometry**

Effect of excitation voltage on the peak height and S/N ratio of Li⁺ (−▲−), Na⁺ (−●−) and K⁺ (−■−) peaks (0.5 mM) obtained using injected gallium electrodes in quad geometry with an excitation frequency of 220 kHz

To allow accurate comparison of the three electrode geometries under investigation, the optimum excitation frequency and voltage of the remaining two electrode configurations (parallel and anti-parallel) were determined. The frequency optimisation data for the parallel and anti-parallel geometries displayed the same general trend and optimum value (220 kHz) as the quad geometry (see Appendix). One exception to this was observed to be the lithium peak data for the anti-parallel electrodes, which showed maximum peak height and S/N ratio values at an excitation frequency of 200 kHz. However, as this was against the trend observed for all other frequency optimisation plots it was considered an anomaly and an optimised excitation frequency of 220 kHz was chosen for the anti-parallel geometry as well.

The excitation voltage optimisation peak height and S/N ratio analysis plots for parallel and anti-parallel electrode geometries are presented in Figure 41 and Figure 42 respectively. In the case of the parallel electrode geometry, considering the peak data presented in Figure 41, the largest peak heights and S/N ratios for the lithium, sodium and potassium cations were obtained using an excitation voltage of 4.5 V. However, for the anti-parallel electrode geometry, considering the peak data presented in Figure 42 the optimum excitation voltage for all three cations was 5.5 V. The optimised input signal parameters determined for each of the three electrode geometries investigated are summarised in Table 10 and were used for all further experiments.
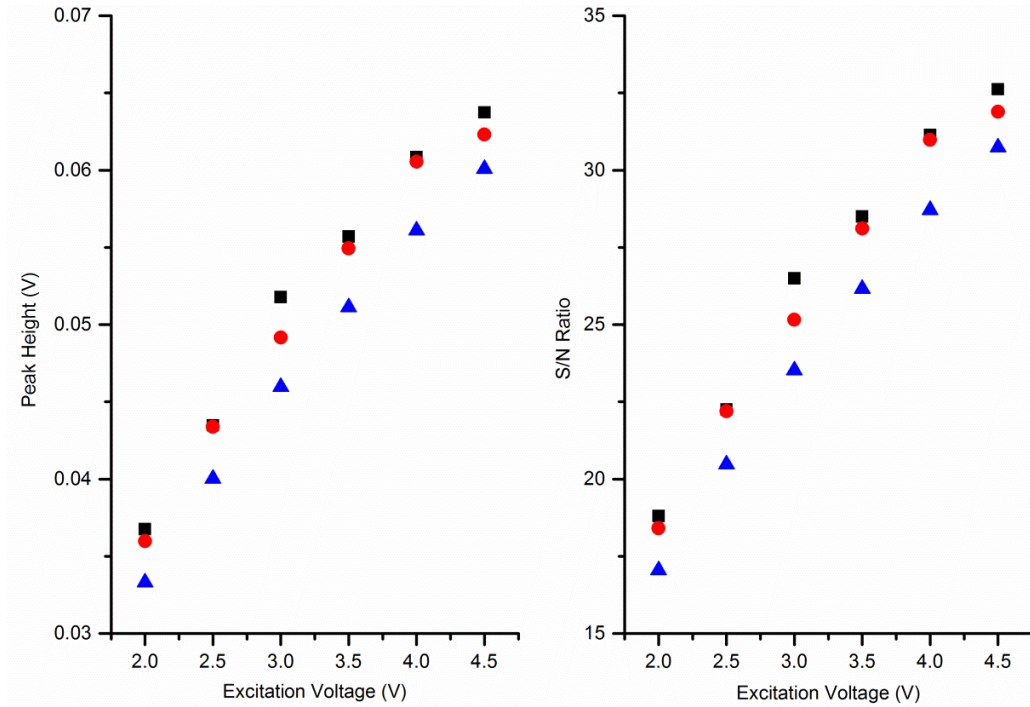
Figure 41   **Effect of excitation voltage on model analyte peaks using parallel geometry**

Peak heights and S/N ratios of Li$^+$ (−▲−), Na$^+$ (−●−) and K$^+$ (−■−) peaks (0.5 mM) obtained using injected gallium electrodes in parallel geometry with an excitation frequency of 220 kHz
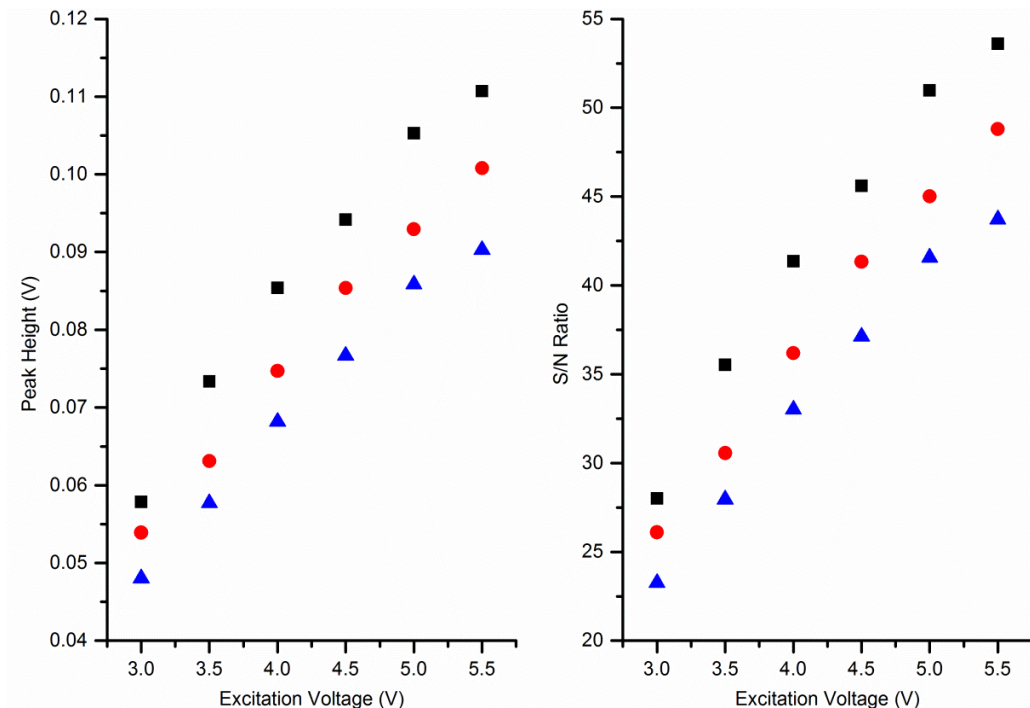
Figure 42   **Effect of excitation voltage on model analyte peaks using anti-parallel geometry**

Peak heights and S/N ratios of Li$^+$ (−▲−), Na$^+$ (−●−) and K$^+$ (−■−) peaks (0.5 mM) obtained using injected gallium electrodes in anti-parallel geometry with an excitation frequency of 220 kHz

Table 10   **Optimised input signal parameters for each electrode geometry**

Geometry	Optimised excitation frequency (kHz)	Optimised excitation voltage (V)
Quad	220	1.5
Parallel	220	4.5
Anti-parallel	220	5.5

To determine which of the three electrode geometries provided the best overall analytical performance the optimised input signal parameters for each were used to perform multiple analyses of a lithium, sodium and potassium cation standard (0.5 mM). More specifically, each electrode geometry was evaluated by performing three separate analyses, of three replicates each (n = 9), of the same cation standard over the course of a single day. The resulting mean peak heights and S/N ratios with their associated standard deviations using each of the electrode geometries is presented in Figure 43 and Figure 44 respectively.
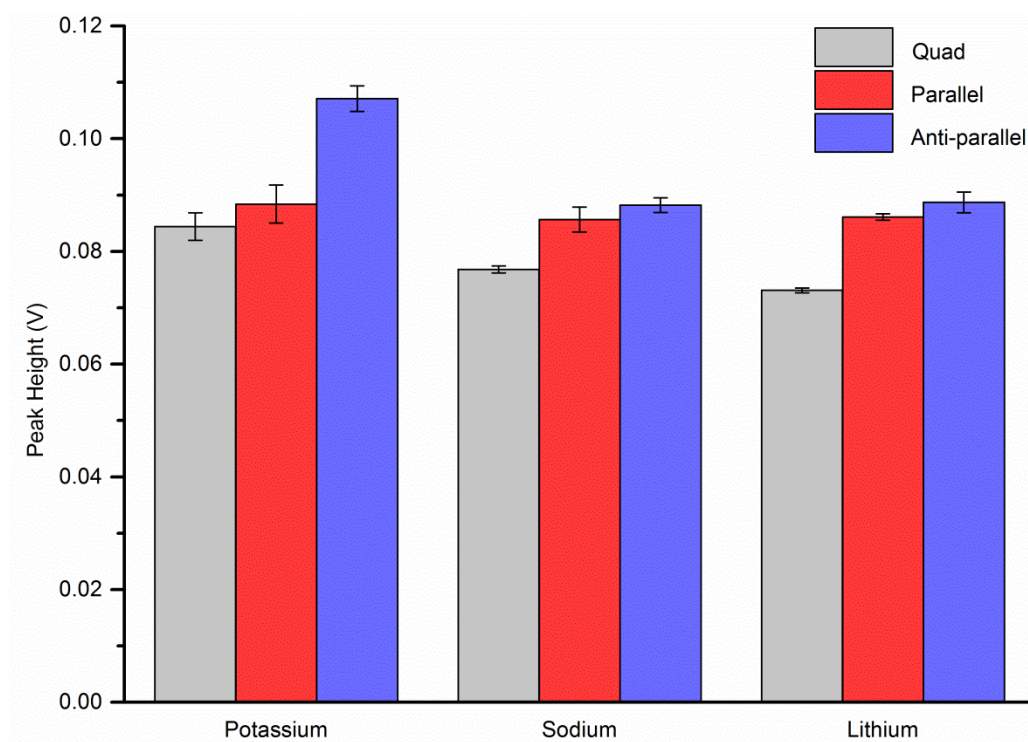
Figure 43   **Comparison of mean analyte peak heights**

Obtained using injected gallium electrodes in quad, parallel and anti-parallel geometries
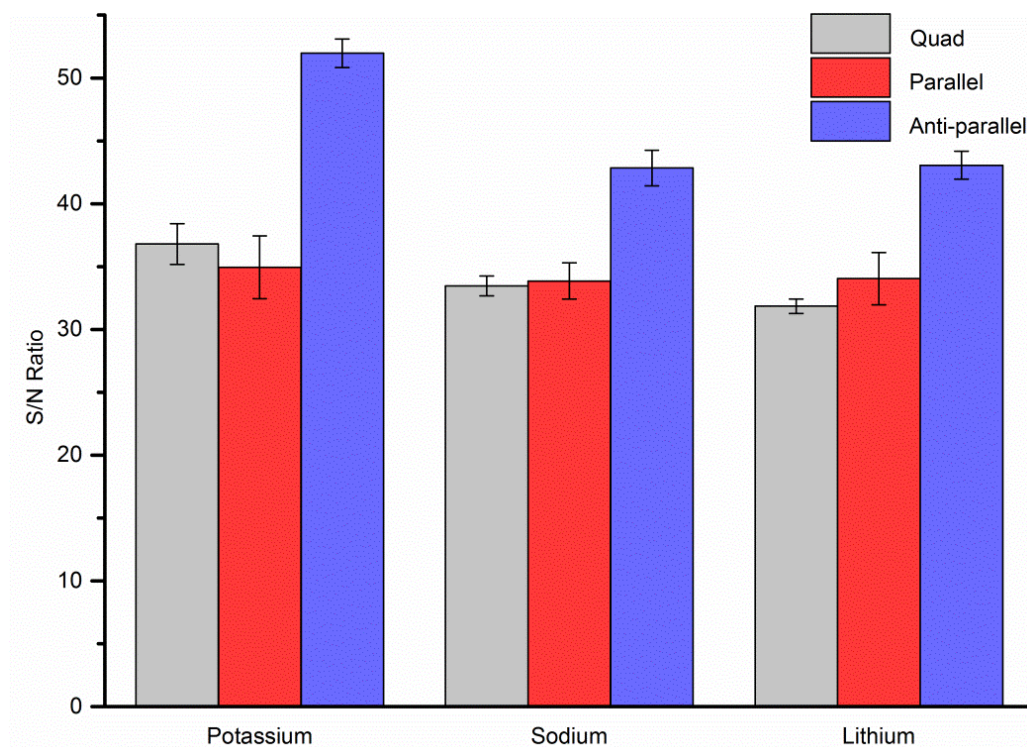
Figure 44   **Comparison of mean analyte peak S/N ratios**

Obtained using injected gallium electrodes in quad, parallel and anti-parallel geometries

Of the three electrode geometries trialled the largest mean peak heights for all three analytes were achieved using anti-parallel C^{4}D electrodes (Figure 43). In the case of potassium a significant difference between the peak heights of anti-parallel electrodes and parallel (0.019 V) and quad (0.023 V) electrodes was observed. Whereas for both sodium and lithium analytes the difference in peak heights between anti-parallel and parallel electrodes was less pronounced (0.0025 V and 0.0026 V respectively) but again dropped away significantly using quad geometry. A similar trend was observed for the mean S/N ratio of each analyte using the three geometries. Anti-parallel electrodes gave a superior S/N ratio for all analytes, whereas both parallel and quad electrodes gave significantly lower S/N values. The distinctly larger peak heights and S/N ratios observed for the anti-parallel injected gallium electrodes indicated that they offered the most superior analytical performance of the three geometries trialled.

The decreased values observed for both quad and parallel geometries was likely a result of higher background noise present using these setups. The enlarged background was caused by an associated increase in stray capacitance using these geometries. This increase in stray capacitance using the four electrode quad system resulted from the enhanced direct coupling that arose from the additional transmitting and receiving electrodes in this design. In contrast, the parallel electrode geometry placed singular

transmitting and receiving electrodes on the same side of the separation microchannel. This brought both electrodes closer to one another which decreased the effectiveness of the grounded shielding between them and gave rise to an increased stray capacitance. The hypothesis of quad and parallel electrodes allowing a greater level of stray capacitance is further supported by the previous experiments to determine the optimum input signal excitation voltage for each geometry. Due to constraints previously explained the maximum excitation voltage was determined to be 1.5 V, 4.5 V and 5.5 V for quad, parallel and anti-parallel electrodes respectively. The lower maximum excitation voltage observed for quad and parallel electrodes suggested more direct coupling, as a result of stray capacitance between transmitting and receiving electrodes, was present in these designs. Therefore, given electrodes in anti-parallel geometry were found to provide superior analytical performance all subsequent optimisation experiments were performed using this geometry.

4.4.2   Optimisation of electrode distance from separation microchannel

The sensitivity of C^{4}D systems is heavily dependent on the magnitude of the distance between the electrodes and the separation microchannel, otherwise known as the dielectric layer (Figure 45). Analytical performance in C^{4}D is known to decrease with increasing thickness of the dielectric [231-232]. Typical minimum thicknesses reported for C^{4}D microdevices incorporating electrodes in the same plane as the sample microchannel range from 0.1 μm to 40 μm [156]. In addition, the dielectric needs to be thick enough to electrically insulate the electrodes to ensure contactless mode capacitive measurement. This translates to the ideal dielectric being the minimum value that can effectively insulate the electrodes from the sample mixture.

electrode to separation
microchannel channel distance
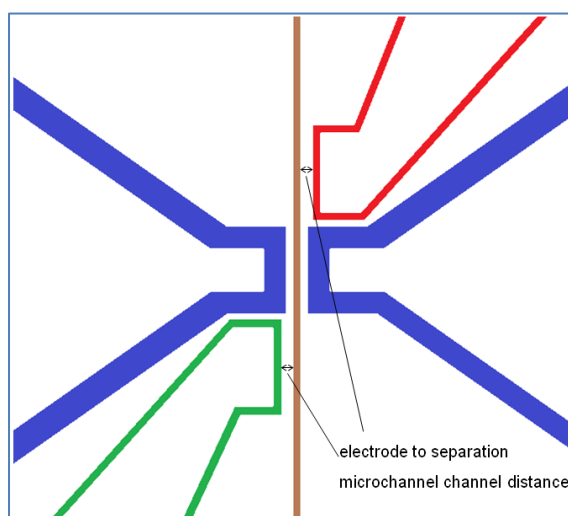
Figure 45   **Illustration of the electrode distance from separation channel parameter**

In the case of the in-plane injected gallium electrode C^{4}D system the dielectric thickness relates directly to the distance between the electrodes and the separation microchannel. Therefore, at reduced distances the dielectric thickness of the insulating PDMS layer is smaller. In the present system, the minimum distance between the injected gallium electrodes and separation microchannel is dictated by the limitation of using soft lithographic techniques to fabricate the PDMS microchips. A minimum distance of 50 μm was required to ensure the integrity of the bonding between the two PDMS sheets was not compromised. Therefore, in this investigation the distances between the electrode and separation channel used to determine the effect of this parameter were 50, 75 and 100 μm. As for electrode geometry experiments initially the excitation frequency and voltage of the three distances was optimised to accurately evaluate the analytical performance of each. The first distance investigated was 50 μm and the peak heights and S/N ratios obtained at the different frequencies and voltages trialled are presented in Figure 46 and Figure 47.

Evaluating the peak data presented in Figure 46, the same general trend as seen for the electrode geometry experiments was observed upon increasing the excitation frequency sequentially by 20 kHz. Both the peak height and S/N ratio was seen to increase as the excitation frequency was increased up to a maximum optimum value before decreasing at a similar rate beyond the optimum parameter. The maximum analyte peak heights and S/N ratios were achieved using an excitation frequency of 220 kHz. Further, the maximum peak heights and S/N ratios for all three cations were achieved using an excitation voltage of 3.5 V (Figure 47). Beyond 3.5 V no signal response was recorded due to the limitations of the signal-to-voltage converter previously explained. Therefore, it was determined that an excitation signal with a frequency of 220 kHz and a voltage of 3.5 V was the optimum for the anti-parallel injected gallium electrode system with an electrode to separation microchannel distance of 50 μm.

Figure 46   **Effect of excitation frequency on model analyte peaks using a 50 μm gap**

Peak heights and S/N ratios of Li⁺ (−▲−), Na⁺ (−●−) and K⁺ (−■−) peaks (0.5 mM) obtained using injected gallium electrodes with an electrode distance from separation microchannel of 50 μm and an excitation voltage of 3.5 V
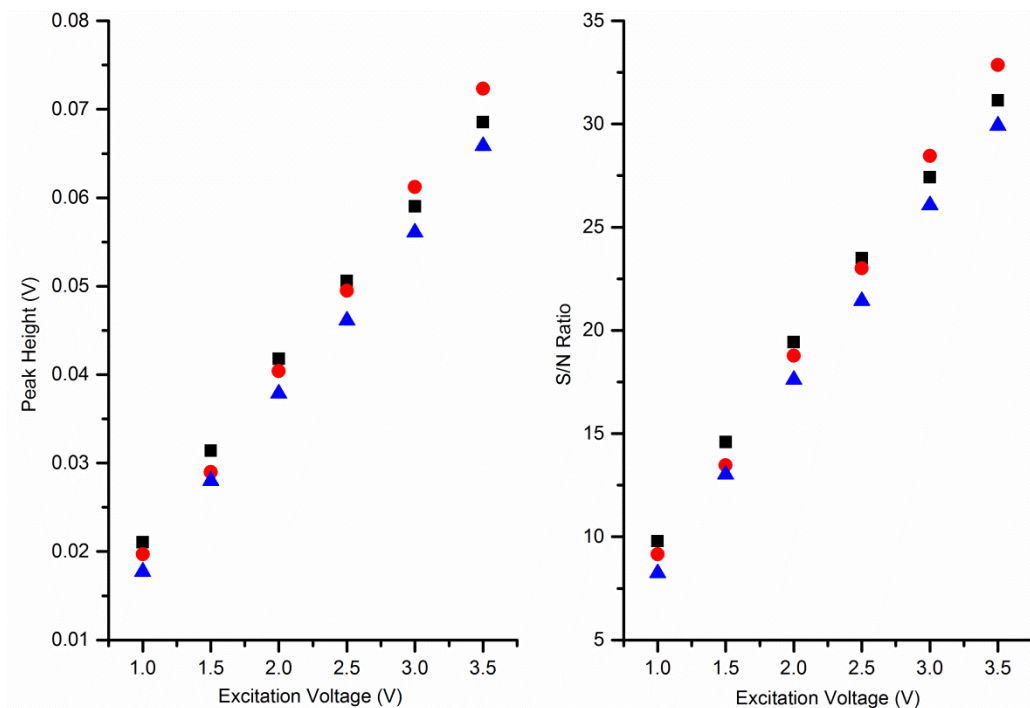
Figure 47   **Effect of excitation voltage on model analyte peaks using a 50 μm gap**

Peak heights and S/N ratios of Li⁺ (−▲−), Na⁺ (−●−) and K⁺ (−■−) peaks (0.5 mM) obtained using injected gallium electrodes with an electrode distance from separation microchannel of 50 μm and an excitation frequency of 220 kHz

Optimum excitation signal parameters for the electrode to separation microchannel distance of 75 μm were determined as part of the electrode geometry optimisation. Therefore the optimum excitation frequency and voltage of the 100 μm distance were subsequently determined to complete the current investigation. The frequency optimisation data for the 100 μm distance displayed the same general trend as the 50 μm distance, with the exception of the 200 kHz data point which for all three cations appeared elevated as is seen in Figure 48. This resulted in the 200 kHz peak heights and S/N ratios being similar to the 220 kHz values. As all previous results displayed clear trends with an optimal excitation frequency of 220 kHz the same was assumed for this experiment and the elevated peak heights and S/N ratios associated with the 200 kHz excitation frequency were considered anomalous. The excitation voltage optimisation plots of peak heights and S/N ratios for the 100 μm electrode to separation microchannel distance are shown in Figure 49. The maximum peak heights and S/N ratios for each cation were obtained using an excitation voltage of 6 V. The optimised input signal parameters for each of the three electrode to separation microchannel distances investigated are summarised in Table 11 and were used for all further experiments.

Table 11   **Optimised input signals for each electrode to separation channel distance**

Electrode to separation microchannel distance (μm)	Optimised excitation frequency (kHz)	Optimised excitation voltage (V)
50	220	3.5
75	220	5.5
100	220	6
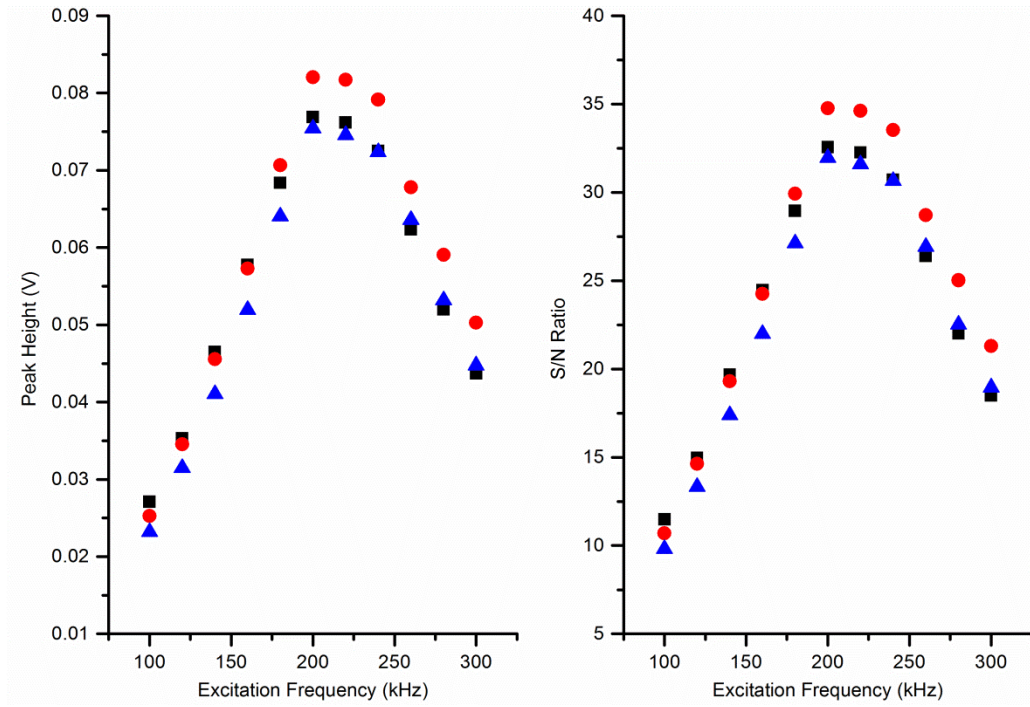
Figure 48   **Effect of excitation frequency on model analyte peaks using a 100 μm gap**

Peak heights and S/N ratios of Li⁺ (−▲−), Na⁺ (−●−) and K⁺ (−■−) peaks (0.5 mM) obtained using anti-parallel injected electrodes with an electrode distance from separation microchannel of 100 μm and an excitation voltage of 6 V
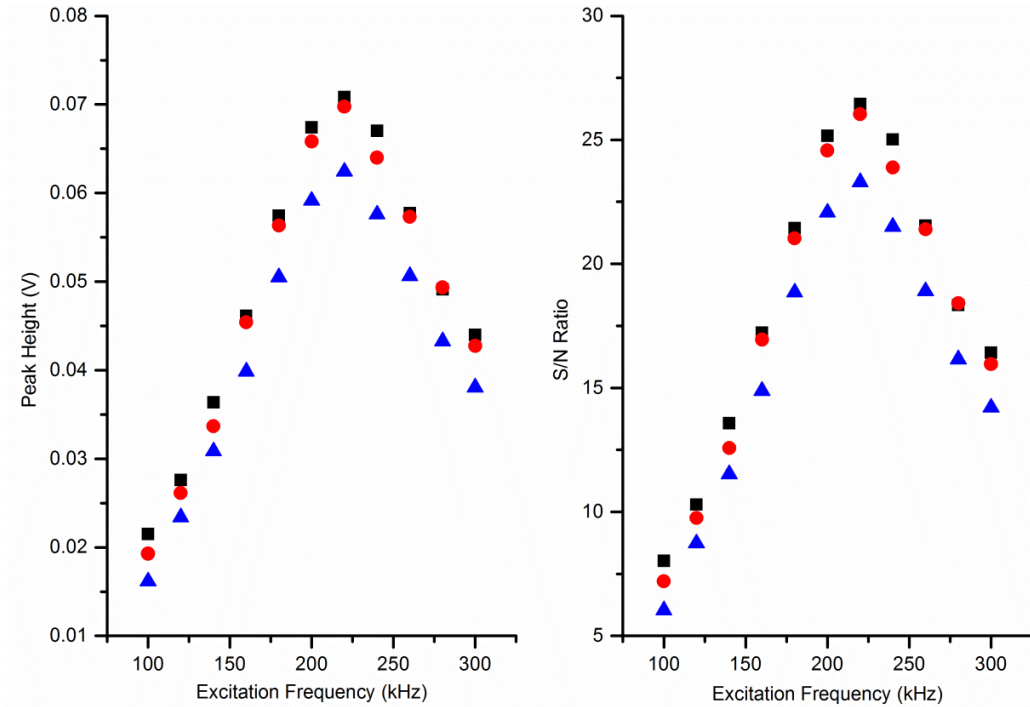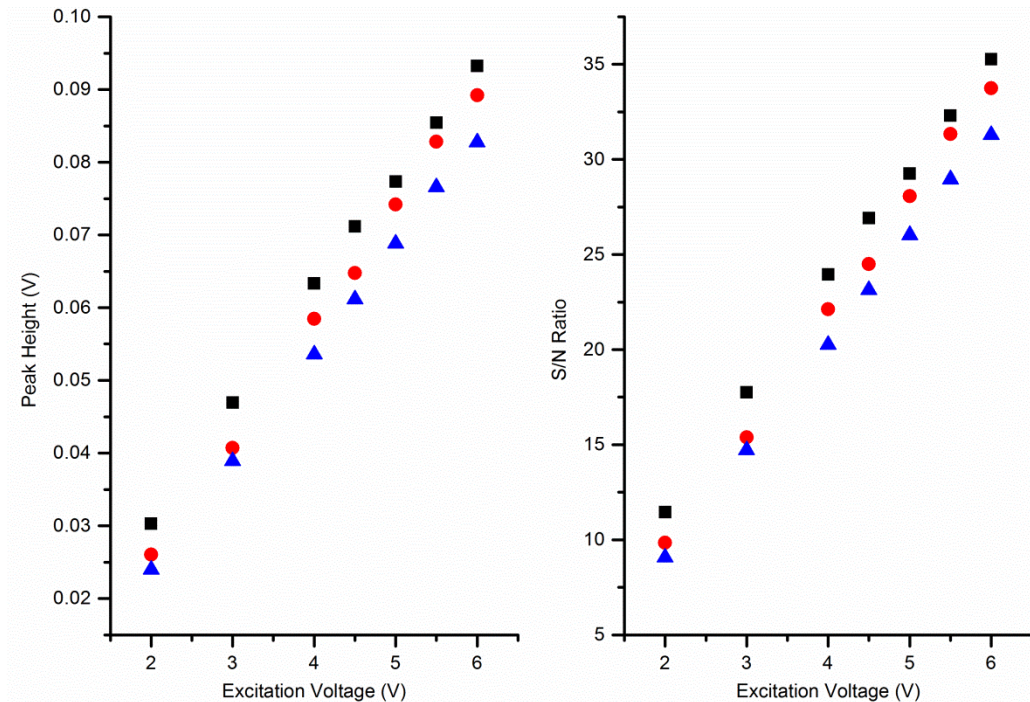

Figure 49   **Effect of excitation voltage on model analyte peaks using a 100 μm gap**

Peak heights and S/N ratios of Li⁺ (−▲−), Na⁺ (−●−) and K⁺ (−■−) peaks (0.5 mM) obtained using anti-parallel injected electrodes with an electrode distance from separation microchannel of 100 μm and an excitation frequency of 220 kHz

To determine which electrode to separation channel distance provided the best analytical performance multiple analyses of a lithium, sodium and potassium cation standard (0.5 mM), using the optimised input signal parameters, were performed. Specifically, three separate three replicate analyses (n = 9) of the cation standard were performed for each electrode to separation channel distance over the course of a single day. The resulting mean peak heights and S/N ratios of the lithium, sodium and potassium peaks, along with their associated standard deviation, at each of the distances are presented in Figure 50 and Figure 51 respectively.
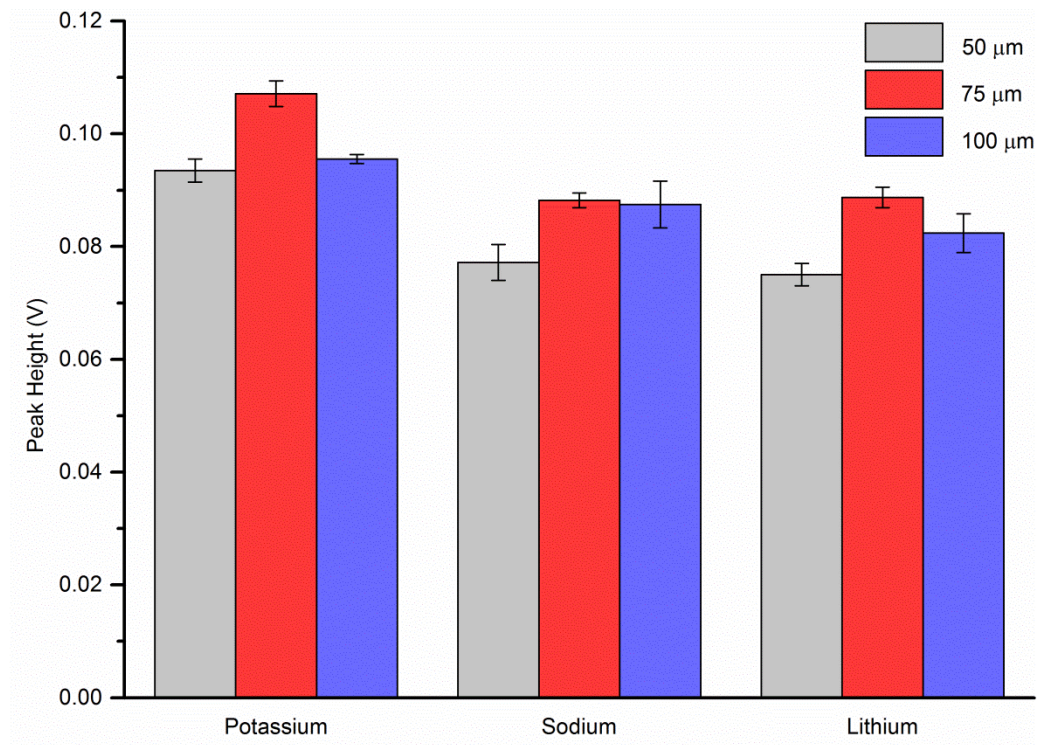
Figure 50   **Comparison of mean analyte peak heights**

Obtained using injected gallium electrodes with an electrode to separation channel distance of 50 μm, 75 μm and 100 μm
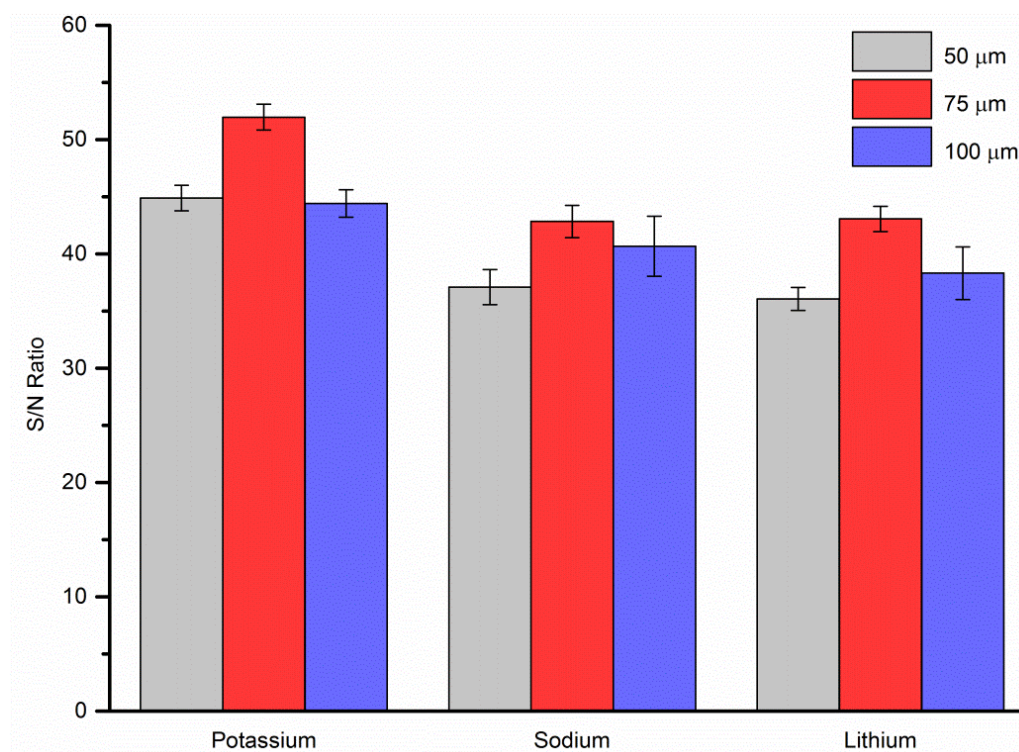
Figure 51   **Comparison of mean analyte S/N ratios**

Obtained using injected gallium electrodes with an electrode to separation channel distance of 50 μm, 75 μm and 100 μm

Considering Figure 50, the largest mean peak heights for both potassium and lithium were observed using an electrode to separation channel distance of 75 μm. The largest mean peak height for sodium was also observed using a 75 μm distance (0.088 $\pm$ 0.0013 V), however it wasn't significantly different from the 100 μm value (0.087 $\pm$ 0.0041 V), as evidenced by the overlap of the mean peak height standard deviation in Figure 50. The same trend was observed for the mean S/N ratios for each analyte using the three electrode to separation channel distances (see Figure 51). The lower peak heights and S/N ratios obtained for the 50 μm gap device were hypothesised to be a result of the decreased shielding capacity inherent in this design. This electrode to separation microchannel distance was equal to that between the integrated in-plane shielding plates and the separation microchannel. Therefore, effective shielding of the stray capacitance was reduced, as the detection electrodes were no longer recessed behind the shielding plates. This in turn resulted in higher background levels due to a greater degree of direct coupling. This limited the maximum excitation voltage able to be used and consequently produced the lower peak heights and S/N ratios at this distance. Conversely, increasing the electrode to separation microchannel gap to 100 μm allowed for the maximum effective shielding of the stray capacitance. This allowed greater excitation voltages to be used; however, the increased separation distance resulted in a significantly decreased coupling ability through the PDMS dielectric layer. This decreased coupling ability

outweighed the extra shielding capacity and resulted in the intermediate peak heights and S/N values observed.

As previously discussed, optimum electrode conditions require a compromise between parameters that will allow greater signal coupling but also decrease the amount of stray capacitance in a system. In the case of electrode to separation channel distance this compromise was achieved using a distance of 75 μm. This distance allowed the electrodes to be recessed 25 μm behind the in-plane shielding plates. This in turn created a more effective shielding arrangement, reducing the amount of stray capacitance in the system. In this design the extra shielding compensated for any reduced signal coupling that was associated with the greater distance from the separation microchannel. Therefore, significantly higher peak heights and S/N ratios for all cations were observed compared to the 50 μm distance and for two out of the three cations compared to the 100 μm distance.

4.4.3 Optimisation of electrode length

Electrode length is an essential parameter to investigate in microchip electrophoresis devices equipped with C^{4}D. This is because altering it can influence both detection sensitivity and resolution of the resulting electrophoretic separations. In the case of the in-plane injected metal electrodes used in this work, electrode length (along the separation microchannel) is analogous to the width of an externally mounted electrode (Figure 52). Therefore, increasing the electrode length results in an increase in the electrode surface area adjacent to the separation microchannel which can give rise to an improved signal intensity. However, larger surface areas can also give rise to an increase in the stray capacitance. Moreover, if the length is increased too much, more than one analyte peak may be able to pass through the detection cell at any one time, negatively impacting on the resolution of the resulting electropherogram. These consequences were carefully considered during the optimisation of the length of the injected gallium C^{4}D electrodes.
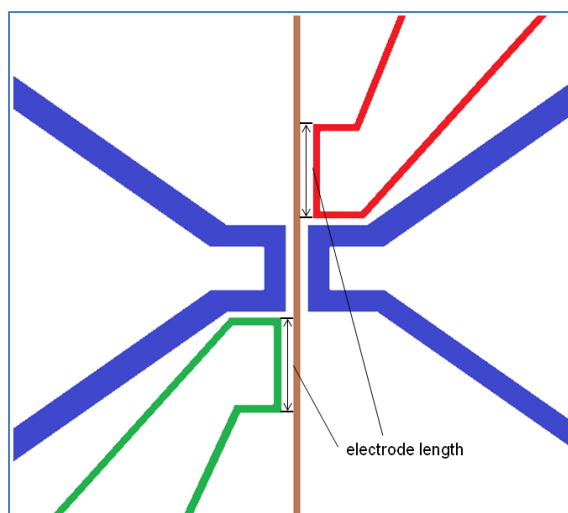
Figure 52   **Illustration of the electrode length parameter**

Electrode lengths of 1000 μm (1 mm) are commonly reported for microchip C^{4}D systems [161, 233-234]. Using this as a guide the lengths used in the optimisation of the injected gallium electrode system were 750 μm, 1000 μm and 1250 μm. These values were chosen to give an indication of the influence of injected gallium electrode length, both above and below the most commonly reported conditions. As was the case for the previous investigations of electrode geometry and distance to separation microchannel parameters, initially the optimum excitation frequency and voltage of the three electrode lengths were determined.

The first length investigated was 750 μm and the peak heights and S/N ratios obtained at the different frequencies and voltages examined are presented in Figure 53 and Figure 54 respectively. The data for these optimisation experiments displayed the same general trends seen for all previous excitation signal optimisation experiments. The maximum analyte peak heights and S/N ratios were achieved using an excitation frequency of 220 kHz (Figure 53) and an excitation voltage of 7.5 V (Figure 54). As optimum parameters for the electrode length 1000 μm were determined as part of the initial electrode geometry optimisation the optimum excitation frequency and voltage of the 1250 μm electrode length were determined to complete the current investigation. Again the excitation frequency data for the 1250 μm electrode peak heights and S/N ratios displayed the same general trends observed previously (see Appendix). The optimum excitation frequency was determined to be 220 kHz. The effect of increasing the excitation voltage on the peak height and S/N ratios of all three cations is displayed in Figure 55. Upon increasing the voltage a subsequent increase in both the peak heights and S/N ratios was observed until a maximum at 6 V. An unexpected drop in the peak height and S/N ratio was recorded using an excitation voltage of 6.5 V, however beyond this the maximum background was reached due to limitations with the feedback resistor

and therefore 6 V was determined as the optimum value. The optimised input signal parameters for each of the three electrode lengths investigated are summarised in Table 12 and were used for all further experiments.
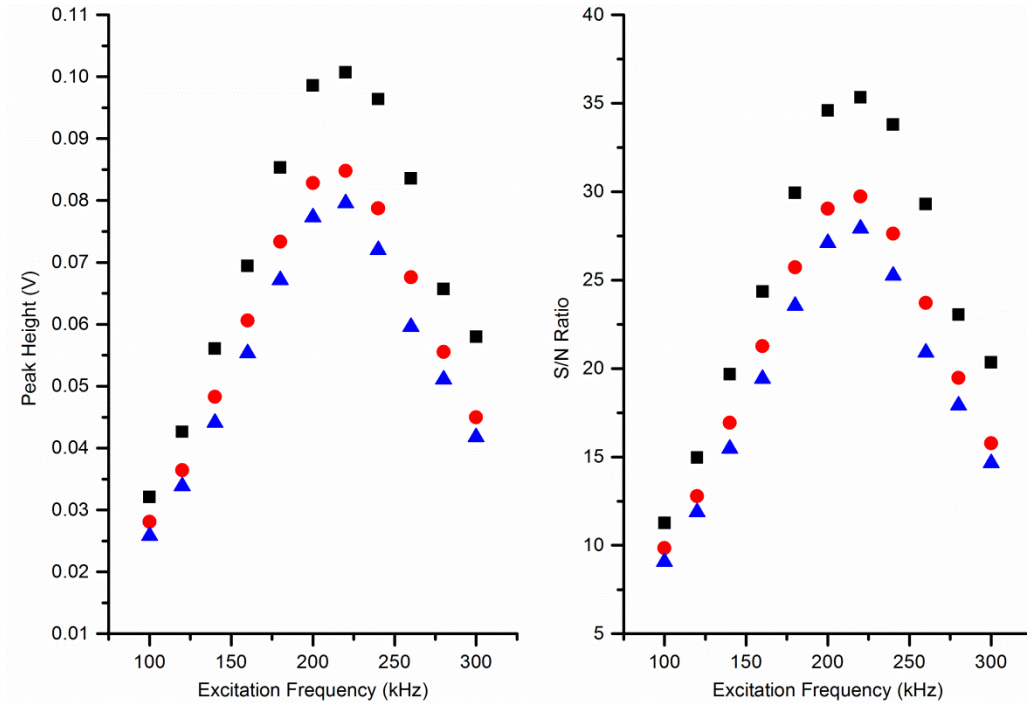
Figure 53   **Effect of excitation frequency on model analyte peaks using 750 μm electrodes**

Peak heights and S/N ratios of Li$^+$ (─▲─), Na$^+$ (─●─) and K$^+$ (─■─) peaks (0.5 mM) obtained using anti-parallel injected gallium electrodes with an electrode length of 750 μm and an excitation voltage of 7.5 V
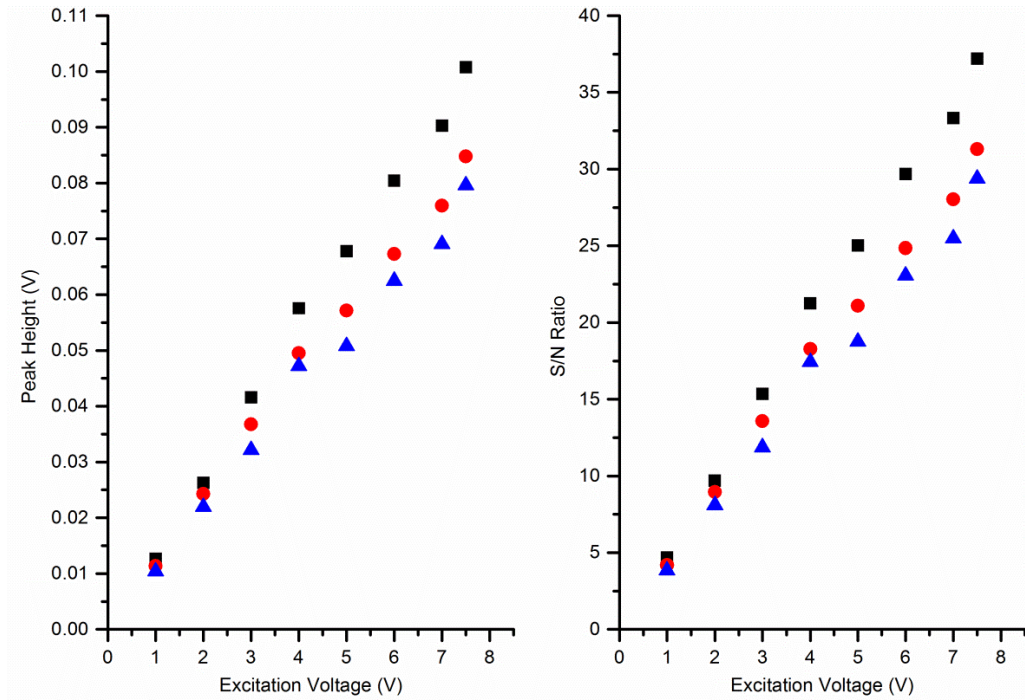
Figure 54   **Effect of excitation voltage on the model analyte peaks using 750 μm electrodes**

Peak heights and S/N ratios of Li$^+$ (−▲−), Na$^+$ (−●−) and K$^+$ (−■−) peaks (0.5 mM) obtained using anti-parallel injected gallium electrodes with an electrode length of 750 μm and an excitation frequency of 220 kHz
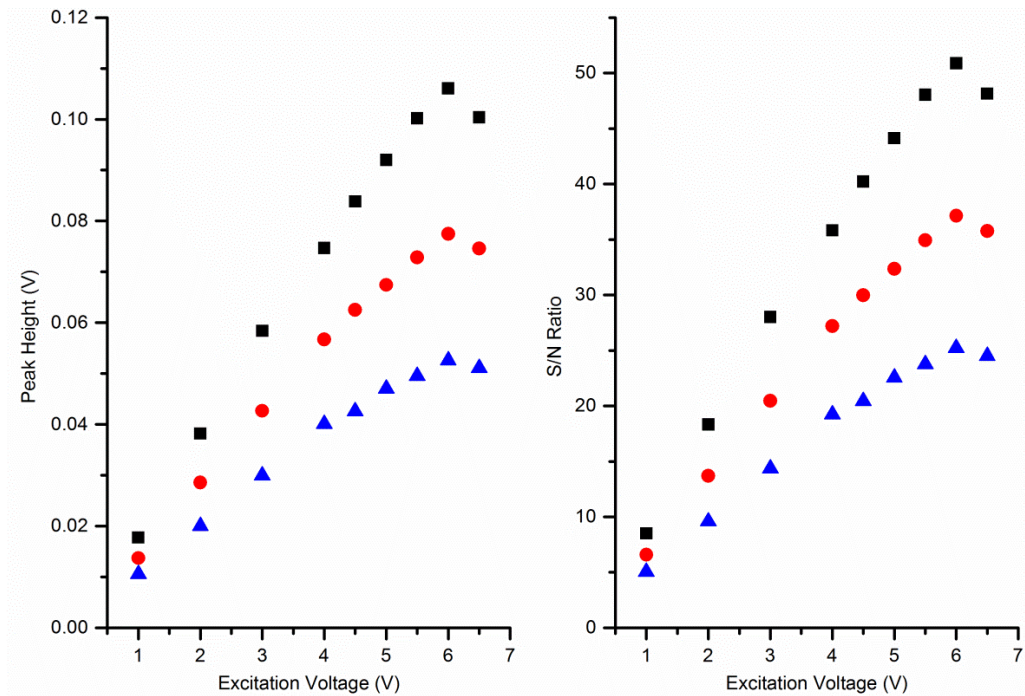
Figure 55   **Effect of excitation voltage on model analyte peaks using 1250 μm electrodes**

Peak heights and S/N ratios of Li$^+$ (−▲−), Na$^+$ (−●−) and K$^+$ (−■−) peaks (0.5 mM) obtained using anti-parallel injected gallium electrodes with an electrode length of 1250 μm and an excitation frequency of 220 kHz

Table 12   **Optimised input signal parameters for each electrode length**

Electrode length (µm)	Optimised excitation frequency (kHz)	Optimised excitation voltage (V)
750	220	7.5
1000	220	5.5
1250	220	6

As for electrode geometry and distance to separation microchannel investigations multiple analyses of a lithium, sodium and potassium cation standard (0.5 mM) using each optimised electrode length were performed. The resulting mean peak heights and S/N ratios of the lithium, sodium and potassium peaks, along with their associated standard deviation, at each of the electrode lengths is presented in Figure 56 and Figure 57 respectively.
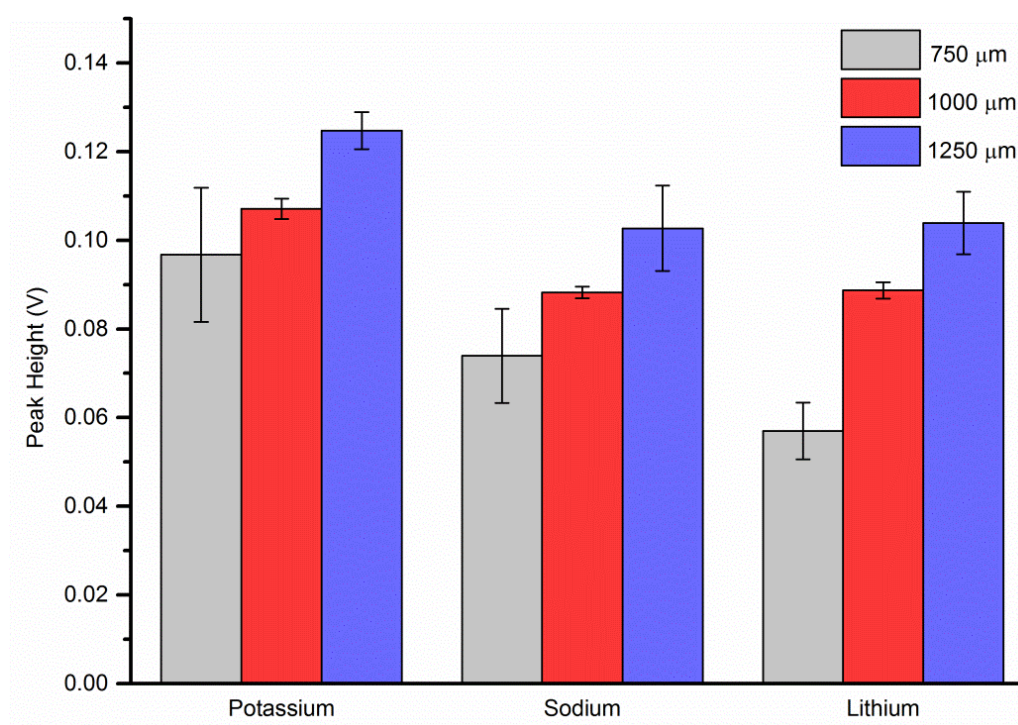
Figure 56   **Comparison of mean analyte peak heights**

Obtained using injected gallium electrodes with an electrode length of 750 µm, 1000 µm and 1250 µm
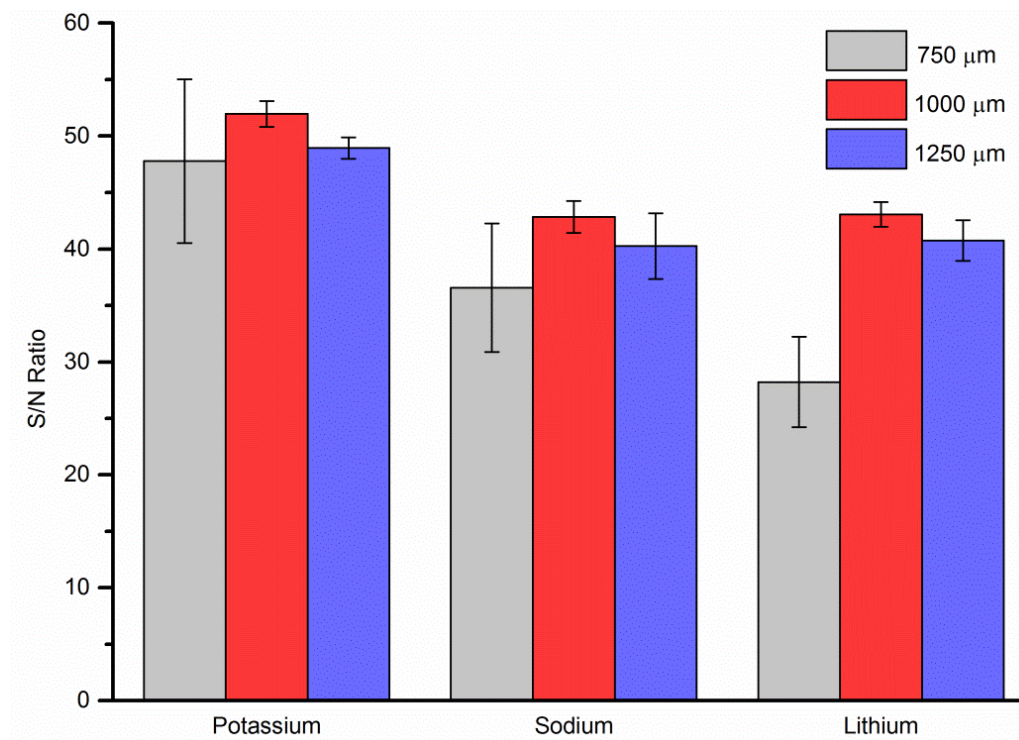
Figure 57   **Comparison of mean analyte S/N ratios**

Obtained using injected gallium electrodes with an electrode length of 750 µm, 1000 µm and 1250 µm

Of the electrode lengths examined 1250 µm gave the highest peak heights for all three analytes whilst 1000 µm gave the highest S/N ratios. Conversely, the lowest peak heights and S/N ratios were achieved using the 750 µm electrodes. Measurements using these electrodes also attracted the highest error values as evidenced by the significantly larger standard deviations in the data observed in both Figure 56 and Figure 57. As expected the 750 µm electrode setup allowed for more effective shielding of the stray capacitance, confirmed by the larger excitation voltage permitted. However, the lower peak height and S/N ratios were a product of lower signal coupling through the microchannel resulting from the smaller transmitting and pickup electrode surface areas. Increasing the electrode length to 1000 µm increased both the peak height (Figure 56) and S/N ratio (Figure 57) observed. The larger electrode surface area permitted greater signal coupling through the fluid in the microchannel, which subsequently outweighed any effect from increased stray capacitance. Further increasing the electrode length to 1250 µm produced increased peak height values (Figure 56); however the S/N ratio values recorded were lower than that for the 1000 µm electrodes (Figure 57). Despite a larger electrode surface area, allowing more signal coupling through the microchannel, a concurrent large increase in stray capacitance resulted in higher background noise levels adversely affecting the S/N ratios. As a result of this work an electrode length of 1000 µm was employed for all further electrophoretic separations due to its superior S/N ratios and

increased repeatability as observed by its comparatively low error values compared to the 750 and 1250 μm electrode lengths.

4.4.4 Detection limits of model analytes using optimised electrode parameters

To assess the overall analytical performance of the optimised injected gallium electrode detection system an external calibration of the model analytes used throughout this work (K$^+$, Na$^+$ and Li$^+$) was conducted. Utilising the optimised conditions a series of mixed cation standards over the range 0.1 mM to 0.7 mM were analysed. The resultant calibration curves (Figure 58) were found to be linear over the tested range with linear regressions of Y = 0.291X − 0.014 (R^2 = 0.987), Y = 0.368X - 0.0238 (R^2 = 0.994) and Y = 0.405X − 0.0240 (R^2 = 0.998) for K$^+$, Na$^+$ and Li$^+$ respectively. Where Y is the C^{4}D signal peak area in V and X is the relevant cation concentration in mM. Further analytical figures of merit are reported in Table 13.
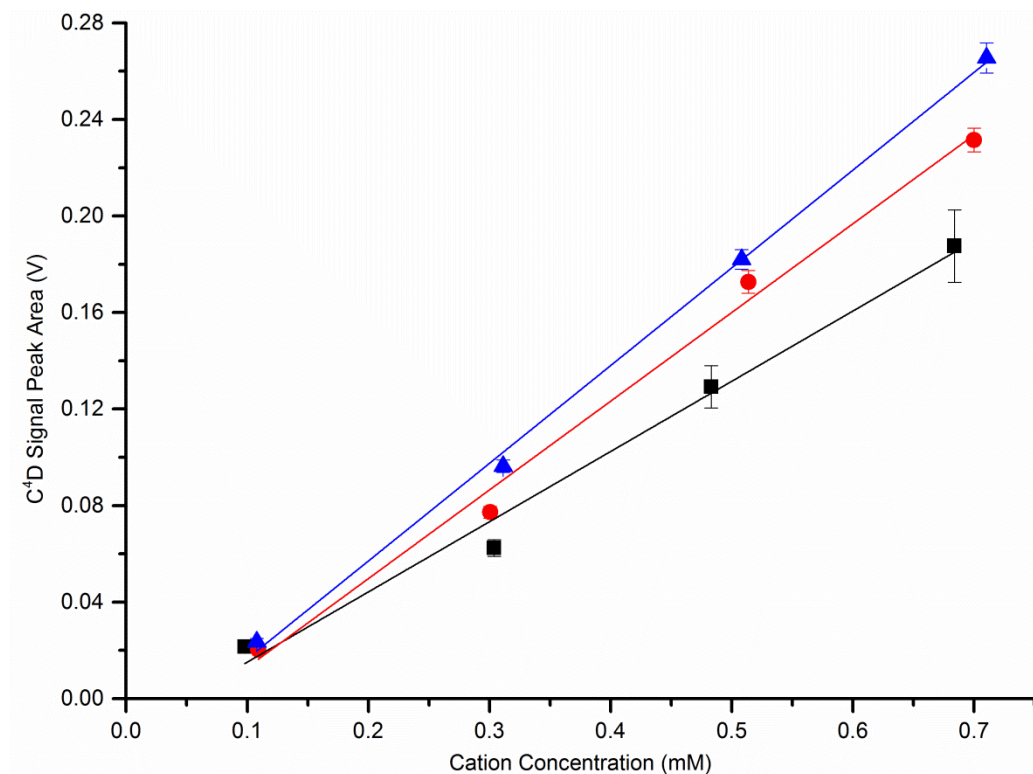
Figure 58   **Calibration plots of model analytes using optimised electrode parameters**

Illustrating linear lines of best fit for K$^+$ (−■−), Na$^+$ (−●−) and Li$^+$ (−▲−) peak areas obtained using optimised injected gallium electrode parameters with an excitation voltage of 5.5 V and frequency of 220 kHz

Table 13   **Analytical figures of merit for K⁺, Na⁺ and Li⁺ calibrations**

	K⁺	Na⁺	Li⁺
Linear function	Y = 0.291X − 0.014	Y = 0.368X − 0.0238	Y = 0.405X − 0.0240
Linear regression (R²)	0.987	0.994	0.998
Limit of detection (µM)	8.7	6.9	6.2
Limit of quantitation (µM)	12.7	10.0	9.1

Using the linear calibrations the limits of detection (LODs) and limits of quantitation (LOQs) were calculated using Equation 10 and Equation 11 respectively, where $S_{analyte}$ is the average signal noise for an analyte blank, $\sigma_{analytre}$ is the standard deviation for the analyte blanks signal noise and k is the slope of the linear calibration function.

Equation 10   **Determination of limit of detection**

$$LOD = S_{analyte} + 3.3\sigma_{analytre} / k$$

Equation 11   **Determination of limit of quantitation**

$$LOQ = S_{analyte} + 10\sigma_{analytre} / k$$

LODs of around 30 µM have been most commonly reported with integrated C⁴D using similar electrode parameters to those used in this study [108, 172]. Therefore, the injected gallium electrodes introduced in this work demonstrated slightly superior detection limits than those reported for similar devices. A previous report also indicated that applying a digital filter treatment by the fast Fourier transform (FFT) algorithm was able to improve detection limits by reducing the noise level in the electropherograms ~3-5 fold [235]. Therefore, to investigate whether detection limits could be improved in this way an FFT algorithm using a low-pass filter (cut-off: 1 Hz) was applied to all electropherograms to remove background noise. The analytical figures of merit obtained using the calibration curves resulting from the filtered data are presented in Table 14.

Table 14   **Revised analytical figures of merit for K$^+$, Na$^+$ and Li$^+$ calibrations**

Calculated after applying a post run FFT digital filter treatment

	K$^+$	Na$^+$	Li$^+$
Linear function	Y = 0.296X – 0.0152	Y = 0.364X – 0.0215	Y = 0.404X – 0.0240
Linear regression (R^2)	0.987	0.996	0.999
Limit of detection (μM)	4.9	4.0	3.6
Limit of quantitation (μM)	9.0	7.3	6.6

The application of an FFT low-pass filter to the calibration electropherograms resulted in a 2.3 fold reduction in the background noise level without the loss of peak shape as observed in Figure 59. However, as shown in Table 14, this resulted in only a small improvement in both the LODs (1.7 – 1.8 fold) and LOQs (1.4 fold) using the filtered data. Therefore, although only small, it was confirmed that applying such a filter to the resulting electropherograms can result in improved detection limits using C^{4}D devices. As mentioned previously, these detection limits compare favourable to those reported in literature using similar electrode parameters. As a result injected gallium electrodes were demonstrated as a viable and competitive alternative to traditional electrode setups. The significant advantage of the presented system was the ability to incorporate both electrode and electrophoresis microchannels into the same lithographic process. This allowed for the subsequent integration of electrodes through the injection of liquid gallium. This process was fast, simple, low-cost and highly reproducible alignment of electrodes on the chip was easily achieved.
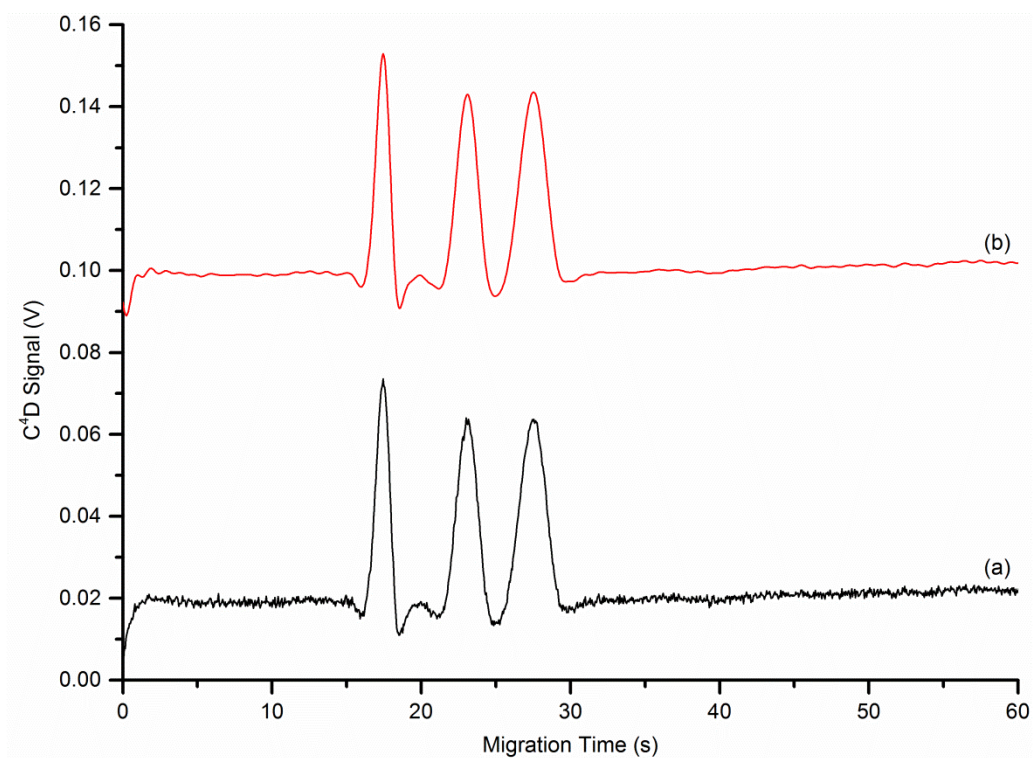
Figure 59   **Comparison of electropherograms before and after FFT filtering**

(a) Unfiltered and (b) FFT filtered (cut-off: 1 Hz) electropherograms showing separation of 0.3 mM model analytes

4.5   Concluding remarks

In these studies, the optimisation of physical parameters of injected gallium electrodes for C^4D detection in PDMS microchips was demonstrated. Most reported methods for the integration of C^4D with microchip electrophoresis systems require multi-step electrode patterning/fabrication processes which in turn leads to difficulty in consistently aligning detection electrodes. These limitations have the potential to compromise analytical performance of the electrodes and increase the time and cost of device production. These investigations show a simplified approach for C^4D electrode integration with PDMS microchips by utilising 'injected' gallium electrodes using a fabrication process that is fast, highly reproducible, and eliminates difficulties with electrode alignment. Using this approach C^4D can be readily achieved in any microchip by simply adding extra 'electrode' channels to the microchip design.

The design flexibility afforded by the injected gallium electrode system allowed for straightforward optimisation of the three electrode parameters investigated. The overall optimised parameters were determined to be an anti-parallel electrode geometry with a 75 μm electrode distance from separation channel and a 1000 μm electrode length. Using the optimised parameters to perform a calibration of the model analytes, Li^+, Na^+ and K^+, yielded detections limits ranging from 6.2 to 8.7 μM and limits of quantitation ranging from 9.1 to 12.7 μM. Upon application of an FFT low-pass filter to the calibration electropherograms a 2.3 fold reduction in the background noise level was observed. However, this resulted in only a small improvement of 1.7 to 1.8 fold and 1.4 fold for the reported LODs and LOQs respectively. After FFT filtering of the data detection limits for the three model analytes ranged from 3.6 to 4.9 μM and limits of quantitation ranged from 6.6 to 9.0 μM.

5. Application: Determination of Histamine Levels in Frozen Fish Samples

5.1   Chapter overview

The determination of histamine levels in fish and related products is of significant importance as it is known to be the toxin responsible for food poisoning in a number of fish species. In Australia, the maximum limit for histamine in certain fish and fish products is 100 μg.g^{-1} as a result of decomposition or 200 μg.g^{-1} as a result of hygiene and handling [191]. Here, the development and optimisation of a direct detection method for histamine using the previously explained PDMS microchip with injected gallium electrodes for C^{4}D is presented. The adaptation of a histamine extraction protocol for fish flesh samples is outlined and the applicability of the new methodology is displayed through the determination of histamine levels in frozen fish samples purchased from a local supermarket.

5.2   Introduction

Histamine is a primary amine formed by the decarboxylation of the amino acid L-histidine [180] and belongs to a group of compounds known as biogenic amines (BAs). BAs are synthesised by microbial, vegetable or animal metabolisms and are known to be the causative agents in a number of food poisoning cases; which is due to their ability to initiate a variety of pharmacological reactions [180-181]. High levels of BAs during food intake are unable to be metabolised by the body, to sufficiently eliminate the toxins, leading to food poisoning symptoms ranging from migraines to hypertension [182-183]. BAs can be present in certain foods, such as some fruit and vegetables (e.g., spinach and bananas) with concentrations dependant on maturity [184]; however they are normally formed as a result of uncontrolled microbial action [184], resulting in elevated levels in food and beverage products after degradation. This is usually as a result of poor quality raw materials, contamination or unsuitable conditions during food processing and storage [184]. Typically, elevated levels of BAs above safe limits are found in fish and fish products, dairy products, meat and meat products as well as fermented products such as vegetable, soy and alcoholic beverages [181-182]. The maximum limits are BA dependant with important BAs present in food and beverages including histamine, *β-phenylethylamine*, tyramine, tryptamine, putrescine, cadaverine, spermine and spermidine [182, 185].

In particular histamine has been reported as the toxin responsible for scombroid fish poisoning [186-188] a type of food poisoning arising from the incorrect handling and storage of scombroid fish products [189]. The current maximum limit for histamine in certain fish and fish products ranges from 50 $\mu g.g^{-1}$ in the United States [190] and up to 100 $\mu g.g^{-1}$ for decomposition or 200 $\mu g.g^{-1}$ as a result of hygiene and handling in Australia and New Zealand [191]. Elevated levels of histamine have also been reported in fermented wines [185, 192]. Therefore, simple portable quantitative methods for the determination of histamine levels in food and beverage products are of increasing interest to allow monitoring of food spoilage and quality during processing and storage.

Numerous quantification methods for biogenic amines, including histamine, have been developed and are the subject of multiple reviews [193-195]. The most common approaches to BA detection have been coupling fluorescence or UV based detection with analytical separation methods such as high performance liquid chromatography (HPLC) [196-198] and capillary electrophoresis (CE) [199-201]. The lack of chromophore in histamine is the major drawback of these methods which means derivatisation with other highly fluorescent or UV active compounds is required to achieve adequate sensitivity [194-195]. Often this results in time intensive indirect analysis methods. LC methods have also been coupled with mass spectrometric (MS) detection [202-203] for the

determination of histamine but this still required histamine derivatisation. CE has also been coupled with chemiluminescence [204], amperometry [205] and conductivity [206] detection systems. Whilst providing sensitive detection, CE techniques are restricted to laboratory settings and cannot be deployed for simple in-field analysis in their traditional format. Furthermore, analytical methods that have been reported for the determination of histamine include thin layer chromatography (TLC) [207-208], gas chromatography-mass spectrometry (GC-MS) [209-210] and biosensor/assay based techniques [211-212]. Of these methods TLC is the most simple and does not require complex instrumentation but is often time consuming and only semi-quantitative [194]. GC is not commonly applied for BA analysis with only one example not requiring derivatisation [209]. Biosensors are simple, portable, low cost and have inherently short analysis times; however, most only produce semi-quantitative determinations. Ideally, the timely and efficient monitoring of food quality and spoilage would be done using a simple portable technique that negates the need for derivatisation.

More recently, the use of portable analytical devices coupled with different detection techniques have been reported for the quantification of a range of BAs, including histamine. Microchip electrophoresis with indirect fluorescence detection has been reported for the detection of histamine and other common BAs in fermented beverages [213-214], fish products [215] and standards [216-217]. A novel chemiluminescene detection system has also been used with microchip electrophoresis for the indirect detection of BAs including histamine in urine samples [218]. Whilst the reported systems symbolise a shift towards the desire to achieve greater portability, most still contained laboratory scale detection components and require a derivatisation step. There remains a need for the development of a truly portable device with miniaturised detection components for quantitative histamine analysis.

This chapter focuses on the development and optimisation of a method for the direct detection of histamine using the PDMS microchip with injected gallium electrodes for C^4D. Particularly, detailed investigations into the optimal electrolyte conditions to achieve histamine resolution from other BAs and sample matrix are outlined. The adaption and further optimisation of a histamine extraction protocol from fish samples into a standard extraction procedure is explained. The applicability of the new approach is then illustrated through the quantitative analysis of histamine levels in frozen fish samples purchased from a local supermarket.

5.3   Experimental

5.3.1   Instrumentation

All experiments in this chapter were performed using the optimised microchip electrophoresis instrument with injected gallium electrodes for capacitively coupled contactless conductivity detection as described previously in Chapter 2.

5.3.2   Chemicals and samples

Unless otherwise specified, all chemicals were of analytical grade, purchased from Sigma-Aldrich (Australia) and used as received. Background electrolyte (BGE) components 2-(*N*-morpholino)ethanesulphonic acid (MES), 2-amino-2-hydroxymethyl-propane-1,3-diol (Tris), 2-(cyclohexyl amino)ethanesulphonic acid (CHES) and 3-(cyclohexylamino)-1-propanesulphonic acid (CAPS) were investigated before the final optimised BGE solution for electrophoretic separation was determined to be 2-[4-(2-hydroxyethyl)piperazin-1yl] ethanesulphonic acid (HEPES) (50 mM) and histidine (His) (5 mM) in 5% v/v isopropanol (pH=6.03). Standard stock solutions of histamine, tyramine and 2-phenylethylamine at concentrations of 200 mg.L^{-1} were prepared by dissolving the respective amines in 5% v/v isopropanol. Working standard solutions containing the three biogenic amines were prepared fresh by dilution of the stock solutions with BGE. All solutions were degassed by ultrasonication prior to use. Frozen yellowfin tuna (*thunnus albacores)* samples were purchased from a local supermarket and stored at -20 °C prior to thawing at 4 °C before extraction.

5.3.3   Electrophoresis procedure

Electrophoretic separations were performed in PDMS microchips as previously described in Chapter 2. Standards and samples were introduced electrokinetically using an applied voltage of 1 kV for a period of 5 s. The separation potential was 1.2 kV and the C^{4}D operated at 216 kHz (sinusoidal) and 10 V (peak to peak amplitude). Before the first analysis of the day the PDMS microchannels were sequentially washed with Milli-Q water for 2 min, BGE containing n-dodecyl β-D-maltoside (DDM) (0.4 mM) for 10 min, Milli-Q water for 2 min and finally BGE for 5 min. After each analysis the microchannels were flushed with BGE for 1.5 min. All analyses were carried out at ambient temperature (20 – 25 °C).

5.3.4   Histamine calibration

Standard curves for histamine were obtained by injecting (in triplicate) five or six working standards containing histamine at concentration levels ranging from 1 to 10 mg.L^{-1} with

final standard concentrations determined gravimetrically. The histamine peak heights from the resulting electropherograms were determined and plotted versus analyte concentration. A linear regression was performed on the standard curve using the least-squares method and the obtained regression equations were used to estimate the concentration of histamine in the frozen fish samples. Peak integration and statistical analysis were carried out with the software OriginPro 9.0 (OriginLab, Northhampton, MA, USA). LOD and LOQ determinations were performed as outlined in Chapter 4.

5.3.5 Optimised histamine extraction and solid phase extraction (SPE) cleanup procedure

Extractions were performed using 2 g of homogenised fish flesh weighed directly into 10 mL capped polyethylene centrifuge tubes. For recovery experiments, a stock standard solution containing histamine (8.07 $g.L^{-1}$) was used to spike the samples. Histamine extraction was then performed using a method modified from Hwang *et al.* [209] Namely, 10 mL of methanol alkalised with 40 µL of concentrated ammonia (28-30%) was added to the sample tubes. Solutions were manually homogenised for 1 min followed by ultrasonication for 5 min. Samples were then centrifuged for 5 min at 3000 rpm to separate the solid fish flesh matrix from the aqueous phase. After centrifugation, 2-5 mL of supernatant was removed from each tube by micropipette and evaporated to dryness under N_2. Extracts were then reconstituted in the same volume of Milli-Q water and filtered through a 0.45 µm nylon membrane prior to SPE cleanup.

SPE cleanup of aqueous histamine extracts were performed using C18 cartridges (Phenomonex, Australia). Prior to cleanup 1 mL of filtered aqueous extract was alkalised with 10 µL of concentrated ammonia solution (28-30%) in order to increase histamine retention on the C18 column. The cartridges were first conditioned and equilibrated with 1.2 mL of methanol and Milli-Q water respectively. This was followed by loading of 1 mL of the alkalised aqueous extract, washing with 5 mL of Milli-Q water and elution of histamine with 1 mL of optimised BGE. This produced a matrix matched histamine extract ready for injection into the microchip electrophoresis device. Where required fish extracts were diluted with BGE prior to injection to ensure they fitted within the reported linear range for histamine analysis.

5.4   Results and Discussion

5.4.1   Investigation of suitable BGE for biogenic amine analysis

The first aim of this study was to find a suitabile BGE for analysing biogenic amines using microchip electrophoresis with C^4D. Traditionally, low conductivity buffer systems containing MES and histidine are used for the separation of cationic mixtures in microchip electrophoresis devices coupled with C^4D. However; attempting to use this BGE with 3% v/v isopropanol, to prevent the BAs from precipitating out of solution in the microchannels, yielded very low signals for all three analytes (Figure 60). As the method was to be applied to the detection of histamine in real samples the best sensitivity was required and therefore, this BGE was considered unsuitable given the relatively high concentration of the individual standards analysed.
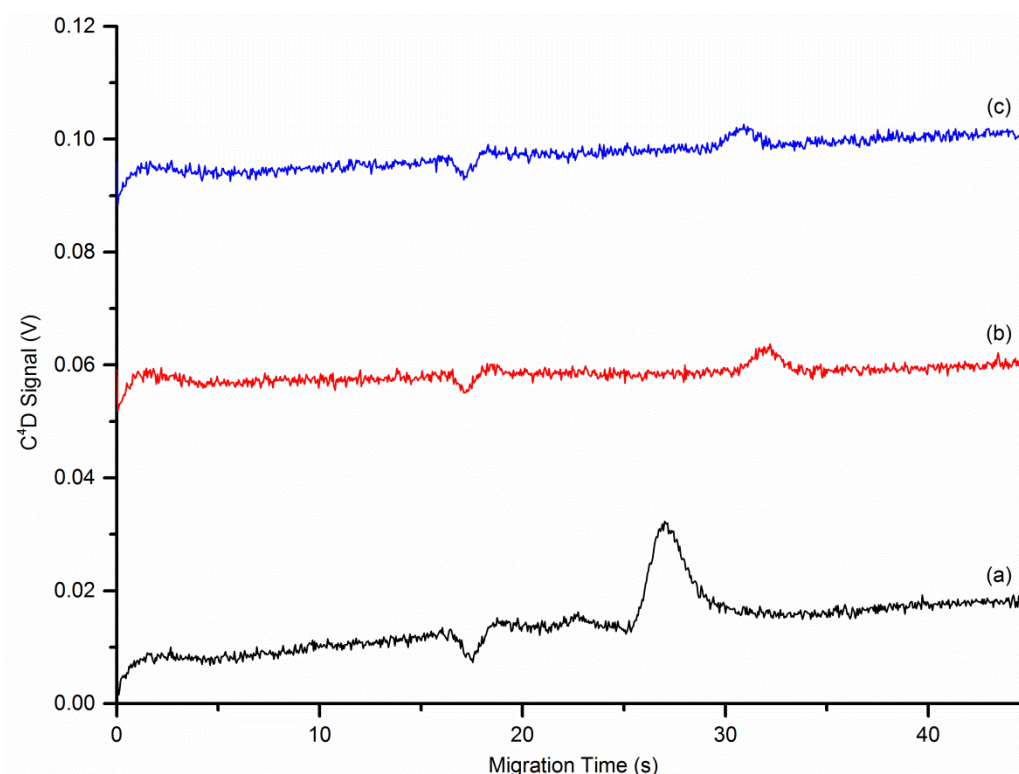
Figure 60   **Analysis of biogenic amines using MES/His BGE**
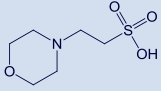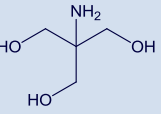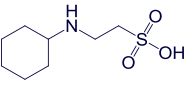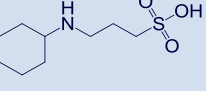
Electropherograms of 10 mg.L^{-1} (a) histamine, (b) tyramine and (c) 2-phenylethylamine standards using 15 mM MES/his BGE in 3% v/v isopropanol. Operating conditions: microchip 57/37 mm total/effective length; injection voltage 1.0 kV for 5 s; separation voltage 1.4 kV. C^4D detector: sine waveform of 216 kHz, 10 V_{p-p}

In order to find an appropriate BGE, alternative buffer components HEPES, Tris, CHES and CAPS were investigated for their suitability for this application. These particular

alternatives were chosen due to their structural similarities and range of pKa values, as demonstrated in Table 15.

Table 15 **Properties and characterisation of low conductivity BGEs**

For application to histamine analysis in PDMS microchips

BGE (15 mM)	Structure and pKa	pH	Mean* Conductivity (µS) (n=3)	Mean µEOF ($cm^2V^{-1}S^{-1}$) (n=3)
Mes/His	*6.15*	6.26	359 ± 3.06	2.64 ± 0.07 x 10^{-4}
HEPES/ His	*7.50*	6.97	109 ± 2.08	4.47 ± 0.04 x 10^{-4}
Tris/His	*8.07*	8.93	177 ± 1.55	4.31 ± 0.03 x 10^{-4}
CHES/ His	*9.30*	7.72	27.0 ± 0.10	3.80 ± 0.08 x 10^{-4}
CAPS/ His	*10.40*	7.87	21.1 ± 0.22	6.29 ± 0.28 x 10^{-4}

Initially, the conductivity and electro-osmotic flow mobility (µEOF) of the alternative BGEs were determined to assess their properties in PDMS microchips with C^4D (Table 15). All of the investigated alternatives produced BGEs with lower conductivities and larger µEOFs than that of MES/histidine as seen in Table 15. Lower conductivities were considered advantageous as using these BGE systems in conjunction with C^4D should result in improved signal to noise ratios, attributed to lower background conductivity levels, and potentially improved detection limits. Subsequent analysis of individual BA standards using the alternative BGE systems found that both CHES/histidine and CAPS/histidine were unsuitable for this analysis as a result of heavily distorted peak shapes. Of the remaining alternatives Figure 61 shows that Tris/histidine produced only a low intensity signal for histamine and no discernable signal for tyramine or 2-phenylethylamine whereas HEPES/histidine produced signals for all analytes greater than that originally observed using MES/histidine BGE (Figure 60). As a result HEPES/histidine was chosen as the preferred BGE for further optimisation.
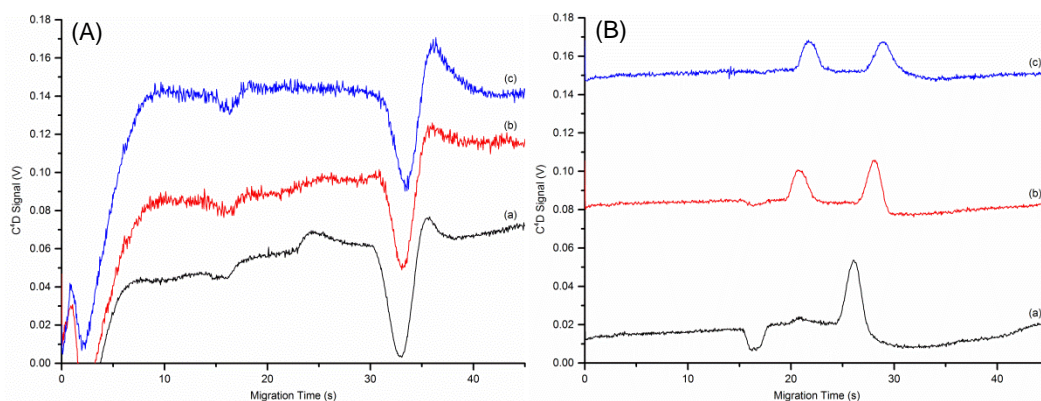
Figure 61 **Analysis of biogenic amines using Tris/His and HEPES/His BGEs**

Electropherograms using (A) 15 mM Tris/his BGE in 3% v/v isopropanol and (B) 15 mM HEPES/his BGE in 3% v/v isopropanol for the analysis of 10 mg.L^{-1} (a) histamine, (b) tyramine and (c) 2-phenylethylamine standards. Operating conditions: as per Figure 60

5.4.2 Optimisation of HEPES/His BGE

Despite 15 mM HEPES/His BGE in 3% v/v isopropanol providing the best peak heights of all BGEs trialled; Figure 62 (a) shows that the three BA analytes were poorly resolved when analysed together in a mixed standard (10 mg.L^{-1}). To produce the best sensitivity and resolution in electrophoretic techniques careful optimisation of BGE conditions is often required. Two commonly optimised variables include the addition of organic modifiers and alteration of the BGE ionic strength. These act to alter the μEOF of the system or the electrophoretic mobility of specific analytes.

Initially, the concentration of isopropanol added as an organic modifier to the 15 mM HEPES/His BGE was sequentially increased to inve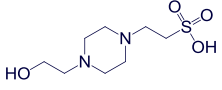stigate its effect on BA resolution. Figure 62 shows shifting of the BA peaks to slightly higher migration times as a result of increasing isopropanol concentration from 3% v/v to 10% v/v. Despite this small shift, there was no signififcant improvement in BA resolution observed. Isopropanol concentrations above 10% v/v were not trialled due to the incompatibility of organic solvents with PDMS microchips [5]. Overall, minimal improvement in BA resolution was observed upon increasing isopropanol concentration. However, the presence of an additional unknown peak (approx. 23 s) observed in individual tyramine and 2-PE standards (see Figure 61 (B)) using 3% v/v isopropanol was no longer present using concentrations of 5% v/v and 10% v/v. Therefore, for all further experiments 5% v/v isopropanol was chosen as optimum concentration for the organic modifier in the BGE.
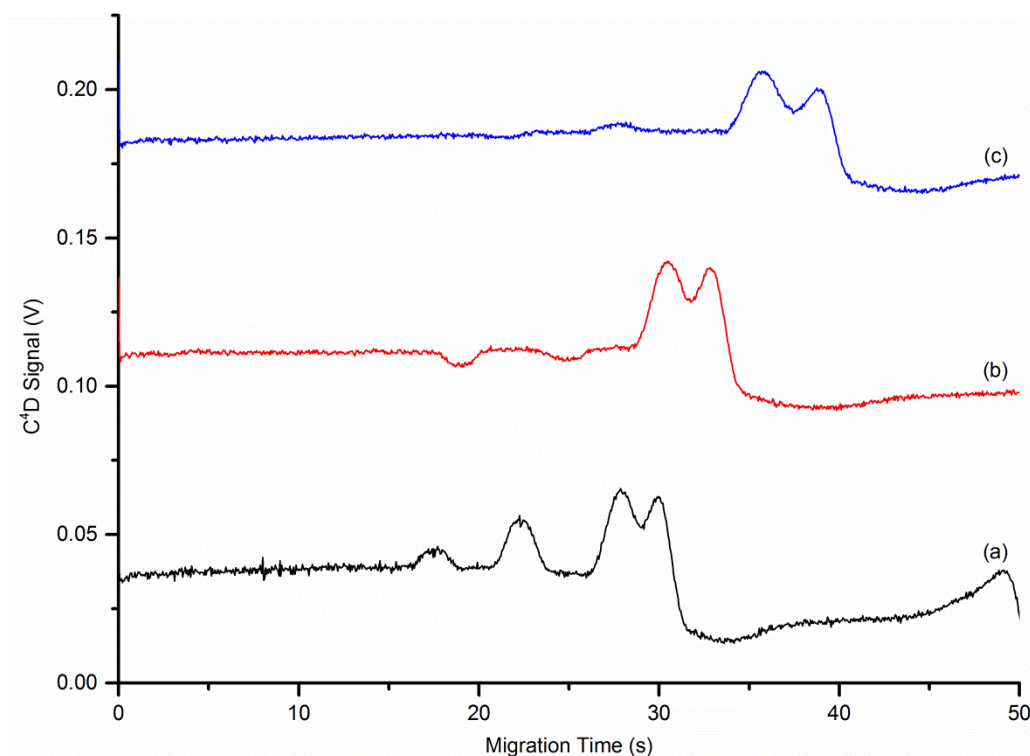
Figure 62   **Effect of altering the organic modifier concentration on BA separation**

Electropherograms of a standard containing the BAs histamine (10 mg.L^{-1}), tyramine (10 mg.L^{-1}) and 2-phenylethylamine (10 mg.L^{-1}) in 15 mM HEPES/his BGE containing (a) 3% v/v isopropanol, (b) 5% v/v isopropanol and (c) 10% v/v isopropanol as organic modifier. Operating conditions: as per Figure 60

An additional variable that is easily manipulated to achieve enhanced resolution is BGE ionic strength. For this application low conductivity BGEs were essential due to the use of C^{4}D. This ruled out the addition of high conductivity additives to increase this parameter. Therefore, altering ionic strength was achieved two ways. Firstly, by altering the ratio of the BGE components whilst maintaining the same overall concentration and secondly, after the ratio was optimised, by increasing the concentration of both BGE components whilst maintaining the same overall ratio. The electropherograms that resulted from altering the BGE component ratio are shown in Figure 63.
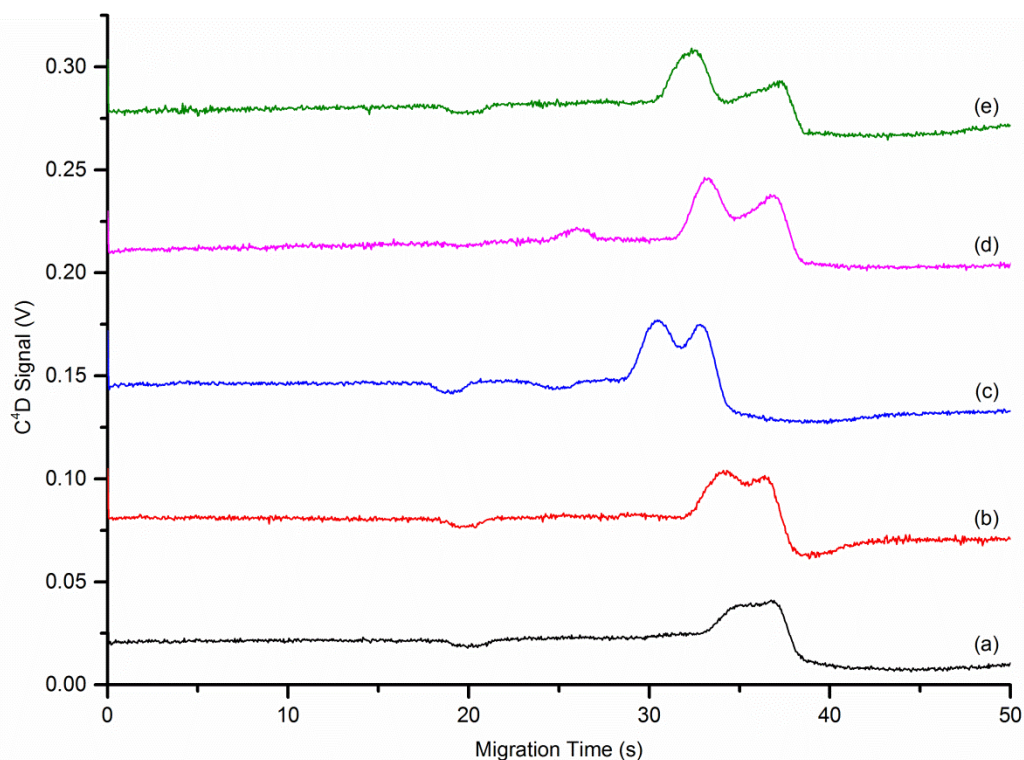
Figure 63   **Effect of altering the HEPES:His ratio on BA separation**

Electropherograms of a standard containing the biogenic amines histamine (10 mg.L^{-1}), tyramine (10 mgL^{-1}) and 2-phenylethylamine (10 mg.L^{-1}) using BGE with HEPES:His ratios of (a) 1:5 (pH 7.23), (b) 1:2 (pH 6.94), (c) 1:1 (pH 6.97), (d) 2:1 (pH 6.59) and (e) 5:1 (pH 6.32). Operating conditions: as per Figure 60

Increasing the HEPES:His ratio was expected to reduce the overall ionic strength of the BGE as zwitterions are known not to contribute to the ionic strength of a solution [236]. However, upon incrementally increasing the ratio from 1:5 to 2:1 the resolution of the histamine peak from tyramine and 2-phenylethylamine peaks improved with baseline resolution achieved using a final ratio of 5:1 (Figure 63). The increased resolution observed was attributed to the ability of the zwitterions to interact electrostatically with solvent and other charged molecules [236] combined with the decreased pH achieved at higher HEPES:His ratios.

To study the effect of increasing the overall BGE ionic strength the molar concentrations of HEPES and histidine were increased incrementally whilst maintaining the previously optimised 5:1 HEPES:His ratio. A trend of greater resolution of the three BAs was observed as the BGE molar concentration was increased (Figure 64). However, increased resolution was at the expense of peak height. As histamine was fully resolved from tyramine and 2-phenylethylamine using the intermediate concentrations of 50 mM HEPES and 10 mM histidine this BGE was chosen for additional optimisation.
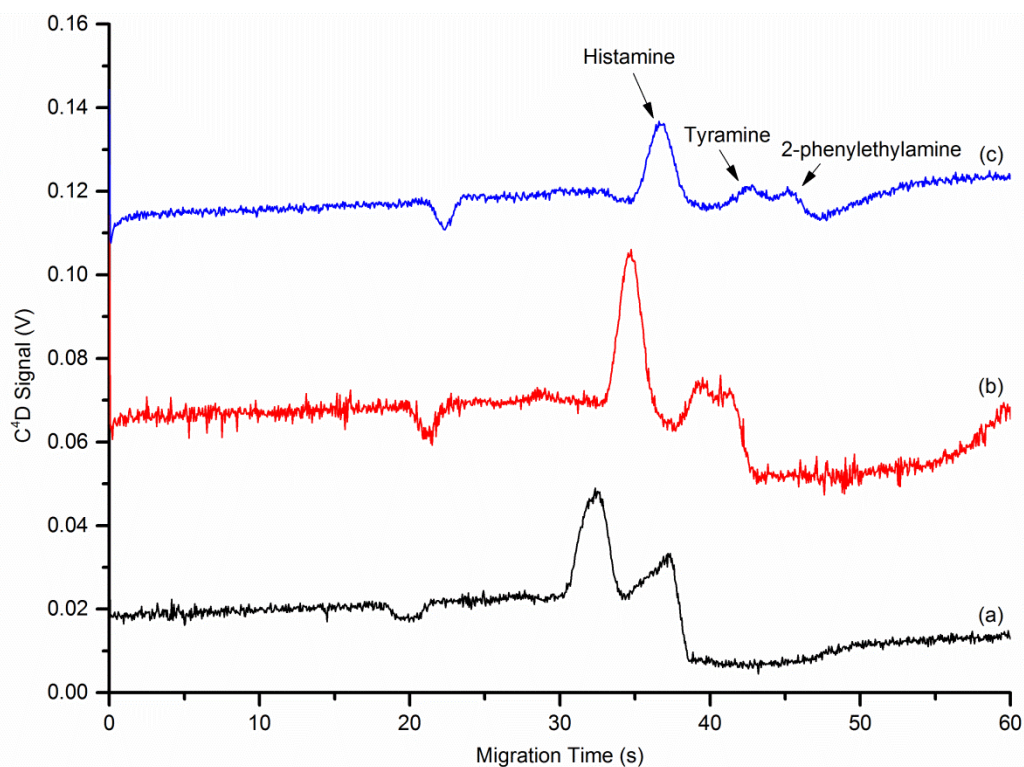
Figure 64   **Effect of altering the overall BGE ionic strength on BA separation**

Electropherograms of a standard containing the biogenic amines histamine (10 mgL^{-1}), tyramine (10 mgL^{-1}) and 2-phenylethylamine (10 mgL^{-1}) using (a) 25 mM HEPES/5 mM histidine BGE in 5% v/v isopropanol (ph 6.32), (b) 50 mM HEPES/10 mM histidine BGE in 5% v/v isopropanol (pH 6.31) and (c) 100 mM HEPES/20 mM histidine BGE in 5% v/v isopropanol (pH 6.30). Operating conditions: as per Figure 60

To complete the optimisation of the HEPES/His BGE for histamine analysis the ratio of HEPES:His at the higher BGE concentrations was again investigated. Specifically, molar concentration ratios of 5:1, 10:1 and 20:1 were trialled to see if resolution could be further improved. As shown in Figure 65 it was found that increasing the ratio from 5:1 to 10:1 slightly increased the resolution of tyramine and 2-phenylthylamine; however baseline resolution of the two analytes was still not achieved. Furthermore, analysis using the high 20:1 ratio resulted in significantly decreased peak heights for all analytes. Therefore, a ratio of 10:1 corresponding to 50 mM HEPES and 5 mM histidine in 5% v/v isopropanol was chosen as the final optimum BGE for histamine analysis as it provided optimum resolution and peak heights for the analysis of histamine (Figure 65).
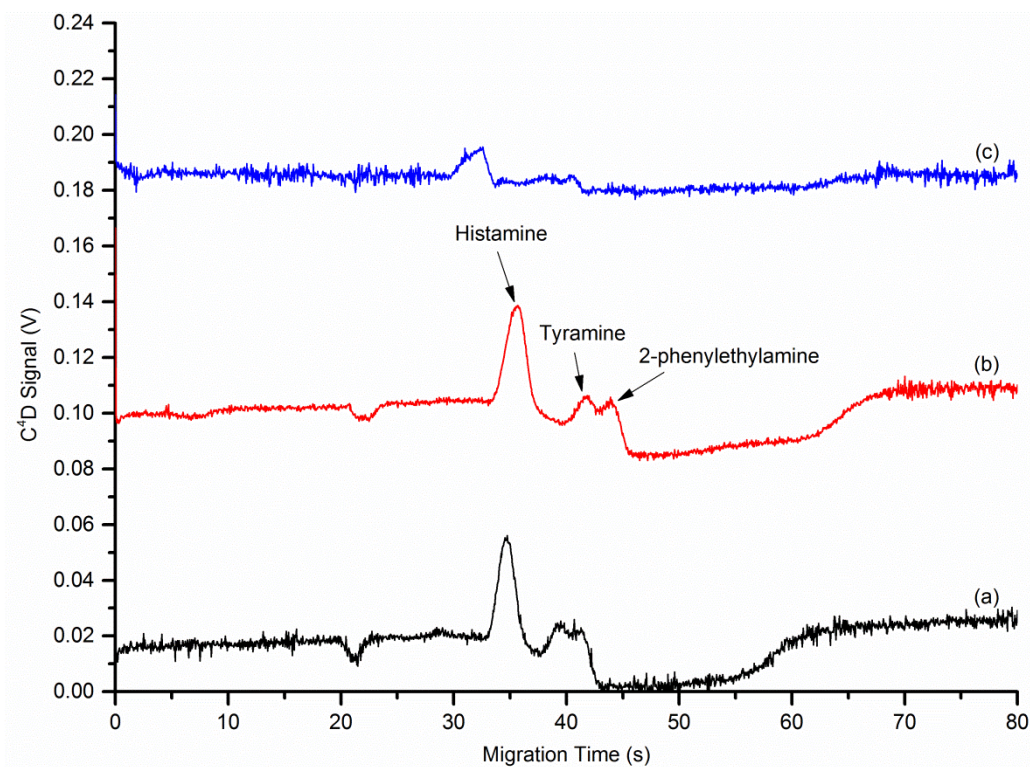
Figure 65   **Optimisation of the HEPES:His ratio for histamine analysis**

Electropherograms of a standard containing the biogenic amines histamine (10 mg.L-1), tyramine (10 mg.L-1) and 2-phenylethylamine (10 mg.L-1) using (a) 50 mM HEPES/10 mM histidine BGE in 5% v/v isopropanol (ph 6.31), (b) 50 mM HEPES/5 mM histidine BGE in 5% v/v isopropanol (pH 6.03) and (c) 50 mM HEPES/2.5 mM histidine BGE in 5% v/v isopropanol (pH 6.01). Operating conditions: as per Figure 60

5.4.3 Direct histamine quantification

After optimisation of the BGE the developed ME method was applied to a series of histamine calibration standards (1.07 mg.L^{-1} to 8.62 mg.L^{-1}) to determine its suitability for quantitative histamine analysis. The resulting histamine calibration curve and analytical figures of merit are shown in Figure 66 and Table 16 respectively. The linearity of the standard curve over the evaluated concentration range was confirmed with an R^2 value of 0.997. In addition, the relative standard deviation (%RSD) of migration time was 1.32 (n=15) reflecting the excellent repeatability and analytical performance of the system for the quantitative analysis of histamine. The instrumental limit of detection (LOD) and limit of quantification (LOQ) were determined using the equations outlined previously (Chapter 4) and were comparable to other reported methods for the direct detection of histamine using electrophoresis [200, 206]. Whilst more sensitive detection using indirect methods with electrophoresis have been reported [201, 215, 218], direct detection using conductivity was considered advantageous as it did not require lengthy histamine derivatisation steps prior to analysis. Furthermore, the reported LOD (0.43 mg.L^{-1}) was

only slightly higher than LODs reported for the analysis of volatile aliphatic amines in seafood (0.041 – 0.40 mg.L^{-1}) using microchip electrophoresis with C^{4}D [237]. However, the microchip fabrication and C^{4}D electrode integration approaches utilised in this work are considerably simpler [177]. The reported LOD and LOQ were also considered adequate for the determination of elevated histamine levels in food and beverage samples. When combined with an efficient extraction procedure; the limits reported in Table 16 will permit detection in samples that contain histamine below the maximum allowed levels in fish and fish products in the USA (50 µg.g^{-1}) [190].
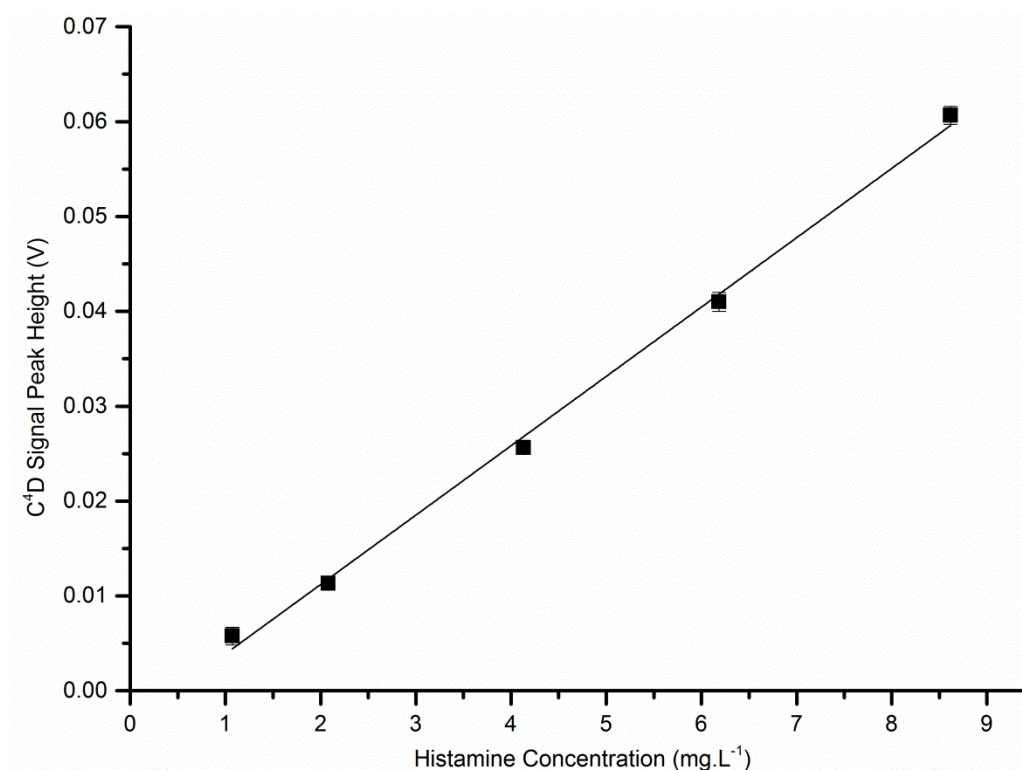
Figure 66   **Calibration plot with linear line of best fit for histamine peak heights**

Table 16   **Analytical figures of merit for the quantitative determination of histamine**

Analyte	Equation	R^2	LOD (mg.L^{-1})	LOQ (mg.L^{-1})	Migration time RSD (%) (n=15)
Histamine	$y = 0.0073x - 0.0034$	0.997	0.43	0.69	1.32

5.4.4 Development of a histamine extraction procedure from frozen fish

The applicability of the developed microchip electrophoresis-C^{4}D method was demonstrated through the determination of histamine levels in fish flesh. To extract histamine from flesh samples an extraction method reported by Hwang *et al.* [209], used for the determination of histamine by GC-MS, was adapted. The adapted method is outlined in Figure 67 and first involved the extraction of histamine from the flesh samples into methanol alkalised with concentrated ammonia. After extraction, the samples were centrifuged, the supernatant removed and then evaporated. The extracts were then reconstituted in water. Due to the complex nature of biological samples the flesh extracts required a cleanup step prior to analysis on the microchip electrophoresis device.
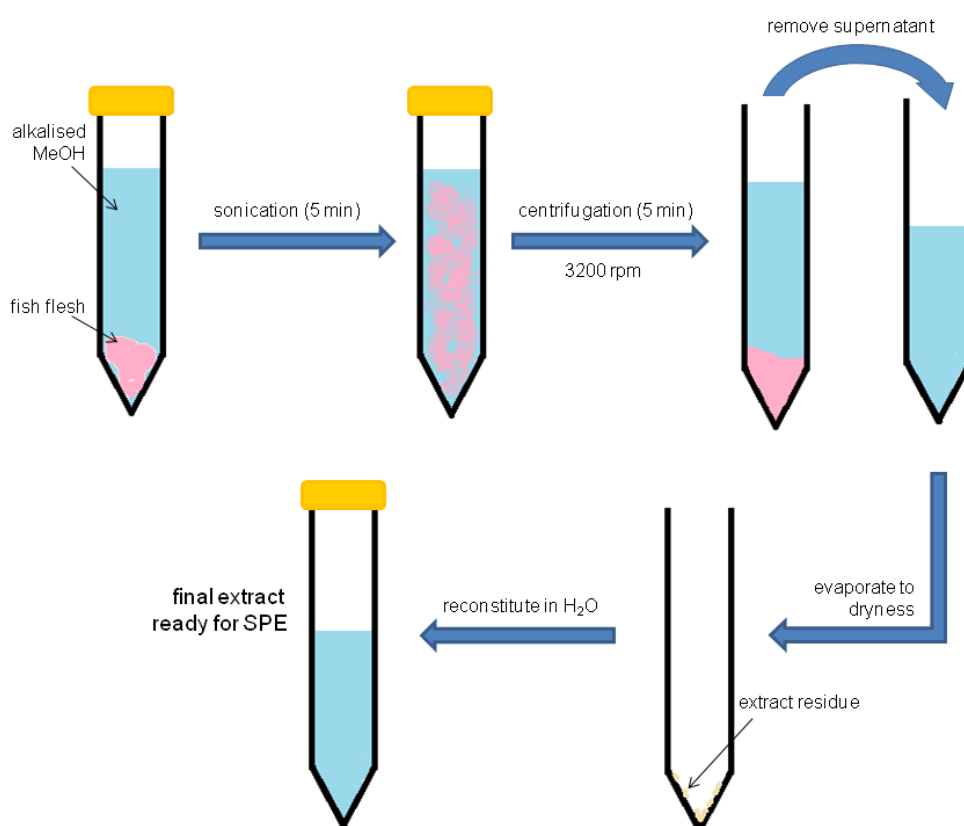
Figure 67 **Schematic of procedure used for histamine extraction from fish flesh**

A solid phase extraction (SPE) using C18 cartridge was chosen to cleanup the fish flesh extracts prior to analysis. Initially, a standard SPE procedure was adjusted from a method reported by Oguri *et al.* [238] for the analysis of histamine in food samples. The method published by Oguri *et al.* is outlined in Table 17 along with the proposed method adjusted for histamine extraction from the fish flesh extracts in this study.

Table 17   Comparison of SPE methods for the cleanup of fish extracts

SPE step	Oguri *et al.* method [238]	This method
SPE material	C18	C18
Condition	Methanol	Methanol
Equilibrate	Water x 2	Water
Load	Food extract	Fish extract
Wash	Nil	Water
Elute	Nil	BGE

The published method achieved sample cleanup by introducing food extracts containing histamine in a phosphate buffer (pH 3.0) and collecting the resulting eluent for analysis. This was found to provide samples that were free of other BAs as they were retained on the C18 cartridge allowing for the selective analysis of histamine [238]. Alternatively, for the current study the cleanup procedure was employed to eliminate organic compounds in the extracts that may interfere with analysis using microchip electrophoresis. To achieve this, samples were introduced in water to allow histamine and other BAs to be retained on the C18 cartridge. This was followed by a washing step using water and a final elution of the histamine using the optimised BGE (pH 6.03). This produced final extracts that were matrix matched for electrokinetic injection under non-stacking conditions. To confirm good recoveries of histamine were obtained using the proposed SPE cleanup method a simple test was performed on two water samples spiked with different amounts of histamine. The recoveries achieved are reported in Table 18.

Table 18   Recovery determination of histamine standards after SPE cleanup

Histamine standard	Actual concentration (mg.L^{-1})	Concentration post SPE cleanup (mg.L^{-1})	Recovery (%)
3 mg.L^{-1}	3.1	3.2	101.4
5 mg.L^{-1}	5.1	4.5	87.6

Recoveries obtained for the 3.1 mg.L^{-1} and 5.1 mg.L^{-1} histamine spiked water samples were 101.4% and 87.6% respectively. These results suggested that a degree of overloading may have occurred at the higher concentration resulting in the slightly lower recovery observed. However, as the recoveries for the two concentrations trialled were between the commonly accepted range of 80% – 120% the method was considered fit for the quantitative analysis of histamine [239]. Further validation was performed via spike and recovery experiments using the more complex fish matrices and is discussed in the proceeding section.

5.4.5 Analysis of histamine in frozen fish flesh

Initially, recoveries of tuna samples spiked with known amounts of histamine were determined to validate the extraction procedure outlined in Section 5.4.4. To achieve this thawed tuna flesh samples were spiked with three different amounts of histamine corresponding to a low, medium and high level in the range 40 – 190 μg.g^{-1}. The histamine peak was confirmed by the increase in peak height observed after spiking as demonstrated in the typical electropherogram for a spiked tuna extract displayed in Figure 68. As shown in Table 19, tuna flesh used in this experiment initially contained 17.7 ± 0.7 μg.g^{-1} of histamine, determined using the optimised method. The mean recovery of histamine using the standard extraction procedure ranged from 88.8 to 112.5% and all showed acceptable relative standard deviation values (%RSD<13%). These results strongly indicated that the extraction procedure in conjunction with the electrophoretic separation and direct detection via C^{4}D produced reliable measurements of histamine levels in the tuna flesh samples.
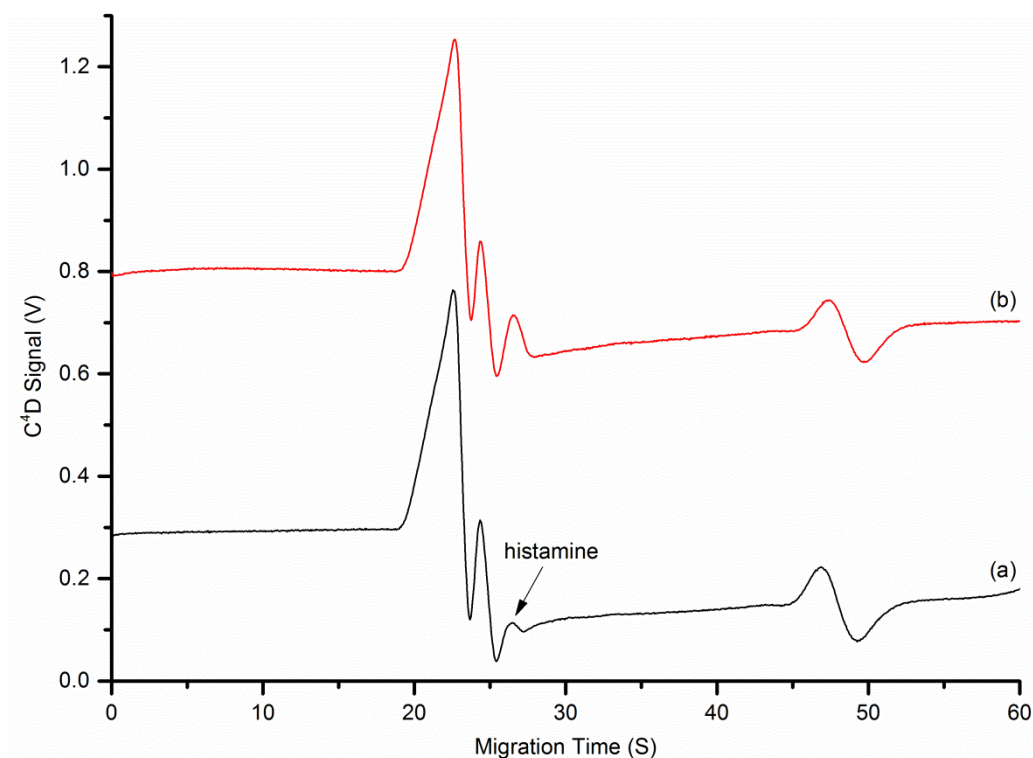
Figure 68   **Electropherograms of a tuna flesh extract pre and post histamine spike**

(a) without spike and (b) with a 47.5 μg.g^{-1} histamine spike using optimised BGE.
Operating conditions: as per Figure 60

Table 19   **Spike and recovery determination of histamine from tuna flesh**

Sample	Histamine content ($\mu g.g^{-1}$)			Mean recovery[b] (%)	RSD (%)
	Initial[a]	Spike[a]	Detected[a]		
Tuna flesh	17.7 ± 0.7	43.1 ± 7.2	61.1 ± 7.8	100.8	12.8
		91.9 ± 11.1	121.1 ± 7.9	112.5	6.5
		187.3 ± 4.9	184.0 ± 21.3	88.8	11.6

[a] Each histamine determination was performed in triplicate and final amount is reported as mean ± S.D.

[b] Recovery of spiked histamine from samples was calculated using [(detected histamine content-initial histamine content)/spiked histamine content] x 100%.

To demonstrate the versatility of the developed methodology it was used to determine the histamine content of a number of additional frozen fish samples purchased at a local supermarket. In total, histamine content was determined for four species of frozen fish. Table 20 shows that the fish samples analysed contained histamine levels ranging from 17.7 to 63.3 $\mu g.g^{-1}$. Both basa and pacific cod fillets contained histamine above the US FDA recommended 50 $\mu g.g^{-1}$ however, all were well below (<65 $\mu g.g^{-1}$) the Australian and New Zealand food safety standards maximum histamine content of 200 $\mu g.g^{-1}$. These results demonstrated the versatility of the developed methodology for determining histamine concentration in a variety of fish flesh samples. The significant advantage of employing microchip electrophoresis coupled with C^4D for this type of analysis was its simple instrumental setup with enhanced portability; which combined with simplified sample preparation, negating lengthy histamine derivatisation, and a rapid electrophoretic separation (< 50 s) allowed fast analysis timeframes.

Table 20   **Histamine contents of various species of frozen fish**

All samples purchased from a local supermarket

Frozen fish sample	Mean histamine content ($\mu g.g^{-1}$) (n=3)
Yellowfin tuna (*thunnus albacares*)	17.7 ± 0.7
Atlantic salmon (*salmo salar*)	43.4 ± 5.0
Basa (*pangasius hypophthalmus*)	63.3 ± 3.3
Pacific cod (*gadus macrocephalus*)	57.4 ± 2.6

To further demonstrate the applicability of the developed methodology the histamine content of tuna steaks during decomposition were determined. To achieve this, yellowfin tuna steaks were portioned into three approximately equal pieces and left at ambient temperature (~23 °C) in a fume cupboard for between 2 and 8 hours. Histamine extractions were performed at the time intervals 2, 4 and 8 hours with the resulting concentrations determined using the developed method shown in Table 21. A significant increase in histamine levels from the initial 17.7 ± 0.7 $\mu g.g^{-1}$ (determined previously) to 40.3 ± 4.5 $\mu g.g^{-1}$ was observed over the 8 hour decomposition period. However, the

histamine content after this time was still well below the Australia and New Zealand food standards maximum level for decomposition of 100 μg.g^{-1} [191] indicating that yellowfin tuna samples would need to be left for greater than 8 hours at ambient temperature before they produce histamine above the regulated levels. These results show that the method has the potential to be further optimised and applied for food monitoring in a production line setting, potentially during fish processing. The increased portability of this method compared to traditional high performance liquid chromatography methods could produce both cost and time benefits for this application.

Table 21   **Histamine contents of Yellowfin tuna steaks during decomposition**

Performed at ambient temperature

Decomposition time (hours)	Mean histamine content (μg.g^{-1}) (n=3)
0	17.7 ± 0.7
2	29.2 ± 1.4
4	30.5 ± 0.5
8	40.3 ± 4.5

5.5   Concluding remarks

The development of an alternative direct detection method for the analysis of histamine in fish samples using microchip electrophoresis with C^4D has been demonstrated. The method was optimised to produce detection limits for histamine of 0.43 mg.L^{-1} (S/N = 3) using calibration data in the linear range 1.07 - 8.62 mg.L^{-1} with a regression coefficient (R^2) of 0.997. Optimised BGE conditions included a mixed electrolyte containing 50 mM HEPES and 5 mM histidine in 5% v/v isopropanol to prevent precipitation of histamine in the microchannels during electrophoretic separation. After optimisation, the new method was used in conjunction with an adapted histamine extraction and cleanup procedure for the analysis of histamine levels in frozen fish samples. Spike and recovery experiments were performed at three concentration levels producing mean recoveries in all cases greater than 88.8% (n = 3) and relative standard deviations ≤ 12.8%. Further application of the direct detection method was demonstrated by determining the histamine content of four frozen fish samples sourced from local supermarkets and undertaking a decomposition study on yellowfin tuna. All fish samples were found to contain histamine below the maximum allowed limit for decomposition in Australia (100 μg.g^{-1}) [191].

This new method represents the first use of microchip electrophoresis coupled with C^4D for the direct analysis of histamine. This approach negates the need for derivatisation, required for the detection of these analytes using optical detection techniques, and incorporates the significant advantage of enhanced analysis portability for potential on-site analysis. The reported method has comparable LODs with other direct detection approaches and its suitability has been demonstrated for histamine recovery in yellowfin tuna flesh samples. Furthermore, the versatility of this new approach was demonstrated by determining the histamine content in a number of frozen fish samples. This approach has potential to be further optimised for the determination of additional biogenic amines in a large range of food and beverage samples. It is possible that with further extraction method development it could be implemented for monitoring of food quality during processing and storage.

6. Conclusions and Future Work

6.1   Conclusions

Prior to this work, the integration of C^{4}D with microfluidic chips was limited by multi-step electrode patterning/fabrication processes which in turn led to difficulty in consistently aligning detection electrodes. These limitations can compromise analytical performance of the electrodes and increase the time and cost of device production. Chapter 2 describes the first design and implementation of injected metal electrodes for C^{4}D detection on PDMS microfluidic chips. This simplified approach utilised additional electrode guide microchannels fabricated into the microchip, for integration of injected gallium electrodes, in the same photolithographic process as the electrophoresis microchannels. C^{4}D electrode integration utilising injected gallium electrodes was fast, highly reproducible, eliminated difficulties with alignment and produced electrodes which were easily connected to external electronic circuitry using a custom designed PCB. Using this approach C^{4}D can be readily achieved in any microchip by simply adding extra 'electrode' channels to the microchannel design.

The optimisation of a microchip electrophoresis method, with the novel C^{4}D electrode setup, for the analysis of a model analyte system comprising of K$^+$, Na$^+$ and Li$^+$ is described in Chapter 3. As a result of this study it was determined that stable electro-osmotic flows of 2.00 $\pm$ 0.11 x 10^{-4} cm^2 V^{-1} s^{-1} were achieved via an intermittent dynamic surfactant modification of the microchannel surfaces using 15 mM MES/His BGE with 0.4 mM DDM. Furthermore, the optimised electrophoresis BGE, separation and injection conditions were as follows; BGE contained 15 mM MES/His, separation voltage: 1400 V, electrokinetic injection voltage: 800 V and an electrokinetic injection time: 10 s. The analytical repeatability of the optimised electrophoresis method was confirmed with intra-day %RSDs for migration times and peak heights being below 1.2 and 2.5 respectively for all analytes. Moreover, the inter-day %RSDs for migration time and peak height were below 3.4 and 2.6 respectively for all analytes.

Following the development of an optimised electrophoresis method, physical parameters of the injected gallium electrodes were optimised in Chapter 4 to achieve sensitive detection. The design flexibility afforded by the injected gallium electrode system allowed for straightforward optimisation of the electrode geometry, distance from separation channel and length. Overall, the optimised parameters were determined to be anti-parallel electrode geometry with a 75 μm electrode distance from separation channel and a 1000 μm electrode length. Using these parameters, a calibration of the model analytes Li$^+$, Na$^+$ and K$^+$ yielded detections limits ranging from 6.2 to 8.7 μM and limits of quantitation ranging from 9.1 to 12.7 μM. Upon applying an FFT low-pass filter to the raw data a 2.3 fold reduction in the background noise level was observed. This in turn

resulted in a small improvement of 1.7 to 1.8 fold and 1.4 fold for the reported LODs and LOQs respectively.

The ability of the novel electrode system to perform sensitive and quantitative analysis is demonstrated in Chapter 5. In this work an alternative direct detection method for the analysis of histamine in fish samples using the microchip electrophoresis with optimised C^4D was developed. This new method represented the first use of microchip electrophoresis coupled with C^4D for the direct determination of histamine. This approach negated the need for derivatisation, a step required for the detection of these analytes using optical detection techniques, and incorporated the significant advantage of enhanced analysis portability for potential on-site analysis. The reported method had comparative LODs with other direct detection approaches and its suitability was demonstrated for histamine recovery in yellowfin tuna flesh samples. Furthermore, the versatility of this new approach was demonstrated by determining the histamine content in a number of frozen fish species. We believe this approach has potential to be further optimised for the determination of additional biogenic amines in a large range of food and beverage samples and could even be implemented for food quality monitoring during processing and storage.

6.2   Future work

6.2.1   Microchip electrophoresis instrumental setup

The microfluidic channel network used throughout this work was designed to perform simple and rapid electrophoretic separations with electrokinetic injection capability. As a result separation of a simple model system (Li$^+$, Na$^+$ and K$^+$) and histamine from a more complex matrix was achieved using an effective separation length of 37 mm. However, theory predicts that analyte resolution can be significantly improved upon increasing the effective separation length [81, 88] and this would further aid in the separation of more complex analyte mixtures such as the biogenic amines discussed in Chapter 5. An increased effective length could be achieved on a similar sized microchip by incorporating a serpentine shaped sequence before straightening again at the detection electrodes [240-241]. This would allow for additional separation length without increasing the overall size of the microchip potentially extending the analysis capability of the developed device.

PDMS was chosen as the microchip substrate for all investigations in this work due to its fabrication simplicity, low cost and similar properties to that of glass. However, as documented, electrophoresis microchannels in PDMS require treatment to provide stable surface chemistries and consequently stable μEOFs during electrophoresis. Additionally, compared to more stable alternatives, such as glass and polycarbonate, PDMS microchips can display shorter lifetimes due to the variable nature of its μEOF [242]. A full investigation into substrate alternatives such as glass and polycarbonate chips would add value in identifying the optimum material to use. Important factors that should be considered in such an investigation should include microchip lifetime, fabrication simplicity and cost and ease of electrophoretic separations (ie: surface treatments). Due to the fabrication methods used for constructing glass chips it may prove challenging to incorporate injected gallium electrodes with the same optimised parameters as those described in this work. This is because common chemical and mechanical etching techniques may not be able to reproduce the electrode and separation microchannels in the same proximity (within 50 μm) used in this work. One potential approach could be the use of plasma etching which has been shown to produce microchannels with near vertical side walls [243]. However, due consideration should be given to the cost and time of producing such devices as these are favourable properties of the presented PDMS system.

Electrophoretic separations in these studies were performed only on positively charged (cationic) species. This limitation was due to the high voltage power supply implemented when building the system only supplying a positive voltage. A logical extension of this

work would be to incorporate additional high voltage capability for the separation and detection of negatively charged (anionic) species. Furthermore, by expanding the capability of the high voltage power supply alternative electrokinetic injection strategies such as pinched injection could be explored. Pinched injection methods are known to prevent leakage both during injection and separation, reducing sample plug size and stabilising background levels during repetitive analysis runs [244-245]. The implementation of such an injection strategy could lead to improved resolution due to smaller sample plug sizes. An additional separation approach that could be investigated to improve the overall sensitivity of the developed device would be isotachophoresis (ITP). ITP is known as a moving boundary electrophoresis technique that utilises two buffer systems to create leading and terminating electrolytes effectively sandwiching the analyte zones [246]. As a result it has been shown to be an effective on-chip sample preconcentration technique [247-248]

6.2.2 C[4]D system

The electronic setup of the C[4]D used in this work was adapted from a previously reported system due to its simplicity and availability of parts. A detailed study into the electronic setup of the C[4]D system could result in improved instrument sensitivity and consequently its application detection limits. Particularly it would be of interest to look at the implementation of a recent advance where a series resonance detection approach is achieved by incorporating a quartz crystal as an ideal inductor [235, 249-250]. This has been reported to result in the cancellation of unwanted capacitance in the system ultimately producing improved sensitivity by reducing background noise. The result of implementing such a system would be improved detection limits and the ability to apply the chip to less conductive analytes.

Gallium metal was chosen as the electrode material in this work due to its low melting point (29.8 °C), ease of handling and low toxicity. However, its low melting point could also be detrimental for truly portable systems required for in field under potentially fluctuating temperatures. Therefore a more robust electrode material may be required for these applications. A number of other low melting point alloys are available and have been reported for use as injected electrodes in alternative applications [173, 175-176]. Namely, eutectic gallium indium alloy containing 75% gallium and 25% indium (mp 15.7 °C), Field's metal consisting of 51% indium, 32.5% bismuth and 16.5% tin (mp 62 °C) and Wood's metal consisting of 50% bismuth, 26.7% lead, 13.3% tin and 10% cadmium (mp 70 °C). Each of these has been reported as materials for injected electrodes. Despite the increased toxicity of both Wood's and Field's metal a thorough investigation comparing all of the alloys performances as an electrode material would be worthwhile and add to this field of research. Another alternative electrode material would be ionic liquids or salt solutions. Saturated sodium chloride solutions have been previously

reported as an electrode material in PDMS microfluidic devices for droplet generation [251]. It would be an interesting extension to examine the suitability of these materials for C^4D applications as they are readily available and inexpensive compared to liquid metals. Although salt solutions may not possess a conductivity sufficient to carry the required high voltage signals, this investigation would be an important contribution to the field.

The basic design of the electrode guide channels used throughout this work was implemented due to its similarity to externally mounted solid metal electrodes. Although multiple electrode geometries (parallel, anti-parallel and quad) were studied it is possible that alternative electrode shapes and designs may provide enhanced instrument sensitivity. The aim of this research was to investigate if injected gallium electrodes were able to be easily implemented and used for C^4D on a microchip and as such additional electrode shapes and designs were not investigated. A previous report found electrodes with semi-circular ends adjacent the separation microchannel offered improved sensitivity over conventional rectangular electrodes [171]. Although soft lithography fabrication limits the distance that microchannels can be from one another; it is possible that further work into alternate electrode shapes and guide channel designs could provide valuable data to this field of research and lead to a detection system with improved sensitivity.

6.2.3 Application extension to additional biogenic amines and samples

In this study, the developed microchip electrophoresis device with C^4D was applied to the detection of histamine in fish flesh samples. Its successful use for the determination of histamine opens up a number of potential avenues for further work in this area. Firstly, it would be advantageous if the developed method could be further optimised to separate additional BAs such as tyramine and 2-phenylethylamine [185]. A number of BAs are known to be causative agents for food poisoning in a large range of foods and beverages so the ability to determine these in addition to histamine would allow for more comprehensive monitoring using the developed methodology. With the incorporation of a lengthened separation channel mentioned previously it could be possible to separate additional BAs using the methods outlined in this work. Additionally, potential improvements to the C^4D system (Section 6.2.2) could also assist with achieving lower limits of detection for these compounds.

The extraction and cleanup methods reported in these studies were adapted from previous reports and were optimised for the analysis of histamine only. As mentioned, the capability to efficiently extract and quantitatively determine an extended range of BAs would be very valuable. Therefore an important future work investigation would be to further develop and optimise the reported extraction method to include more BA

compounds. This could be achieved using an alternative SPE material or with ultrasound assisted microextraction which has been reported for the extraction of BAs that were determined using HPLC [252] and GC-MS [253]. In addition it would also be of significant interest to expand the extraction and cleanup methods to a range of different food and beverages. Samples including fermented beverages, fresh and canned fish products, dairy products and meat products can also contain elevated levels of BAs [185]. Therefore, an efficient extraction and cleanup method producing extracts that could be simply analysed using the microchip electrophoresis-C^4D device developed in these studies would be an exciting extension of this work.

Finally, after the further optimisation and extension of the reported methods outlined above this approach could be implemented as a replacement for traditional methods of food monitoring during food processing and storage. Whilst a thorough investigation into the system's ability to produce the same high quality data of traditional approaches, such as HPLC, would first be required there is no obvious reason why a further optimised system could not be employed for this purpose.

7. Appendix
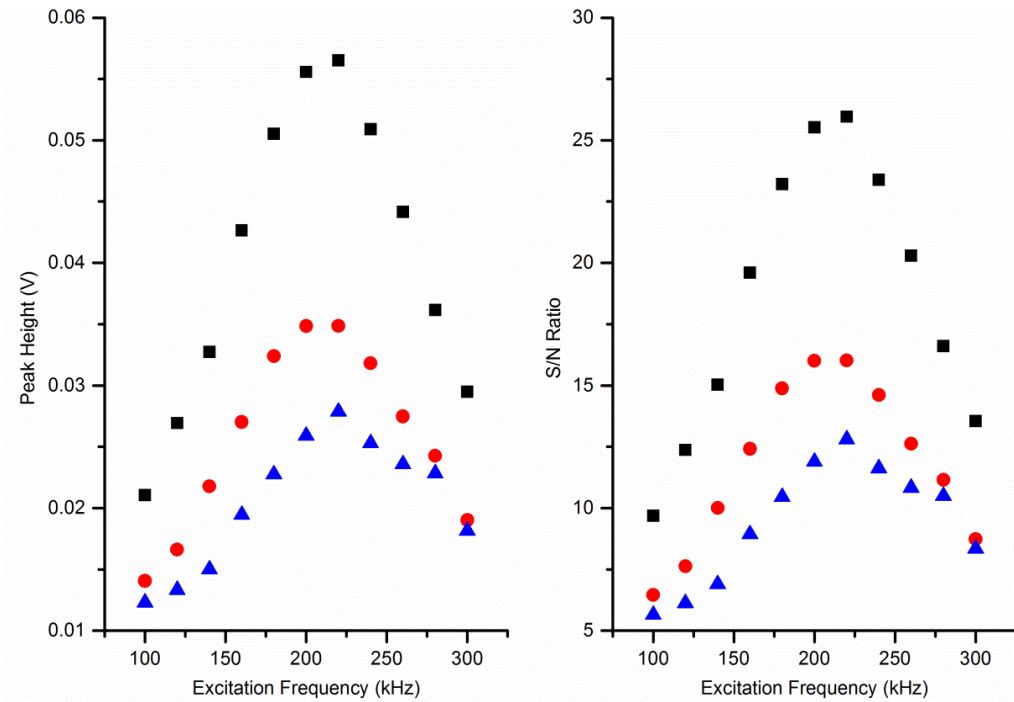
Figure 69   **Effect of excitation frequency on model analyte peaks using parallel geometry**

Peak heights and S/N ratios of Li^+ (−▲−), Na^+ (−●−) and K^+ (−■−) peaks (5 × 10^{-4} M) obtained using injected gallium electrodes in parallel geometry with an excitation voltage of 4.5 V
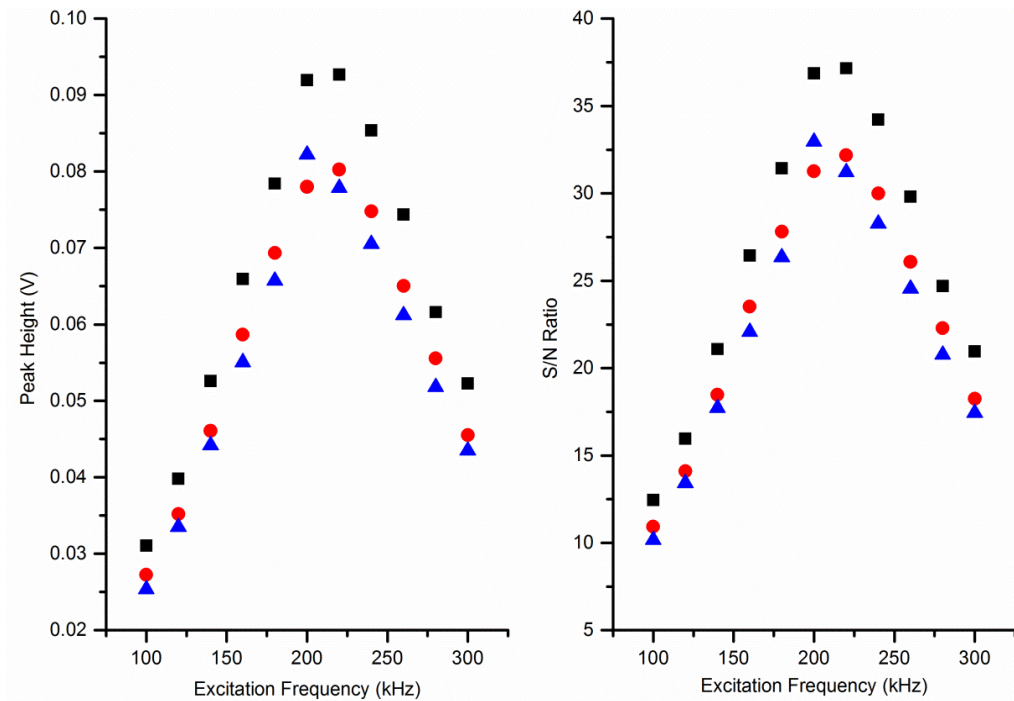
Figure 70   **Effect of excitation frequency on model analyte peaks using anti-parallel geometry**

Peak heights and S/N ratios of Li^+ (−▲−), Na^+ (−●−) and K^+ (−■−) peaks (5 × 10^{-4} M) obtained using injected gallium electrodes in anti-parallel geometry with an excitation voltage of 5.5 V
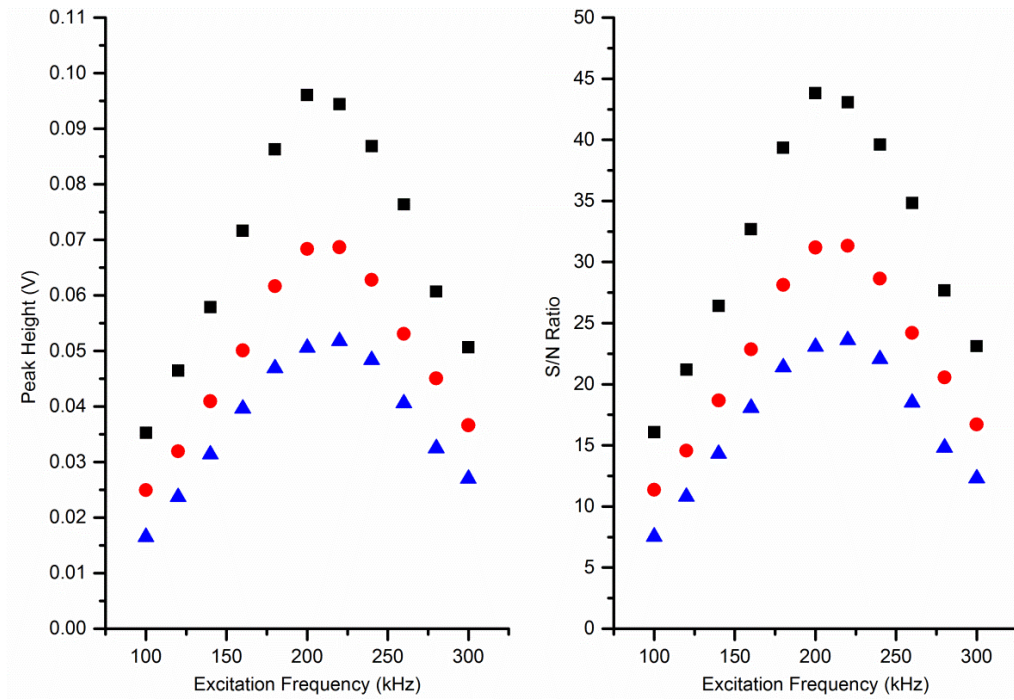
Figure 71   **Effect of excitation frequency on model analyte peaks using 1250 μm electrodes**

Peak heights and S/N ratios of Li⁺ (− ▲ −), Na⁺ (− ● −) and K⁺ (−■−) peaks (5 × 10⁻⁴ M) obtained using anti-parallel injected gallium electrodes with an electrode length of 1250 μm in geometry with an excitation voltage of 6 V

8. References

1. Whitesides, G. M., *The origins and the future of microfluidics*, Nature, 2006. **442**(7101): p. 368-373.

2. Yetisen, A. K. and Volpatti, L. R., *Patent protection and licensing in microfluidics*, Lab on a Chip, 2014. **14**(13): p. 2217-2225.

3. Ohno, K.-i., Tachikawa, K. and Manz, A., *Microfluidics: Applications for analytical purposes in chemistry and biochemistry*, Electrophoresis, 2008. **29**(22): p. 4443-4453.

4. McDonald, J. C., Duffy, D. C., Anderson, J. R., Chiu, D. T., Wu, H., Schueller, O. J. A. and Whitesides, G. M., *Fabrication of microfluidic systems in poly(dimethylsiloxane)*, Electrophoresis, 2000. **21**(1): p. 27-40.

5. McDonald, J. C. and Whitesides, G. M., *Poly(dimethylsiloxane) as a Material for Fabricating Microfluidic Devices*, Accounts of Chemical Research, 2002. **35**(7): p. 491-499.

6. Sia, S. K. and Whitesides, G. M., *Microfluidic devices fabricated in Poly(dimethylsiloxane) for biological studies*, Electrophoresis, 2003. **24**(21): p. 3563-3576.

7. *Microfluidics market by materials (polymers, silicon, glass), pharmaceuticals (microreactors, toxicity, screening, lab on chip, proteomic & genomic analysis) drug delivery devices (microneedles, micropumps), IVD (POC) - Global Trends & Forecast to 2018*, Markets and Markets, 2013.

8. *Microfluidic technologies: Biopharmaceutical and Healthcare Applications 2013-2023*, Visiongain, 2013.

9. Dittrich, P. S. and Manz, A., *Lab-on-a-chip: microfluidics in drug discovery*, Nature Reviews Drug Discovery, 2006. **5**(3): p. 210-218.

10. Horsman, K. M., Bienvenue, J. M., Blasier, K. R. and Landers, J. P., *Forensic DNA Analysis on Microfluidic Devices: A Review*, Journal of Forensic Sciences, 2007. **52**(4): p. 784-799.

11. Paegel, B. M., Blazej, R. G. and Mathies, R. A., *Microfluidic devices for DNA sequencing: sample preparation and electrophoretic analysis*, Current Opinion in Biotechnology, 2003. **14**(1): p. 42-50.

12. Schulte, T. H., Bardell, R. L. and Weigl, B. H., *Microfluidic technologies in clinical diagnostics*, Clinica Chimica Acta, 2002. **321**(1–2): p. 1-10.

13. Chin, C. D., Linder, V. and Sia, S. K., *Commercialization of microfluidic point-of-care diagnostic devices*, Lab on a Chip, 2012. **12**(12): p. 2118-2134.

14. Fortier, M.-H., Bonneil, E., Goodley, P. and Thibault, P., *Integrated*

Microfluidic Device for Mass Spectrometry-Based Proteomics and Its Application to Biomarker Discovery Programs, Analytical Chemistry, 2005. **77**(6): p. 1631-1640.

15. Khandurina, J. and Guttman, A., *Bioanalysis in microfluidic devices*, Journal of Chromatography A, 2002. **943**(2): p. 159-183.

16. Jokerst, J. C., Emory, J. M. and Henry, C. S., *Advances in microfluidics for environmental analysis*, Analyst, 2012. **137**(1): p. 24-34.

17. Beebe, D. J., Mensing, G. A. and Walker, G. M., *Physics and Applications of Microfluidics in Biology*, Annual Review of Biomedical Engineering, 2002. **4**(1): p. 261-286.

18. Squires, T. M. and Quake, S. R., *Microfluidics: Fluid physics at the nanoliter scale*, Reviews of Modern Physics, 2005. **77**(3): p. 977.

19. Stone, H. A., Stroock, A. D. and Ajdari, A., *Engineering flows in small devices: Microfluidics toward a lab-on-a-chip*, Annual Review of Fluid Mechanics, 2004. **36**: p. 381-411.

20. Zhou, G. and Yao, S.-C., *Effect of surface roughness on laminar liquid flow in micro-channels*, Applied Thermal Engineering, 2011. **31**(2–3): p. 228-234.

21. Weibel, D. B. and Whitesides, G. M., *Applications of microfluidics in chemical biology*, Current Opinion in Chemical Biology, 2006. **10**(6): p. 584-591.

22. Figeys, D. and Pinto, D., *Lab-on-a-Chip: A Revolution in Biological and Medical Sciences*, Analytical Chemistry, 2000. **72**(9): p. 330 A-335 A.

23. Sharp, K. V. and Adrian, R. J., *Transition from laminar to turbulent flow in liquid filled microtubes*, Experiments in Fluids, 2004. **36**(5): p. 741-747.

24. Gervais, T. and Jensen, K. F., *Mass transport and surface reactions in microfluidic systems*, Chemical Engineering Science, 2006. **61**(4): p. 1102-1121.

25. Guo, Z.-Y. and Li, Z.-X., *Size effect on single-phase channel flow and heat transfer at microscale*, International Journal of Heat and Fluid Flow, 2003. **24**(3): p. 284-298.

26. Manz, A., Effenhauser, C. S., Burggraf, N., Harrison, D. J., Seiler, K. and Fluri, K., *Electroosmotic pumping and electrophoretic separations for miniaturized chemical analysis systems*, Journal of Micromechanics Microengineering, 1994. **4**: p. 257-265.

27. Locascio, L. E., Perso, C. E. and Lee, C. S., *Measurement of electroosmotic flow in plastic imprinted microfluid devices and the effect*

of protein adsorption on flow rate, Journal of Chromatography A, 1999. **857**(1-2): p. 275-284.

28.   Zhao, B., Moore, J. S. and Beebe, D. J., *Surface-Directed Liquid Flow Inside Microchannels*, Science, 2001. **291**(5506): p. 1023-1026.

29.   Pollack, M. G., Fair, R. B. and Shenderov, A. D., *Electrowetting-based actuation of liquid droplets for microfluidic applications*, Applied Physics Letters, 2000. **77**(11): p. 1725-1726.

30.   Prins, M. W. J., Welters, W. J. J. and Weekamp, J. W., *Fluid Control in Multichannel Structures by Electrocapillary Pressure*, Science, 2001. **291**(5502): p. 277-280.

31.   Marle, L. and Greenway, G. M., *Microfluidic devices for environmental monitoring*, TrAC Trends in Analytical Chemistry, 2005. **24**(9): p. 795-802.

32.   Lee, K. B. and Lin, L., *Surface micromachined glass and polysilicon microchannels using MUMPs for BioMEMS applications*, Sensors and Actuators A: Physical, 2004. **111**(1): p. 44-50.

33.   Chien, R.-D., *Micromolding of biochip devices designed with microchannels*, Sensors and Actuators A: Physical, 2006. **128**(2): p. 238-247.

34.   McCormick, R. M., Nelson, R. J., Alonso-Amigo, M. G., Benvegnu, D. J. and Hooper, H. H., *Microchannel Electrophoretic Separations of DNA in Injection-Molded Plastic Substrates*, Analytical Chemistry, 1997. **69**(14): p. 2626-2630.

35.   Shen, J.-Y., Chan-Park, M. B.-E., Feng, Z.-Q., Chan, V. and Feng, Z.-W., *UV-embossed microchannel in biocompatible polymeric film: Application to control of cell shape and orientation of muscle cells*, Journal of Biomedical Materials Research Part B: Applied Biomaterials, 2006. **77B**(2): p. 423-430.

36.   Wolfe, D. B., Qin, D. and Whitesides, G. M., *Rapid Prototyping of Microstructures by Soft Lithography for Biotechnology*, Humana Press, 2010, p. 81-107.

37.   Neill, P. F., Ben Azouz, A., Vázquez, M., Liu, J., Marczak, S., Slouka, Z., Chang, H. C., Diamond, D. and Brabazon, D., *Advances in three-dimensional rapid prototyping of microfluidic devices for biological applications*, Biomicrofluidics, 2014. **8**(5): p. 052112.

38.   Andersson, H., van der Wijngaart, W., Enoksson, P. and Stemme, G., *Micromachined flow-through filter-chamber for chemical reactions on beads*, Sensors and Actuators B: Chemical, 2000. **67**(1-2): p. 203-208.

39. Attia, U., Marson, S. and Alcock, J., *Micro-injection moulding of polymer microfluidic devices*, Microfluidics and Nanofluidics, 2009. **7**(1): p. 1-28.

40. Elders, J., Jansen, H. V., Elwenspoek, M. and Ehrfeld, W., presented in part at the The Eighth IEEE International Conference on Micro Electro Mechanical Systems, Amsterdam, Netherlands, 1995.

41. Hanemann, T., Pfleging, W., Haußelt, J. and Zum, K. H., *Laser micromaching and light induced reaction injection molding as suitable process sequence for the rapid fabrication of microcomponents*, Microsystem Technologies, 2002. **7**(5): p. 209-214.

42. Becker, H. and Heim, U., *Hot embossing as a method for the fabrication of polymer high aspect ratio structures*, Sensors and Actuators A: Physical, 2000. **83**(1-3): p. 130-135.

43. Becker, H. and Heim, U., Silicon as tool material for polymer hot embossing, *Proceedings of Twelfth IEEE International Conference on Micro Electro Mechanical Systems*, Orlando, Florida, 1999.

44. Papautsky, I., in *Bio-MEMS*, CRC Press, 2006, p. 117-140.

45. Pun Pang, S., Knopf, G. K., Ostojic, M. and Nikumb, S., Rapid Fabrication of Micromolds for Polymeric Microfluidic Devices, *Proceedings of Canadian Conference on Electrical and Computer Engineering*, Vancouver, 2007.

46. Schutte, J., Freudigmann, C., Benz, K., Bottger, J., Gebhardt, R. and Stelzle, M., *A method for patterned in situ biofunctionalization in injection-molded microfluidic devices*, Lab on a Chip, 2010. **10**(19): p. 2551-2558.

47. Qi, S., Liu, X., Ford, S., Barrows, J., Thomas, G., Kelly, K., McCandless, A., Lian, K., Goettert, J. and Soper, S. A., *Microfluidic devices fabricated in poly(methyl methacrylate) using hot-embossing with integrated sampling capillary and fiber optics for fluorescence detection*, Lab on a Chip, 2002. **2**(2): p. 88-95.

48. Xia, Y. and Whitesides, G. M., *Soft Lithography*, Annual Review of Materials Science, 1998. **28**(1): p. 153-184.

49. Zaouk, R., Park, B. Y. and Madou, M. J., in *Microfluidic Techniques*, ed. Shelley D. Minteer, Humana Press, 2006, vol. 321, p. 17-21.

50. Lee, J. N., Park, C. and Whitesides, G. M., *Solvent Compatibility of Poly(dimethylsiloxane)-Based Microfluidic Devices*, Analytical Chemistry, 2003. **75**(23): p. 6544-6554.

51. Sollier, E., Murray, C., Maoddi, P. and Di Carlo, D., *Rapid prototyping polymers for microfluidic devices and high pressure injections*, Lab on a

Chip, 2011. **11**(22): p. 3752-3765.

52. Miyaki, K., Zeng, H.-L., Nakagama, T. and Uchiyama, K., *Steady surface modification of polydimethylsiloxane microchannel and its application in simultaneous analysis of homocysteine and glutathione in human serum*, Journal of Chromatography A, 2007. **1166**(1-2): p. 201-206.

53. Schrott, W., Svoboda, M., Slouka, Z., Pribyl, M. and Snita, D., *PDMS microfluidic chips prepared by a novel casting and pre-polymerization method*, Microelectronic Engineering. **87**(5-8): p. 1600-1602.

54. Berdichevsky, Y., Khandurina, J., Guttman, A. and Lo, Y. H., *UV/ozone modification of poly(dimethylsiloxane) microfluidic channels*, Sensors and Actuators B: Chemical, 2004. **97**(2-3): p. 402-408.

55. Zhou, J., Ellis, A. V. and Voelcker, N. H., *Recent developments in PDMS surface modification for microfluidic devices*, Electrophoresis 2010. **31**(1): p. 2-16.

56. Bodas, D. and Khan-Malek, C., *Formation of more stable hydrophilic surfaces of PDMS by plasma and chemical treatments*, Microelectronic Engineering. **83**(4-9): p. 1277-1279.

57. Wong, I. and Ho, C.-M., *Surface molecular property modifications for poly(dimethylsiloxane) (PDMS) based microfluidic devices*, Microfluidics and Nanofluidics, 2009. **7**(3): p. 291-306.

58. Seethapathy, S. and Górecki, T., *Applications of polydimethylsiloxane in analytical chemistry: A review*, Analytica Chimica Acta, 2012. **750**: p. 48-62.

59. Eteshola, E. and Leckband, D., *Development and characterization of an ELISA assay in PDMS microfluidic channels*, Sensors and Actuators B: Chemical, 2001. **72**(2): p. 129-133.

60. Zheng, B., Roach, L. S. and Ismagilov, R. F., *Screening of Protein Crystallization Conditions on a Microfluidic Chip Using Nanoliter-Size Droplets*, Journal of the American Chemical Society, 2003. **125**(37): p. 11170-11171.

61. Herrmann, M., Roy, E., Veres, T. and Tabrizian, M., *Microfluidic ELISA on non-passivated PDMS chip using magnetic bead transfer inside dual networks of channels*, Lab on a Chip, 2007. **7**(11): p. 1546-1552.

62. Carlborg, C. F., Haraldsson, T., Oberg, K., Malkoch, M. and van der Wijngaart, W., *Beyond PDMS: off-stoichiometry thiol-ene (OSTE) based soft lithography for rapid prototyping of microfluidic devices*, Lab on a Chip, 2011. **11**(18): p. 3136-3147.

63. Scharnweber, T., Truckenmuller, R., Schneider, A. M., Welle, A., Reinhardt, M. and Giselbrecht, S., *Rapid prototyping of microstructures in polydimethylsiloxane (PDMS) by direct UV-lithography*, Lab on a Chip, 2011. **11**(7): p. 1368-1371.

64. *U.S. Pat.,* 4575330 A, 1986.

65. Shallan, A. I., Smejkal, P., Corban, M., Guijt, R. M. and Breadmore, M. C., *Cost-Effective Three-Dimensional Printing of Visibly Transparent Microchips within Minutes*, Analytical Chemistry, 2014. **86**(6): p. 3124-3130.

66. Zein, I., Hutmacher, D. W., Tan, K. C. and Teoh, S. H., *Fused deposition modeling of novel scaffold architectures for tissue engineering applications*, Biomaterials, 2002. **23**(4): p. 1169-1185.

67. Vaezi, M., Seitz, H. and Yang, S., *A review on 3D micro-additive manufacturing technologies*, The International Journal of Advanced Manufacturing Technology, 2013. **67**(5-8): p. 1721-1754.

68. Zhang, Y.-L., Chen, Q.-D., Xia, H. and Sun, H.-B., *Designable 3D nanofabrication by femtosecond laser direct writing*, Nano Today, 2010. **5**(5): p. 435-448.

69. Zhu, F., Macdonald, N. P., Cooper, J. M. and Wlodkowic, D., Additive manufacturing of lab-on-a-chip devices: promises and challenges, *Proceedings of Micro/Nano Materials, Devices, and Systems*, Melbourne, 2013.

70. Sachs, E., Cima, M. and Cornie, J., *Three-dimensional printing: rapid tooling and prototypes directly from a CAD model*, CIRP Annals-Manufacturing Technology, 1990. **39**(1): p. 201-204.

71. Kesner, S. B. and Howe, R. D., *Design Principles for Rapid Prototyping Forces Sensors using 3D Printing*, IEEE/ASME transactions on mechatronics : a joint publication of the IEEE Industrial Electronics Society and the ASME Dynamic Systems and Control Division, 2011. **PP**(99): p. 1-5.

72. Kitson, P. J., Rosnes, M. H., Sans, V., Dragone, V. and Cronin, L., *Configurable 3D-Printed millifluidic and microfluidic 'lab on a chip' reactionware devices*, Lab on a Chip, 2012. **12**(18): p. 3267-3271.

73. Lee, K. G., Park, K. J., Seok, S., Shin, S., Kim, D. H., Park, J. Y., Heo, Y. S., Lee, S. J. and Lee, T. J., *3D printed modules for integrated microfluidic devices*, RSC Advances, 2014. **4**(62): p. 32876-32880.

74. Erkal, J. L., Selimovic, A., Gross, B. C., Lockwood, S. Y., Walton, E. L.,

McNamara, S., Martin, R. S. and Spence, D. M., *3D printed microfluidic devices with integrated versatile and reusable electrodes*, Lab on a Chip, 2014. **14**(12): p. 2023-2032.

75.   Krejcova, L., Nejdl, L., Rodrigo, M. A. M., Zurek, M., Matousek, M., Hynek, D., Zitka, O., Kopel, P., Adam, V. and Kizek, R., *3D printed chip for electrochemical detection of influenza virus labeled with CdS quantum dots*, Biosensors and Bioelectronics, 2014. **54**: p. 421-427.

76.   Comina, G., Suska, A. and Filippini, D., *Low cost lab-on-a-chip prototyping with a consumer grade 3D printer*, Lab on a Chip, 2014. **14**(16): p. 2978-2982.

77.   Harvey, D., *Modern Analytical Chemistry*,International Edition, McGraw-Hill, USA, 1999, p. 1-798.

78.   Landers, J. P., *Handbook of Capillary Electrophoresis*,Second Edition, CRC press, USA, 1996, p. 1-894.

79.   Marina, M. L., Ríos, A. and Valcárcel, M., in *Comprehensive Analytical Chemistry*, eds. A. Ros M.L. Marina and M. Valcrcel, Elsevier, 2005, vol. 45, p. 1-30.

80.   Shallan, A., Guijt, R. and Breadmore, M., in *Encyclopedia of Forensic Sciences*, eds. Jay A. Siegel, Pekka J. Saukko and Max M. Houck, Academic Press, Waltham, 2013, p. 549-559.

81.   Jorgenson, J. W. and Lukacs, K. D., *Capillary zone electrophoresis*, Science, 1983. **222**(4621): p. 266-272.

82.   Landers, J. P., *Handbook of Capillary and Microchip Electrophoresis and Associated Microtechniques*,3rd Edition, CRC Press, London, New York, 2009, p. 1-1567.

83.   Horvath, J. and Dolník, V., *Polymer wall coatings for capillary electrophoresis*, Electrophoresis 2001. **22**(4): p. 644-655.

84.   Heiger, D. N., *High Performance Capillary Electrophoresis: An Introduction*,3rd Edition, Hewlett Packard Company, France, 1997, p. 1-136.

85.   Takayanagi, T., Wada, E. and Motomizu, S., *Electrophoretic Mobility Study of Ion Association Between Aromatic Anions and Quaternary Ammonium Ions in Aqueous Solution*, Analyst, 1997. **122**(1): p. 57-62.

86.   Wang, W., Zhou, F., Zhao, L., Zhang, J.-R. and Zhu, J.-J., *Measurement of electroosmotic flow in capillary and microchip electrophoresis*, Journal of Chromatography A, 2007. **1170**(1–2): p. 1-8.

87.   Lacher, N. A., Garrison, K. E., Martin, R. S. and Lunte, S. M., *Microchip*

capillary electrophoresis/ electrochemistry, Electrophoresis, 2001. **22**(12): p. 2526-2536.

88. Jacobson, S. C., Hergenroder, R., Koutny, L. B. and Ramsey, J. M., *High-speed separations on a microchip*, Analytical Chemistry, 1994. **66**(7): p. 1114-1118.

89. Li, S. F. Y. and Kricka, L. J., *Clinical Analysis by Microchip Capillary Electrophoresis*, Clinical Chemistry, 2006. **52**(1): p. 37-45.

90. Hofgärtner, W. T., Hühmer, A. F. R., Landers, J. P. and Kant, J. A., *Rapid Diagnosis of Herpes Simplex Encephalitis Using Microchip Electrophoresis of PCR Products*, Clinical Chemistry, 1999. **45**(12): p. 2120-2128.

91. Verpoorte, E., *Microfluidic chips for clinical and forensic analysis*, Electrophoresis, 2002. **23**(5): p. 677-712.

92. Reyes, D. R., Lossifidis, D., Auroux, P.-A. and Manz, A., *Micro total analysis systems. 1. Introduction, theory, and technology*, Analytical Chemistry, 2002. **74**(12): p. 2623-2636.

93. Tudos, A. J., Besselink, G. A. J. and Schasfoort, R. B. M., *Trends in miniaturized total analysis systems for point-of-care testing in clinical chemistry*, Lab on a Chip, 2001. **1**(2): p. 83-95.

94. Auroux, P. A., Koc, Y., deMello, A., Manz, A. and Day, P. J. R., *Miniaturised nucleic acid analysis*, Lab on a Chip, 2004. **4**(6): p. 534-546.

95. Vilkner, T., Janasek, D. and Manz, A., *Micro total analysis systems. Recent developments*, Analytical Chemistry, 2004. **76**(12): p. 3373-3386.

96. Dittrich, P. S., Tachikawa, K. and Manz, A., *Micro total analysis systems. Latest advancements and trends*, Analytical Chemistry, 2006. **78**(12): p. 3887-3908.

97. West, J., Becker, M., Tombrink, S. and Manz, A., *Micro total analysis systems: latest achievements*, Analytical Chemistry, 2008. **80**(12): p. 4403-4419.

98. Arora, A., Simone, G., Salieb-Beugelaar, G. B., Kim, J. T. and Manz, A., *Latest developments in micro total analysis systems*, Analytical Chemistry, 2010. **82**(12): p. 4830-4847.

99. Kartalov, E. P., Anderson, W. F. and Scherer, A., *The Analytical Approach to Polydimethylsiloxane Microfluidic Technology and Its Biological Applications*, Journal of Nanoscience and Nanotechnology, 2006. **6**(8): p. 2265-2277.

100. Yi, C., Li, C.-W., Ji, S. and Yang, M., *Microfluidics technology for*

manipulation and analysis of biological cells, Analytica Chimica Acta, 2006. **560**(1-2): p. 1-23.

101. Makamba, H., Kim, J. H., Lim, K., Park, N. and Hahn, J. H., *Surface modification of poly(dimethylsiloxane) microchannels*, Electrophoresis 2003. **24**(21): p. 3607-3619.

102. García, C. D., Dressen, B. M., Henderson, A. and Henry, C. S., *Comparison of surfactants for dynamic surface modification of poly(dimethylsiloxane) microchips*, Electrophoresis, 2005. **26**(3): p. 703-709.

103. Guan, Q., Noblitt, S. D. and Henry, C. S., *Electrophoretic separations in poly(dimethylsiloxane) microchips using mixtures of ionic, nonionic and zwitterionic surfactants*, Electrophoresis 2012. **33**(18): p. 2875-2883.

104. Guan, Q., Noblitt, S. D. and Henry, C. S., *Electrophoretic separations in poly(dimethylsiloxane) microchips using a mixture of ionic and zwitterionic surfactants*, Electrophoresis 2012. **33**(2): p. 379-387.

105. Jung, B., Bharadwaj, R. and Santiago, J. G., *Thousandfold signal increase using field-amplified sample stacking for on-chip electrophoresis*, Electrophoresis, 2003. **24**(19-20): p. 3476-3483.

106. Lichtenberg, J., Verpoorte, E. and de Rooij, N. F., *Sample preconcentration by field amplification stacking for microchip-based capillary electrophoresis*, Electrophoresis 2001. **22**(2): p. 258-271.

107. Blow, N., *Microfluidics: The Great Divide*, Nature Methods, 2009. **6**(9): p. 683-686.

108. Kubán, P. and Hauser, P. C., *Capacitively coupled contactless conductivity detection for microseparation techniques – recent developments*, Electrophoresis 2011. **32**(1): p. 30-42.

109. Santiago, J. G. and Chen, C.-H., *Special issue on fundamental principles and techniques in microfluidics*, Lab on a Chip, 2009. **9**(17): p. 2423-2424.

110. Dolník, V., Liu, S. and Jovanovich, S., *Capillary electrophoresis on microchip*, Electrophoresis, 2000. **21**(1): p. 41-54.

111. Swinney, K. and Bornhop, D. J., *Detection in capillary electrophoresis*, Electrophoresis 2000. **21**(7): p. 1239-1250.

112. Götz, S. and Karst, U., *Recent developments in optical detection methods for microchip separations*, Analytical and Bioanalytical Chemistry, 2007. **387**(1): p. 183-192.

113. Kuswandi, B., Nuriman, Huskens, J. and Verboom, W., *Optical sensing*

systems for microfluidic devices: A review, Analytica Chimica Acta, 2007. **601**(2): p. 141-155.

114. Schulze, P. and Belder, D., *Label-free fluorescence detection in capillary and microchip electrophoresis*, Analytical and Bioanalytical Chemistry 2009. **393**(2): p. 515-525.

115. Effenhauser, C. S., Bruin, G. J. M., Paulus, A. and Ehrat, M., *Integrated Capillary Electrophoresis on Flexible Silicone Microdevices: Analysis of DNA Restriction Fragments and Detection of Single DNA Molecules on Microchips*, Analytical Chemistry, 1997. **69**(17): p. 3451-3457.

116. Chabinyc, M. L., Chiu, D. T., McDonald, J. C., Stroock, A. D., Christian, J. F., Karger, A. M. and Whitesides, G. M., *An Integrated Fluorescence Detection System in Poly(dimethylsiloxane) for Microfluidic Applications*, Analytical Chemistry, 2001. **73**(18): p. 4491-4498.

117. Ryu, G., Huang, J., Hofmann, O., Walshe, C. A., Sze, J. Y. Y., McClean, G. D., Mosley, A., Rattle, S. J., deMello, J. C., deMello, A. J. and Bradley, D. D. C., *Highly sensitive fluorescence detection system for microfluidic lab-on-a-chip*, Lab on a Chip, 2011. **11**(9): p. 1664-1670.

118. Kettlitz, S. W., Valouch, S., Sittel, W. and Lemmer, U., *Flexible planar microfluidic chip employing a light emitting diode and a PIN-photodiode for portable flow cytometers*, Lab on a Chip, 2012. **12**(1): p. 197-203.

119. Yang, F., Li, X.-c., Zhang, W., Pan, J.-b. and Chen, Z.-g., *A facile light-emitting-diode induced fluorescence detector coupled to an integrated microfluidic device for microchip electrophoresis*, Talanta, 2011. **84**(4): p. 1099-1106.

120. He, X., Chen, Q., Zhang, Y. and Lin, J.-M., *Recent advances in microchip-mass spectrometry for biological analysis*, TrAC Trends in Analytical Chemistry, 2014. **53**: p. 84-97.

121. Lin, S.-L., Lin, T.-Y. and Fuh, M.-R., *Recent developments in microfluidic chip-based separation devices coupled to MS for bioanalysis*, Bioanalysis, 2013. **5**(20): p. 2567-2580.

122. Ibanez, C., Simo, C., Garcia-Canas, V., Cifuentes, A. and Castro-Puyana, M., *Metabolomics, peptidomics and proteomics applications of capillary electrophoresis-mass spectrometry in Foodomics: A review*, Analytica Chimica Acta, 2013. **802**: p. 1-13.

123. Timerbaev, A. R. and Timerbaev, R. M., *Recent progress of capillary electrophoresis in studying the speciation of actinides*, Trac-Trends in Analytical Chemistry, 2013. **51**: p. 44-50.

124. Wang, X., Li, K. F., Adams, E. and Van Schepdael, A., *Capillary Electrophoresis-Mass Spectrometry in Metabolomics: The Potential for Driving Drug Discovery and Development*, Current Drug Metabolism, 2013. **14**(7): p. 807-813.

125. Xie, J., Miao, Y. N., Shih, J., Tai, Y. C. and Lee, T. D., *Microfluidic platform for liquid chromatography-tandem mass spectrometry analyses of complex peptide mixtures*, Analytical Chemistry, 2005. **77**(21): p. 6947-6953.

126. Yin, H., Killeen, K., Brennen, R., Sobek, D., Werlich, M. and van de Goor, T., *Microfluidic chip for peptide analysis with an integrated HPLC column, sample enrichment column, and nanoelectrospray tip*, Analytical Chemistry, 2005. **77**(2): p. 527-533.

127. Lazar, I. M., Trisiripisal, P. and Sarvaiya, H. A., *Microfluidic liquid chromatography system for proteomic applications and biomarker screening*, Analytical Chemistry, 2006. **78**(15): p. 5513-5524.

128. Hoffmann, P., Hausig, U., Schulze, P. and Belder, D., *Microfluidic glass chips with an integrated nanospray emitter for coupling to a mass spectrometer*, Angewandte Chemie-International Edition, 2007. **46**(26): p. 4913-4916.

129. Chambers, A. G., Mellors, J. S., Henley, W. H. and Ramsey, J. M., *Monolithic Integration of Two-Dimensional Liquid Chromatography-Capillary Electrophoresis and Electrospray Ionization on a Microfluidic Device*, Analytical Chemistry, 2011. **83**(3): p. 842-849.

130. Fritzsche, S., Hoffmann, P. and Belder, D., *Chip electrophoresis with mass spectrometric detection in record speed*, Lab on a Chip, 2010. **10**(10): p. 1227-1230.

131. Sikanen, T., Aura, S., Franssila, S., Kotiaho, T. and Kostiainen, R., *Microchip capillary electrophoresis-electrospray ionization-mass spectrometry of intact proteins using uncoated Ormocomp microchips*, Analytica Chimica Acta, 2012. **711**: p. 69-76.

132. Batz, N. G., Mellors, J. S., Alarie, J. P. and Ramsey, J. M., *Chemical vapor deposition of aminopropyl silanes in microfluidic channels for highly efficient microchip capillary electrophoresis-electrospray ionization-mass spectrometry*, Analytical Chemistry, 2014. **86**(7): p. 3493-3500.

133. Nordman, N., Sikanen, T., Moilanen, M.-E., Aura, S., Kotiaho, T., Franssila, S. and Kostiainen, R., *Rapid and sensitive drug metabolism studies by SU-8 microchip capillary electrophoresis-electrospray*

ionization mass spectrometry, Journal of Chromatography A, 2011. **1218**(5): p. 739-745.

134. Mellors, J. S., Black, W. A., Chambers, A. G., Starkey, J. A., Lacher, N. A. and Ramsey, J. M., *Hybrid Capillary/Microfluidic System for Comprehensive Online Liquid Chromatography-Capillary Electrophoresis-Electrospray Ionization-Mass Spectrometry*, Analytical Chemistry, 2013. **85**(8): p. 4100-4106.

135. Li, X., Xiao, D., Ou, X.-M., McCullm, C. and Liu, Y.-M., *A microchip electrophoresis-mass spectrometric platform for fast separation and identification of enantiomers employing the partial filling technique*, Journal of Chromatography A, 2013. **1318**: p. 251-256.

136. Kubán, P. and Hauser, P. C., *Fundamentals of electrochemical detection techniques for CE and MCE*, Electrophoresis 2009. **30**(19): p. 3305-3314.

137. Vandaveer, W. R., Pasas-Farmer, S. A., Fischer, D. J., Frankenfeld, C. N. and Lunte, S. M., *Recent developments in electrochemical detection for microchip capillary electrophoresis*, Electrophoresis 2004. **25**(21-22): p. 3528-3549.

138. Kappes, T. and Hauser, P. C., *Potentiometric detection in capillary electrophoresis with a metallic copper electrode*, Analytica Chimica Acta, 1997. **354**(1-3): p. 129-134.

139. Macka, M., Gerhardt, G., Andersson, P., Bogan, D., Cassidy, R. M. and Haddad, P. R., *Capillary electrophoresis with end-capillary potentiometric detection using a copper electrode*, Electrophoresis 1999. **20**(12): p. 2539-2546.

140. Zakaria, P., Macka, M., Gerhardt, G. and Haddad, P. R., *Pulsed potentiometric detection in capillary electrophoresis using platinum electrodes*, Analyst, 2000. **125**(9): p. 1519-1523.

141. Mark, J. J., Scholz, R. and Matysik, F.-M., *Electrochemical methods in conjunction with capillary and microchip electrophoresis*, Journal of Chromatography A, 2012. **1267**: p. 45-64.

142. Ghanim, M. H. and Abdullah, M. Z., *Integrating amperometric detection with electrophoresis microchip devices for biochemical assays: Recent developments*, Talanta, 2011. **85**(1): p. 28-34.

143. Gunasekara, D. B., Hulvey, M. K. and Lunte, S. M., *In-channel amperometric detection for microchip electrophoresis using a wireless isolated potentiostat*, Electrophoresis 2011. **32**(8): p. 832-837.

144. Kang, C. M., Joo, S., Bae, J. H., Kim, Y.-R., Kim, Y. and Chung, T. D., *In-*

channel electrochemical detection in the middle of microchannel under high electric field, Analytical Chemistry, 2011. **84**(2): p. 901-907.

145. Lin, K.-W., Huang, Y.-K., Su, H.-L. and Hsieh, Y.-Z., *In-channel simplified decoupler with renewable electrochemical detection for microchip capillary electrophoresis*, Analytica Chimica Acta, 2008. **619**(1): p. 115-121.

146. Omiatek, D. M., Santillo, M. F., Heien, M. L. and Ewing, A. G., *Hybrid capillary-microfluidic device for the separation, lysis, and electrochemical detection of vesicles*, Analytical Chemistry, 2009. **81**(6): p. 2294-2302.

147. Zhang, S., Cao, W., Li, J. and Su, M., *MCE enzyme immunoassay for carcinoembryonic antigen and alpha-fetoprotein using electrochemical detection*, Electrophoresis 2009. **30**(19): p. 3427-3435.

148. Kovachev, N., Canals, A. and Escarpa, A., *Fast and selective microfluidic chips for electrochemical antioxidant sensing in complex samples*, Analytical Chemistry, 2010. **82**(7): p. 2925-2931.

149. Piccin, E., Dossi, N., Cagan, A., Carrilho, E. and Wang, J., *Rapid and sensitive measurements of nitrate ester explosives using microchip electrophoresis with electrochemical detection*, Analyst, 2009. **134**(3): p. 528-532.

150. Brito-Neto, J. G. A., Fracassi da Silva, J. A., Blanes, L. and do Lago, C. L., *Understanding Capacitively Coupled Contactless Conductivity Detection in Capillary and Microchip Electrophoresis. Part 1. Fundamentals*, Electroanalysis, 2005. **17**(13): p. 1198-1206.

151. Guijt, R. M., Armstrong, J. P., Candish, E., Lefleur, V., Percey, W. J., Shabala, S., Hauser, P. C. and Breadmore, M. C., *Microfluidic chips for capillary electrophoresis with integrated electrodes for capacitively coupled conductivity detection based on printed circuit board technology*, Sensors and Actuators B: Chemical, 2011. **159**(1): p. 307-313.

152. Coltro, W. K. T., da Silva, J. A. F. and Carrilho, E., *Fabrication and integration of planar electrodes for contactless conductivity detection on polyester-toner electrophoresis microchips*, Electrophoresis 2008. **29**(11): p. 2260-2265.

153. Coltro, W. K. T., Fracassi da Silva, J. A. and Carrilho, E., *Rapid prototyping of polymeric electrophoresis microchips with integrated copper electrodes for contactless conductivity detection*, Analytical Methods, 2011. **3**(1): p. 168-172.

154. Kuban, P. and Hauser, P. C., *Evaluation of microchip capillary*

electrophoresis with external contactless conductivity detection for the determination of major inorganic ions and lithium in serum and urine samples, Lab on a Chip, 2008. **8**(11): p. 1829-1836.

155.   Kubán, P. and Hauser, P. C., *Contactless conductivity detection for analytical techniques: Developments from 2010 to 2012*, Electrophoresis 2013. **34**(1): p. 55-69.

156.   Coltro, W. K. T., Lima, R. S., Segato, T. P., Carrilho, E., de Jesus, D. P., do Lago, C. L. and da Silva, J. A. F., *Capacitively coupled contactless conductivity detection on microfluidic systems-ten years of development*, Analytical Methods, 2012. **4**(1): p. 25-33.

157.   Martin, P., *Contactless conductivity detection for microfluidics: Designs and applications*, Talanta, 2007. **74**(3): p. 358-364.

158.   Kubán, P. and Hauser, P. C., *A review of the recent achievements in capacitively coupled contactless conductivity detection*, Analytica Chimica Acta, 2008. **607**(1): p. 15-29.

159.   Elbashir, A. A. and Aboul-Enein, H. Y., *Applications of capillary electrophoresis with capacitively coupled contactless conductivity detection (CE-C4D) in pharmaceutical and biological analysis*, Biomedical Chromatography, 2010. **24**(10): p. 1038-1044.

160.   Guijt, R. M., Baltussen, E., van der Steen, G., Frank, H., Billiet, H., Schalkhammer, T., Laugere, F., Vellekoop, M., Berthold, A., Sarro, L. and van Dedem, G. W. K., *Capillary electrophoresis with on-chip four-electrode capacitively coupled conductivity detection for application in bioanalysis*, Electrophoresis 2001. **22**(12): p. 2537-2541.

161.   Vazquez, M., Frankenfeld, C., Coltro, W. K. T., Carrilho, E., Diamond, D. and Lunte, S. M., *Dual contactless conductivity and amperometric detection on hybrid PDMS/glass electrophoresis microchips*, Analyst, 2010. **135**(1): p. 96-103.

162.   Shang, T., Teng, E., Woolley, A. T., Mazzeo, B. A., Schultz, S. M. and Hawkins, A. R., *Contactless conductivity detection of small ions in a surface micro-machined CE chip*, Electrophoresis, 2010. **31**(15): p. 2596-2601.

163.   Liu, B., Jin, Q., Zhang, Y., Mayer, D., Krause, H.-J., Zhao, J. and Offenhäusser, A., *A simple poly(dimethylsiloxane) electrophoresis microchip with an integrated contactless conductivity detector*, Microchimica Acta, 2011. **172**(1-2): p. 193-198.

164.   Segato, T. P., Coltro, W. K. T., de Jesus Almeida, A. L., de Oliveira

Piazetta, M. H., Gobbi, A. L., Mazo, L. H. and Carrilho, E., *A rapid and reliable bonding process for microchip electrophoresis fabricated in glass substrates*, Electrophoresis, 2010. **31**(15): p. 2526-2533.

165. Coltro, W. K. T., Neves, R. D., Motheo, A. D., da Silva, J. A. F. and Carrilho, E., *Microfluidic devices with integrated dual-capacitively coupled contactless conductivity detection to monitor binding events in real time*, Sensors and Actuators B-Chemical, 2014. **192**: p. 239-246.

166. Ding, Y. S. and Rogers, K., *Determination of haloacetic acids in water using solid-phase extraction/microchip capillary electrophoresis with capacitively coupled contactless conductivity detection*, Electrophoresis 2010. **31**(15): p. 2602-2607.

167. Mahabadi, K. A., Rodriguez, I., Lim, C. Y., Maurya, D. K., Hauser, P. C. and de Rooij, N. F., *Capacitively coupled contactless conductivity detection with dual top–bottom cell configuration for microchip electrophoresis*, Electrophoresis 2010. **31**(6): p. 1063-1070.

168. Tanyanyiwa, J., Abad-Villar, E. M., Fernandez-Abedul, M. T., Costa-Garcia, A., Hoffmann, W., Guber, A. E., Herrmann, D., Gerlach, A., Gottschlich, N. and Hauser, P. C., *High-voltage contactless conductivity-detection for lab-on-chip devices using external electrodes on the holder*, Analyst, 2003. **128**(8): p. 1019-1022.

169. Ansari, K., Ying, J. Y. S., Hauser, P. C., de Rooij, N. F. and Rodriguez, I., *A portable lab-on-a-chip instrument based on MCE with dual top–bottom capacitive coupled contactless conductivity detector in replaceable cell cartridge*, Electrophoresis 2013. **34**(9-10): p. 1390-1399.

170. Lichtenberg, J., de Rooij, N. F. and Verpoorte, E., *A microchip electrophoresis system with integrated in-plane electrodes for contactless conductivity detection*, Electrophoresis 2002. **23**(21): p. 3769-3780.

171. Lee, C.-Y., Chen, C. M., Chang, G.-L., Lin, C.-H. and Fu, L.-M., *Fabrication and characterization of semicircular detection electrodes for contactless conductivity detector – CE microchips*, Electrophoresis 2006. **27**(24): p. 5043-5050.

172. Henderson, R. D., Guijt, R. M., Andrewartha, L., Lewis, T. W., Rodemann, T., Henderson, A., Hilder, E. F., Haddad, P. R. and Breadmore, M. C., *Lab-on-a-Chip device with laser-patterned polymer electrodes for high voltage application and contactless conductivity detection*, Chemical Communications, 2012. **48**(74): p. 9287-9289.

173. Siegel, A. C., Shevkoplyas, S. S., Weibel, D. B., Bruzewicz, D. A.,

Martinez, A. W. and Whitesides, G. M., *Cofabrication of Electromagnets and Microfluidic Systems in Poly(dimethylsiloxane)*, Angewandte Chemie International Edition, 2006. **45**(41): p. 6877-6882.

174. Priest, C., Gruner, P. J., Szili, E. J., Al-Bataineh, S. A., Bradley, J. W., Ralston, J., Steele, D. A. and Short, R. D., *Microplasma patterning of bonded microchannels using high-precision "injected" electrodes*, Lab on a Chip, 2011. **11**(3): p. 541-544.

175. So, J.-H. and Dickey, M. D., *Inherently aligned microfluidic electrodes composed of liquid metal*, Lab on a Chip, 2011. **11**(5): p. 905-911.

176. Hallfors, N., Khan, A., Dickey, M. D. and Taylor, A. M., *Integration of pre-aligned liquid metal electrodes for neural stimulation within a user-friendly microfluidic platform*, Lab on a Chip, 2013. **13**(4): p. 522-526.

177. Thredgold, L. D., Khodakov, D. A., Ellis, A. V. and Lenehan, C. E., *On-chip capacitively coupled contactless conductivity detection using "injected" metal electrodes*, Analyst, 2013. **138**(15): p. 4275-4279.

178. Thredgold, L. D., Khodakov, D. A., Ellis, A. V. and Lenehan, C. E., Optimization of physical parameters of 'injected' metal electrodes for capacitively coupled contactless conductivity detection on poly(dimethylsiloxane) microchips, *Proceedings of SPIE Micro/Nano Materials, Devices, and Applications*, Melbourne, 2013.

179. Gaudry, A. J., Breadmore, M. C. and Guijt, R. M., *In-plane alloy electrodes for capacitively coupled contactless conductivity detection in poly(methylmethacrylate) electrophoretic chips*, Electrophoresis 2013. **34**(20-21): p. 2980-2987.

180. Taylor, S. L. and Eitenmiller, R. R., *Histamine Food Poisoning: Toxicology and Clinical Aspects*, Critical Reviews in Toxicology, 1986. **17**(2): p. 91-128.

181. Shalaby, A. R., *Significance of biogenic amines to food safety and human health*, Food Research International, 1996. **29**(7): p. 675-690.

182. Bodmer, S., Imark, C. and Kneubühl, M., *Biogenic amines in foods: Histamine and food processing*, Inflammation Research, 1999. **48**(6): p. 296-300.

183. Nollet, L. M. and Toldrá, F., *Safety analysis of foods of animal origin*, CRC Press, 2010, p. 1-1002.

184. Halász, A., Baráth, Á., Simon-Sarkadi, L. and Holzapfel, W., *Biogenic amines and their production by microorganisms in food*, Trends in Food Science & Technology, 1994. **5**(2): p. 42-49.

185. Santos, M. H. S., *Biogenic amines: their importance in foods*, International Journal of Food Microbiology, 1996. **29**(2–3): p. 213-231.

186. Motil, K. J. and Scrimshaw, N. S., *The role of exogenous histamine in scombroid poisoning*, Toxicology Letters, 1979. **3**(4): p. 219-223.

187. Morrow, J. D., Margolies, G. R., Rowland, J. and Roberts, L. J., *Evidence that histamine is the causative toxin of scombroid-fish poisoning*, New England Journal of Medicine, 1991. **324**(11): p. 716-720.

188. Hungerford, J. M., *Scombroid poisoning: A review*, Toxicon, 2010. **56**(2): p. 231-243.

189. Visciano, P., Schirone, M., Tofalo, R. and Suzzi, G., *Biogenic amines in raw and processed seafood*, Frontiers in Microbiology, 2012. **3**(188): p.

190. United States Food and Drug Administration, Decomposition and Histamine Raw, Frozen Tuna and Mahi-Mahi; Canned Tuna; and Related Species Section 540.525, http://www.fda.gov/ICECI/ComplianceManuals/CompliancePolicyGuidanceManual/ucm074506.htm, Accessed 13th November, 2014.

191. Australia New Zealand Food Standards Code, Standard 2.2.3 - Fish and Fish Products http://www.comlaw.gov.au/Details/F2009C01233, Accessed 13th November, 2014.

192. Bauza, T., Blaise, A., Daumas, F. and Cabanis, J. C., *Determination of biogenic amines and their precursor amino acids in wines of the Vallée du Rhône by high-performance liquid chromatography with precolumn derivatization and fluorimetric detection*, Journal of Chromatography A, 1995. **707**(2): p. 373-379.

193. Chiu, T.-C., Lin, Y.-W., Huang, Y.-F. and Chang, H.-T., *Analysis of biologically active amines by CE*, Electrophoresis, 2006. **27**(23): p. 4792-4807.

194. Önal, A., *A review: Current analytical methods for the determination of biogenic amines in foods*, Food Chemistry, 2007. **103**(4): p. 1475-1486.

195. Önal, A., Tekkeli, S. E. K. and Önal, C., *A review of the liquid chromatographic methods for the determination of biogenic amines in foods*, Food Chemistry, 2013. **138**(1): p. 509-515.

196. Šimat, V. and Dalgaard, P., *Use of small diameter column particles to enhance HPLC determination of histamine and other biogenic amines in seafood*, LWT - Food Science and Technology, 2011. **44**(2): p. 399-406.

197. Tahmouzi, S., Khaksar, R. and Ghasemlou, M., *Development and validation of an HPLC-FLD method for rapid determination of histamine in*

skipjack tuna fish (Katsuwonus pelamis), Food Chemistry, 2011. **126**(2): p. 756-761.

198. Latorre-Moratalla, M. L., Bosch-Fusté, J., Lavizzari, T., Bover-Cid, S., Veciana-Nogués, M. T. and Vidal-Carou, M. C., *Validation of an ultra high pressure liquid chromatographic method for the determination of biologically active amines in food*, Journal of Chromatography A, 2009. **1216**(45): p. 7715-7720.

199. Ginterová, P., Marák, J., Staňová, A., Maier, V., Ševčík, J. and Kaniansky, D., *Determination of selected biogenic amines in red wines by automated on-line combination of capillary isotachophoresis–capillary zone electrophoresis*, Journal of Chromatography B, 2012. **904**: p. 135-139.

200. Vitali, L., Valese, A. C., Azevedo, M. S., Gonzaga, L. V., Costa, A. C. O., Piovezan, M., Vistuba, J. P. and Micke, G. A., *Development of a fast and selective separation method to determine histamine in tuna fish samples using capillary zone electrophoresis*, Talanta, 2013. **106**: p. 181-185.

201. Steiner, M.-S., Meier, R., Spangler, C., Duerkop, A. and Wolfbeis, O., *Determination of biogenic amines by capillary electrophoresis using a chameleon type of fluorescent stain*, Microchimica Acta, 2009. **167**(3-4): p. 259-266.

202. La Torre, G. L., Saitta, M., Giorgia Potortì, A., Di Bella, G. and Dugo, G., *High performance liquid chromatography coupled with atmospheric pressure chemical ionization mass spectrometry for sensitive determination of bioactive amines in donkey milk*, Journal of Chromatography A, 2010. **1217**(32): p. 5215-5224.

203. Self, R. L., Wu, W.-H. and Marks, H. S., *Simultaneous Quantification of Eight Biogenic Amine Compounds in Tuna by Matrix Solid-Phase Dispersion followed by HPLC–Orbitrap Mass Spectrometry*, Journal of Agricultural and Food Chemistry, 2011. **59**(11): p. 5906-5913.

204. Liu, Y.-M. and Cheng, J.-K., *Separation of biogenic amines by micellar electrokinetic chromatography with on-line chemiluminescence detection*, Journal of Chromatography A, 2003. **1003**(1–2): p. 211-216.

205. Li, W.-l., Ge, J.-y., Pan, Y.-l., Chu, Q.-c. and Ye, J.-n., *Direct analysis of biogenic amines in water matrix by modified capillary zone electrophoresis with 18-crown-6*, Microchimica Acta, 2012. **177**(1-2): p. 75-80.

206. Gong, X. Y. and Hauser, P. C., *Determination of different classes of*

amines with capillary zone electrophoresis and contactless conductivity detection, Electrophoresis, 2006. **27**(2): p. 468-473.

207. Lapa-Guimarães, J. and Pickova, J., *New solvent systems for thin-layer chromatographic determination of nine biogenic amines in fish and squid*, Journal of Chromatography A, 2004. **1045**(1–2): p. 223-232.

208. Shalaby, A. R., *Simple, rapid and valid thin layer chromatographic method for determining biogenic amines in foods*, Food Chemistry, 1999. **65**(1): p. 117-121.

209. Hwang, B.-S., Wang, J.-T. and Choong, Y.-M., *A rapid gas chromatographic method for the determination of histamine in fish and fish products*, Food Chemistry, 2003. **82**(2): p. 329-334.

210. Fernandes, J. O. and Ferreira, M. A., *Combined ion-pair extraction and gas chromatography–mass spectrometry for the simultaneous determination of diamines, polyamines and aromatic amines in Port wine and grape juice*, Journal of Chromatography A, 2000. **886**(1–2): p. 183-195.

211. Draisci, R., Volpe, G., Lucentini, L., Cecilia, A., Federico, R. and Palleschi, G., *Determination of biogenic amines with an electrochemical biosensor and its application to salted anchovies*, Food Chemistry, 1998. **62**(2): p. 225-232.

212. Lange, J. and Wittmann, C., *Enzyme sensor array for the determination of biogenic amines in food samples*, Analytical and Bioanalytical Chemistry, 2002. **372**(2): p. 276-283.

213. Jayarajah, C. N., Skelley, A. M., Fortner, A. D. and Mathies, R. A., *Analysis of Neuroactive Amines in Fermented Beverages Using a Portable Microchip Capillary Electrophoresis System*, Analytical Chemistry, 2007. **79**(21): p. 8162-8169.

214. Dossi, N., Toniolo, R., Pizzariello, A., Susmel, S. and Bontempelli, G., *A modified electrode for the electrochemical detection of biogenic amines and their amino acid precursors separated by microchip capillary electrophoresis*, Electrophoresis, 2011. **32**(8): p. 906-912.

215. Beard, N. P., Edel, J. B. and deMello, A. J., *Integrated on-chip derivatization and electrophoresis for the rapid analysis of biogenic amines*, Electrophoresis 2004. **25**(14): p. 2363-2373.

216. Beard, N. P. and de Mello, A. J., *A polydimethylsiloxane/glass capillary electrophoresis microchip for the analysis of biogenic amines using indirect fluorescence detection*, Electrophoresis, 2002. **23**(11): p. 1722-

1730.

217. Beard, N. P., Zhang, C.-X. and deMello, A. J., *In-column field-amplified sample stacking of biogenic amines on microfabricated electrophoresis devices*, Electrophoresis, 2003. **24**(4): p. 732-739.

218. Zhao, S., Huang, Y., Shi, M. and Liu, Y.-M., *Quantification of biogenic amines by microchip electrophoresis with chemiluminescence detection*, Journal of Chromatography A, 2009. **1216**(26): p. 5155-5159.

219. Zemann, A. J., *Capacitively coupled contactless conductivity detection in capillary electrophoresis*, Electrophoresis, 2003. **24**(12-13): p. 2125-2137.

220. Kubán, P. and Hauser, P. C., *Contactless Conductivity Detection in Capillary Electrophoresis: A Review*, Electroanalysis, 2004. **16**(24): p. 2009-2021.

221. Li, X.-A., Zhou, D.-M., Xu, J.-J. and Chen, H.-Y., *Determination of chloride, chlorate and perchlorate by PDMS microchip electrophoresis with indirect amperometric detection*, Talanta, 2008. **75**(1): p. 157-162.

222. Bruin, G. J. M., *Recent developments in electrokinetically driven analysis on microfabricated devices*, Electrophoresis 2000. **21**(18): p. 3931-3951.

223. Stone, H. A., Stroock, A. D. and Ajdari, A., *Engineering Flows in Small Devices*, Annual Review of Fluid Mechanics, 2004. **36**(1): p. 381-411.

224. Huang, B., Wu, H., Kim, S. and Zare, R. N., *Coating of poly(dimethylsiloxane) with n-dodecyl-β-d-maltoside to minimize nonspecific protein adsorption*, Lab on a Chip, 2005. **5**(10): p. 1005-1007.

225. Erickson, D., Sinton, D. and Li, D., *Joule heating and heat transfer in poly(dimethylsiloxane) microfluidic systems*, Lab on a Chip, 2003. **3**(3): p. 141-149.

226. Kubán, P. and Hauser, P. C., *Effects of the cell geometry and operating parameters on the performance of an external contactless conductivity detector for microchip electrophoresis*, Lab on a Chip, 2005. **5**(4): p. 407-415.

227. Laugere, F., Guijt, R. M., Bastemeijer, J., van der Steen, G., Berthold, A., Baltussen, E., Sarro, P., van Dedem, G. W. K., Vellekoop, M. and Bossche, A., *On-Chip Contactless Four-Electrode Conductivity Detection for Capillary Electrophoresis Devices*, Analytical Chemistry, 2002. **75**(2): p. 306-312.

228. Liu, B., Zhang, Y., Mayer, D., Krause, H.-J., Jin, Q., Zhao, J. and Offenhäusser, A., *A simplified poly(dimethylsiloxane) capillary electrophoresis microchip integrated with a low-noise contactless*

conductivity detector, Electrophoresis 2011. **32**(6-7): p. 699-704.

229. Tomazelli Coltro, W. K., Fracassi da Silva, J. A. and Carrilho, E., *Rapid prototyping of polymeric electrophoresis microchips with integrated copper electrodes for contactless conductivity detection*, Analytical Methods, 2011. **3**(1): p. 168-172.

230. Guijt, R. M., Evenhuis, C. J., Macka, M. and Haddad, P. R., *Conductivity detection for conventional and miniaturised capillary electrophoresis systems*, Electrophoresis 2004. **25**(23-24): p. 4032-4057.

231. Lima, R. S., Piazzetta, M. H. O., Gobbi, A. L., Segato, T. P., Cabral, M. F., Machado, S. A. S. and Carrilho, E., *Highly sensitive contactless conductivity microchips based on concentric electrodes for flow analysis*, Chemical Communications, 2013. **49**(97): p. 11382-11384.

232. Liu, J., Xu, F., Wang, S., Chen, Z., Pan, J., Ma, X., Jia, X., Xu, Z., Liu, C. and Wang, L., *A polydimethylsiloxane electrophoresis microchip with a thickness controllable insulating layer for capacitatively coupled contactless conductivity detection*, Electrochemistry Communications, 2012. **25**: p. 147-150.

233. Kubán, P. and Hauser, P. C., *Application of an external contactless conductivity detector for the analysis of beverages by microchip capillary electrophoresis*, Electrophoresis, 2005. **26**(16): p. 3169-3178.

234. Kuban, P. and Hauser, P. C., *Effects of the cell geometry and operating parameters on the performance of an external contactless conductivity detector for microchip electrophoresis*, Lab on a Chip, 2005. **5**(4): p. 407-415.

235. Kang, Q., Shen, D., Li, Q., Hu, Q., Dong, J., Du, J. and Tang, B., *Reduction of the impedance of a contactless conductivity detector for microchip capillary electrophoresis: compensation of the electrode impedance by addition of a series inductance from a piezoelectric quartz crystal*, Analytical Chemistry, 2008. **80**(20): p. 7826-7832.

236. Stellwagen, E., Prantner, J. D. and Stellwagen, N. C., *Do zwitterions contribute to the ionic strength of a solution?*, Analytical Biochemistry, 2008. **373**(2): p. 407-409.

237. Mark, J. J. P., Kumar, A., Demattio, H., Hoffmann, W., Malik, A. and Matysik, F.-M., *Combination of Headspace Single-Drop Microextraction, Microchip Electrophoresis and Contactless Conductivity Detection for the Determination of Aliphatic Amines in the Biodegradation Process of Seafood Samples*, Electroanalysis, 2011. **23**(1): p. 161-168.

238. Oguri, S., Enami, M. and Soga, N., *Selective analysis of histamine in food by means of solid-phase extraction cleanup and chromatographic separation*, Journal of Chromatography A, 2007. **1139**(1): p. 70-74.

239. Warlley, P. E., Patrícia, A. S. T. and Maria Beatriz, A. G., *Quality control of the analysis of histamine in fish by proficiency test*, Journal of Physics: Conference Series, 2015. **575**(1): p. 012035.

240. Moore, A. W., Jacobson, S. C. and Ramsey, J. M., *Microchip Separations of Neutral Species via Micellar Electrokinetic Capillary Chromatography*, Analytical Chemistry, 1995. **67**(22): p. 4184-4189.

241. Molho, J. I., Herr, A. E., Mosier, B. P., Santiago, J. G., Kenny, T. W., Brennen, R. A., Gordon, G. B. and Mohammadi, B., *Optimization of Turn Geometries for Microchip Electrophoresis*, Analytical Chemistry, 2001. **73**(6): p. 1350-1360.

242. Coltro, W. K. T., Lunte, S. M. and Carrilho, E., *Comparison of the analytical performance of electrophoresis microchannels fabricated in PDMS, glass, and polyester-toner*, Electrophoresis 2008. **29**(24): p. 4928-4937.

243. Szili, E. J., Al-Bataineh, S. A., Ruschitzka, P., Desmet, G., Priest, C., Griesser, H. J., Voelcker, N. H., Harding, F. J., Steele, D. A. and Short, R. D., *Microplasma arrays: a new approach for maskless and localized patterning of materials surfaces*, RSC Advances, 2012. **2**(31): p. 12007-12010.

244. Fu, L. M., Yang, R. J., Lee, G. B. and Liu, H. H., *Electrokinetic Injection Techniques in Microfluidic Chips*, Analytical Chemistry, 2002. **74**(19): p. 5084-5091.

245. Wu, D., Qin, J. and Lin, B., *Electrophoretic separations on microfluidic chips*, Journal of Chromatography A, 2008. **1184**(1–2): p. 542-559.

246. Beckers, J. L. and Boček, P., *Sample stacking in capillary zone electrophoresis: Principles, advantages and limitations*, Electrophoresis 2000. **21**(14): p. 2747-2767.

247. Wainright, A., Williams, S. J., Ciambrone, G., Xue, Q., Wei, J. and Harris, D., *Sample pre-concentration by isotachophoresis in microfluidic devices*, Journal of Chromatography A, 2002. **979**(1–2): p. 69-80.

248. Jung, B., Bharadwaj, R. and Santiago, J. G., *On-chip millionfold sample stacking using transient isotachophoresis*, Analytical Chemistry, 2006. **78**(7): p. 2319-2327.

249. Huang, Z., Long, J., Xu, W., Ji, H., Wang, B. and Li, H., *Design of*

capacitively coupled contactless conductivity detection sensor, Flow Measurement and Instrumentation, 2012. **27**: p. 67-70.

250. Huang, Z., Jiang, W., Zhou, X., Wang, B., Ji, H. and Li, H., *A new method of capacitively coupled contactless conductivity detection based on series resonance*, Sensors and Actuators B: Chemical, 2009. **143**(1): p. 239-245.

251. Sciambi, A. and Abate, A. R., *Generating electric fields in PDMS microfluidic devices with salt water electrodes*, Lab on a Chip, 2014. **14**(15): p. 2605-2609.

252. Huang, K.-J., Wei, C.-Y., Liu, W.-L., Xie, W.-Z., Zhang, J.-F. and Wang, W., *Ultrasound-assisted dispersive liquid–liquid microextraction combined with high-performance liquid chromatography-fluorescence detection for sensitive determination of biogenic amines in rice wine samples*, Journal of Chromatography A, 2009. **1216**(38): p. 6636-6641.

253. Almeida, C., Fernandes, J. O. and Cunha, S. C., *A novel dispersive liquid–liquid microextraction (DLLME) gas chromatography-mass spectrometry (GC–MS) method for the determination of eighteen biogenic amines in beer*, Food Control, 2012. **25**(1): p. 380-388.